

THERMODYNAMICS OF SKELETAL MUSCLE

A THESIS SUBMITTED TO  
THE GRADUATE SCHOOL OF NATURAL AND APPLIED SCIENCES  
OF  
MIDDLE EAST TECHNICAL UNIVERSITY

BY

EKIN VARLI

IN PARTIAL FULFILLMENT OF THE REQUIREMENTS  
FOR  
THE DEGREE OF DOCTOR OF PHILOSOPHY  
IN  
ENGINEERING SCIENCES

DECEMBER 2022



Approval of the thesis:

**THERMODYNAMICS OF SKELETAL MUSCLE**

submitted by **EKIN VARLI** in partial fulfillment of the requirements for the degree of **Doctor of Philosophy in Engineering Sciences Department, Middle East Technical University** by,

Prof. Dr. Halil KALIPÇILAR  
Dean, Graduate School of **Natural and Applied Sciences**

\_\_\_\_\_

Prof. Dr. Murat Dicleli  
Head of Department, **Engineering Sciences**

\_\_\_\_\_

Assist. Prof. Dr. Senih Gürses  
Supervisor, **Engineering Sciences, METU**

\_\_\_\_\_

**Examining Committee Members:**

Prof. Dr. Feza Korkusuz  
Sports Medicine, Hacettepe University

\_\_\_\_\_

Assist. Prof. Dr. Senih Gürses  
Engineering Sciences, METU

\_\_\_\_\_

Prof. Dr. Dilek Keskin  
Engineering Sciences, METU

\_\_\_\_\_

Prof. Dr. Murat Zinnuroğlu  
Physical Medicine and Rehabilitation, Gazi University

\_\_\_\_\_

Assist. Prof. Dr. Kutluk Bilge Arıkan  
Mechanical Engineering, TED University

\_\_\_\_\_

Date:

**I hereby declare that all information in this document has been obtained and presented in accordance with academic rules and ethical conduct. I also declare that, as required by these rules and conduct, I have fully cited and referenced all material and results that are not original to this work.**

Name, Surname: Ekin Varlı

Signature :

## **ABSTRACT**

### **THERMODYNAMICS OF SKELETAL MUSCLE**

Varlı, Ekin

Ph.D., Department of Engineering Sciences

Supervisor: Assist. Prof. Dr. Senih Gürses

December 2022, 116 pages

The major focus of this study is on creating a statistical thermodynamics and mechanics formalism for muscular contraction. The first part of this thesis previously covered classical mechanics. We must first properly comprehend the structure, function, and interaction of actin and myosin, which together comprise the cross-bridge mechanism, in order to comprehend events that are occurring in the cross-bridge mechanism and build a probabilistic strategy. Our studies in this area suggest that the proteins myosin and actin serve as the building blocks of a generic process for generating cell motion. Along with cell migration, cell division, and shape changes, alterations in intracellular actin distribution also occur. The first model replicated three separate modes of movement via the cell model, including the stationary state of our truss model, friction-induced cell motion in the favored direction, and actin polymerization-induced cell motion. The second hypothesis is based on the facts that the cytoskeleton plays a fundamental role in cell motility and that the cytoplasm is viscoelastic. To that purpose, we provide a viscoelastic model for cell movement based on a hexagonal truss structure that includes the threshold element, viscous elements, and contractile actin molecules. We begin studying statistical mechanics in the second half of this subject. As a result, statistical mechanics provides a framework

for transforming a system's probabilistic, high-dimensional description into a macroscopic one using space distributions. This method allows us to express the likelihood of several alternative microscopic states. In this phase, symmetric and asymmetric decision boundaries are identified using a triangular probability distribution function, notwithstanding the friction force, and the decision-making process is then converted to a mechanism-based approach rather than using manually calculated probabilities. The master equation is generated in this stage in order to do it.

Keywords: skeletal muscle, muscle contraction, cell motility, statistical mechanics, statistical thermodynamics, sliding filament theory, cross bridge mechanism, cell division, cell locomotion,

## ÖZ

### İSKELET KASININ TERMODİNAMİK YAPISI

Varlı, Ekin

Doktora, Mühendislik Bilimleri Bölümü

Tez Yöneticisi: Dr. Öğr. Üyesi. Senih Gürses

Aralık 2022 , 116 sayfa

İstatistiksel mekanik ve istatistiksel termodinamik yaklaşımları kullanılarak iskelet kasının kasılma formalizminin geliştirilmesi bu çalışmanın ana konusunu oluşturmaktadır. Bu yöntemler ile çalışılmadan önce, tezin ilk bölümünde klasik mekanik yani Newton mekaniği incelenmiştir. Çapraz köprü mekanizmasında meydana gelen olayları anlamak ve olasılıksal bir yaklaşım geliştirmek için; öncelikle aktin ve miyozinin yapısını ve işlevini ve bunların çapraz köprü mekanizmasını oluşturan etkileşimlerini tam olarak anlamamız gerekmektedir. Bu bağlamda yaptığımız araştırmalar, miyozin ve aktin proteinlerinin hücre hareketi üretmek için genel bir mekanizmanın temelini oluşturduğunu göstermektedir. Hücre içi aktin dağılımındaki değişiklikler hücre hareketine, hücre bölünmesine ve hücre şekli değişikliklerine sebep olmaktadır. Bu nedenle, bu çalışmada hücre motilite modeli olan yeni bir model geliştirdik ve truss sistemlere kullanarak hücre hareketini modelledik. İlk modelde, hücre modeli boyunca gözlenen üç farklı hareket mekanizmasını simüle edildi. Bunlar, hareketin olmadığı yani hücrenin stabil durduğu durum, tercih edilen yönde sürtünmeye bağlı hücre hareketinin gözlemlendiği durum ve son olarakta aktin polimerizasyonunun etkilediği hücre hareketidir. İkinci modelimiz ise, hücre iskeletinin hücre hareketliliği

için birincil rol oynadığı ve sitoplazmanın viskoelastik olduğu gerçeklerine dayanan modelimizdir. Bu amaçla, eşik elemanını, viskoz elemanları ve son olarak kasılabilen aktin moleküllerini içeren altıgen bir truss sistemi kullanarak hücre hareketi için viskoelastik bir model oluşturduk. Tezimizin ikinci bölümünde ise İstatistiksel mekanik konusunu inceledik. İstatistiksel mekanik, mikroskobik bileşenleri analiz ederek bir sistemin makroskopik davranışını tanımlayan bir araçtır. Bu nedenle istatistiksel mekanik, bir sistemin olasılıksal, yüksek boyutlu tanımından, uzay dağılımları yoluyla makroskopik tanımına geçmek için kullanılır. Bu yaklaşımı kullanarak birçok farklı mikroskobik durumun olasılığını yazabiliriz. Bu bölümde çalışmanın ilk kısmındaki modellerde kullanılan sürtünme kuvvetinin aksine, üçgen olasılık dağılım fonksiyonu üzerindeki simetrik ve asimetrik karar sınırları kullanılarak hareket yönü belirlenmiştir. İkinci kısmın bir sonraki aşamasında ise manuel olarak belirlediğimiz hareket yönü belirleme prosedürü olasılığı, mekanizmaya dayalı olarak değiştirilecektir. Yani hareket yönü olasılığı bir denkleme (master denkleme) bağlanarak çok daha fizyolojik bir hale getirilmiştir.

Anahtar Kelimeler: iskelet kası, kas kasılması, hücre hareketi, istatistiksel mekanik, istatistiksel termodinamik, çapraz köprü mekanizması, hücre bölünmesi, kayan filament teorisi



To My Family

## ACKNOWLEDGMENTS

There are no proper words to convey my deep gratitude and respect for my thesis advisor, Assist. Prof. Dr. Senih Gürses. His invaluable advice, continuous support, and patience carried me through all the stages of writing this thesis. His immense knowledge and plentiful experience have encouraged me in all the time of my academic research and daily life.

I would also like to thank Assoc.Prof.Dr.-Ing. Serdar Göktepe for all the support, assistance, and advice he provided for my thesis over the course of the previous six years. He has also provided insightful discussions about the research.

My sincere thanks goes to my thesis committee chair Prof. Dr. Dilek Keskin for all of her kind help and support. I also thank the rest of my thesis committee: Prof. Dr. Feza Korkusuz, Prof. Dr. Murat Zinnurođlu and Assist. Prof. Dr. Kutluk Bilge Arıkan, for their insightful comments and questions which incited me to widen my research from various perspectives.

I will always be grateful to Gamze akır Kabakcı for her kind spirit and contributions to my life.

I am incredibly appreciative of his friendship and support for Berat Can Cengiz. Thanks also to Kardelen Mermerođlu and Nilgün Mermerođlu. Your support have added a lot to my life.

Endless thanks to Türköz Gargun for his priceless encouragement, support, and kind demeanor towards me during the last six years.

Last but not least, I would like to extend a special thank you to my childhood pals Yasemin Öztemur Islakođlu and Ayşe Atöz for their brilliant comments and suggestions. They never stopped believing in me.

It is impossible to extend enough thanks to my parents Abdullah and Hülya Varlı and

my sister Dilge Varlı for their unconditional love and support. They believed in me throughout this journey and my whole life by having faith in me and giving me the encouragement I required. Without them, I would not have progressed this far.

## TABLE OF CONTENTS

ABSTRACT . . . . .	v
ÖZ . . . . .	vii
ACKNOWLEDGMENTS . . . . .	x
TABLE OF CONTENTS . . . . .	xii
LIST OF TABLES . . . . .	xv
LIST OF FIGURES . . . . .	xvi
CHAPTERS	
1 CELL MOTILITY MODELS . . . . .	1
1.1 INTRODUCTION . . . . .	1
1.2 THE CELL AND CYTOSKELETAL STRUCTURES . . . . .	5
1.3 MECHANISIMS OF CELL MOTILITY . . . . .	9
1.3.1 ACTIN POLYMERIZATION . . . . .	10
1.4 DEFINITION OF THE SUBJECT AND ITS IMPORTANCE . . . . .	12
1.5 LITERATURE REVIEW OF RELEVANT RESEARCH . . . . .	13
1.6 AIM OF THE STUDY . . . . .	16
1.7 2D CELL MOTILITY MODEL . . . . .	17
1.8 ANALYSIS . . . . .	26
1.8.1 Case 1 . . . . .	27

1.8.2	Case 2 . . . . .	29
1.8.3	Case 3 . . . . .	31
1.9	HEXAGONAL CELL MOTILITY MODEL . . . . .	33
1.10	ANALYSIS . . . . .	38
1.10.1	Case 1 . . . . .	38
1.10.2	Case 2 . . . . .	40
1.10.3	Case 3 . . . . .	42
2	PROBABILISTIC MODELS . . . . .	45
2.1	INTRODUCTION . . . . .	45
2.1.1	Entropy . . . . .	46
2.1.2	Energy, Enthalpy and Free Energy . . . . .	46
2.1.3	Probability Theory . . . . .	47
2.2	AIM OF THE STUDY . . . . .	51
2.3	THE MASTER EQUATION . . . . .	53
2.4	THE ONE-STATE MODEL . . . . .	55
2.5	ANALYSIS . . . . .	64
2.5.1	Case 1 . . . . .	64
2.5.2	Case 2 . . . . .	65
2.5.3	Case 3 . . . . .	66
2.6	THE TWO-STATE MODEL . . . . .	68
2.6.1	UNBOUND(DETACHED) . . . . .	69
2.6.2	BOUND (ATTACHED) . . . . .	70
2.7	THE FOUR-STATE MODEL . . . . .	73

REFERENCES . . . . .	79
A APPENDIX A . . . . .	91
B TRIANGULAR PROBABILITY DISTRIBUTION FUNCTION . . . . .	93
C UNBIASED RANDOM WALK . . . . .	105
D ADVECTION-DIFFUSION EQUATION . . . . .	113

## LIST OF TABLES

### TABLES

Table A.1	Table of units . . . . .	91
Table A.2	Table of constants . . . . .	92

## LIST OF FIGURES

### FIGURES

Figure 1.1	Skeletal muscle structure . . . . .	1
Figure 1.2	Four state cross-bridge cycle . . . . .	3
Figure 1.3	Structure of an eukaryotic cell [19]. . . . .	5
Figure 1.4	Structure of Cytoskeleton . . . . .	6
Figure 1.5	Cytoskeletal Filaments. Image reproduced from [25] . . . . .	7
Figure 1.6	A single cell moving across a two-dimensional [43] . . . . .	10
Figure 1.7	Illustration of filopod and lamellipod in cell migration [43] . . . . .	10
Figure 1.8	Rates of association and dissociation of actin monomers at the pointed (-) and barbed (+) end of the filament [43]. . . . .	11
Figure 1.9	Regulation of actin filament polymerization and treadmilling [43].	12
Figure 1.10	Cell motility model . . . . .	18
Figure 1.11	Initial and current body configurations . . . . .	20
Figure 1.12	Algorithmic Flow Chart . . . . .	26
Figure 1.13	Symmetric model for case 1 . . . . .	27
Figure 1.14	The change in x coordinate of the centre of mass of the symmetric truss model with respect to time for case 1 . . . . .	28
Figure 1.15	The change in y coordinate of the centre of mass of the symmetric truss model with respect to time for case 1 . . . . .	28



Figure 1.16	The change in x and y coordinates of the center of mass of the symmetric truss model for case 1 . . . . .	28
Figure 1.17	Non-symmetrical model for case 2 (Symmetry is removed by using friction force) . . . . .	29
Figure 1.18	The change in x coordinate of the centre of mass of the non-symmetric truss model with respect to time for case 2 . . . . .	30
Figure 1.19	The change in y coordinate of the centre of mass of the non-symmetric truss model with respect to time for case 2 . . . . .	30
Figure 1.20	The change in x and y coordinates of the center of mass of the non-symmetric truss model for case ) . . . . .	30
Figure 1.21	Non-symmetrical model for case 3 (Symmetry is removed by polymerizing actin) . . . . .	31
Figure 1.22	Monomer capturing and releasing . . . . .	31
Figure 1.23	The change in x coordinate of the center of mass of the non-symmetric truss model with respect to time for case 3 . . . . .	32
Figure 1.24	The change in y coordinate of the center of mass of the non-symmetric truss model with respect to time for case 3 . . . . .	32
Figure 1.25	The change in x and y coordinates of the center of mass of the non-symmetric truss model for case 2 . . . . .	33
Figure 1.26	Hexagonal Cell motility model . . . . .	33
Figure 1.27	Fully elastic model for case 1 . . . . .	39
Figure 1.28	The change in x coordinate of the centre of mass of the fully elastic hexagonal truss model with respect to time for case 1 . . . . .	39
Figure 1.29	The change in y coordinate of the centre of mass of the fully elastic hexagonal truss model with respect to time for case 1 . . . . .	40

Figure 1.30	The change in $x$ and $y$ coordinates of the center of mass of the fully elastic hexagonal truss model for case 1 . . . . .	40
Figure 1.31	Elastic elements with threshold for case 2 (Symmetry is removed by using friction force) . . . . .	41
Figure 1.32	The change in $x$ coordinate of the centre of mass of the non-symmetric truss model with respect to time for case 2 . . . . .	41
Figure 1.33	The change in $y$ coordinate of the centre of mass of the non-symmetric truss model with respect to time for case 2 . . . . .	42
Figure 1.34	The change in $x$ and $y$ coordinates of the center of mass of the non-symmetric truss model for case . . . . .	42
Figure 1.35	Non-symmetrical model for case 3 (Symmetry is removed by polymerizing actin) . . . . .	43
Figure 1.36	The change in $x$ coordinate of the center of mass of the non-symmetric truss model with respect to time for case 3 . . . . .	43
Figure 1.37	The change in $y$ coordinate of the center of mass of the non-symmetric truss model with respect to time for case 3 . . . . .	44
Figure 1.38	The change in $x$ and $y$ coordinates of the center of mass of the non-symmetric truss model for case 2 . . . . .	44
Figure 2.1	Lattice Model . . . . .	49
Figure 2.2	Active actin sites . . . . .	52
Figure 2.3	Jumping to the Left . . . . .	54
Figure 2.4	Jumping to the Right . . . . .	54
Figure 2.5	No Jump . . . . .	54
Figure 2.6	The free energy of a myosin head moving along an actin filament [97] . . . . .	56

Figure 2.7	The free energy of a myosin head moving along an actin filament [97] . . . . .	57
Figure 2.8	Energy landscape of a one-state model [1] . . . . .	58
Figure 2.9	Lattice Model of ATP . . . . .	61
Figure 2.10	Binding Probabilities (Rate constants are selected constant values)	65
Figure 2.11	Binding Probabilities (Force dependent forward rate constant) . .	66
Figure 2.12	Binding Probabilities ( $[ATP] = 5 \times 10^{-3}$ mM ) . . . . .	67
Figure 2.13	Binding Probabilities ( $[ATP] = 15 \times 10^{-3}$ mM ) . . . . .	67
Figure 2.14	Kinetic diagram for a two-state cross-bridge model . . . . .	68
Figure 2.15	Two State Model for Unbound Case . . . . .	69
Figure 2.16	Two State Model for Bound Case . . . . .	71
Figure 2.17	Four State Model . . . . .	73
Figure 2.18	Four State Model . . . . .	74
Figure B.1	Tent of the position distribution . . . . .	93
Figure B.2	1D Triangular probability distribution . . . . .	94
Figure B.3	. . . . .	97
Figure B.4	. . . . .	98
Figure B.5	Brownian Path . . . . .	98
Figure B.6	Decision making model . . . . .	99
Figure B.7	Triangular Distribution . . . . .	100
Figure B.8	Frequency Histogram of Decisions . . . . .	101
Figure B.9	Cumulative Triangular Distribution . . . . .	101

Figure B.10	Triangular Distribution Histogram . . . . .	102
Figure B.11	Cumulative Triangular Distribution . . . . .	102
Figure B.12	Triangular Distribution Histogram . . . . .	103
Figure B.13	Cumulative Triangular Distribution . . . . .	103
Figure B.14	Distribution for Three case . . . . .	104
Figure C.1	Open-ended in the temporal dimension . . . . .	107
Figure D.1	. . . . .	113
Figure D.2	. . . . .	115

# CHAPTER 1

## CELL MOTILITY MODELS

### 1.1 INTRODUCTION

Conducting a directed movement is one of a live organism's most crucial characteristics. Muscle tissue, which generates motion and exerts force, can be thought of as the fundamental component of human and animal movement mechanics [1]. Skeletal (Striated) muscle, Smooth muscle, and Cardiac muscle are the three categories into which the muscular tissue is generally categorized. Tendons connect skeletal muscle, sometimes known as "voluntary muscle," to bones, allowing it to move the skeleton. Lip, eyelid, and ocular mobility are all controlled by skeletal muscle [2]. Long cylindrical cells make up the skeletal muscles. Fig.1.1 [3] displays a schematic depiction of the skeletal muscle structural hierarchy in vertebrate striated muscle [3].

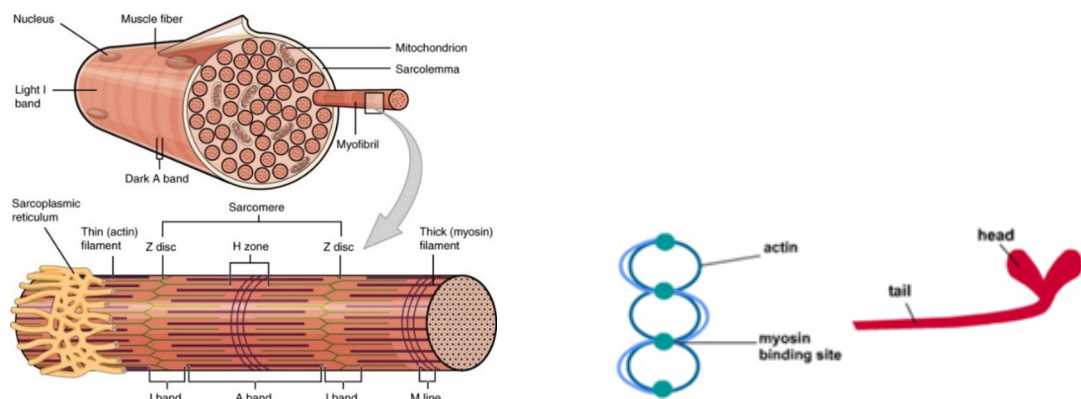


Figure 1.1: Skeletal muscle structure

The muscle fiber is more thoroughly investigated in Fig.1.1. A muscle cell's sar-

cytoplasm and sarcolemma are its cytoplasm and plasma membrane, respectively. Numerous tiny nuclei, mitochondria, and myofibrils can be found in the sarcoplasm. Myofibrils are cylinder-shaped, contractile components. They extend the entire length of the muscle fibre and they are 1 mm in diameter. Each myofibril consists of thick and thin filaments. The thick and thin filaments are protein myosin and protein actin respectively. The basic functional unit of the muscle fibre is sarcomere. The Z-line is the connection line between sarcomeres. A-band is containing the myosin and I-band is between two A-bands and made up only of thin filaments. Thick filaments are connected by the M-line, which runs through the center of the sarcomere. Actin and myosin molecules have twisted protein strands. Protein myosin has a tail and a head and protein actin has a myosin binding site.

The work that is currently being presented is specifically focused on a theoretical model of skeletal muscle that describes the mechanism of the sliding filament theory in terms of energy and stochastic methods. Over the years, the sliding filament theory—and in particular the cross-bridge theory—has been developed and is still being studied [4, 7]. In a nutshell, two separate teams led by Hugh E. and Andrew Fielding Huxley developed the sliding filament idea in the 1950s. The fundamental tenet of the sliding filament theory is that during sarcomere contraction, actin and myosin slide about in the shape of filaments relative to one another. This idea was supported by light microscope findings, but the sliding process itself remained a mystery. There are almost  $10^{14}$  cross-bridges in 1 mg of muscle tissue [8]. The original Huxley cross-bridge theory describes how two proteins, myosin and actin, combine to form the two primary contractile elements of sarcomeres. The cross-bridge theory, developed by Andrew Fielding Huxley in the late 1950s and based on the sliding filament theory, postulates a molecular connection between the contractile proteins actin and myosin. This theory is supported by experiments and accepted as the main explanation of muscle contraction. Myosin and actin molecules exist in the protein filaments. Myosin heads are protruded from the myosin molecules. These myosin heads can cyclically bind to actin filaments and unbind from actin filaments and pull actin filaments towards the centre of sarcomere see in Fig.1.1. Actin and myosin relative sliding is the primary mechanism of muscle shortening and force generation against potential external forces. The temporary connection between myosin and actin filaments is

created when the myosin heads are connected to actin. The cross-bridges are the traditional and illustrative name for these linkages. Figure Fig.1.2 shows the schematic of the four state cross-bridge cycle.

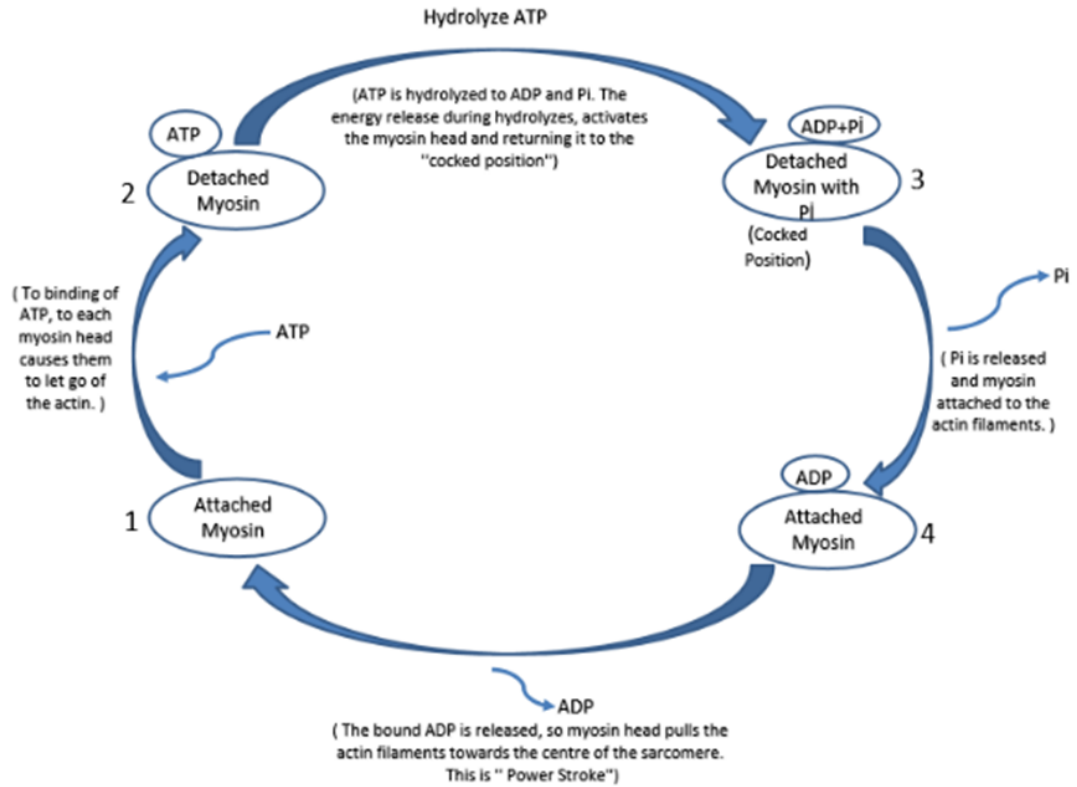


Figure 1.2: Four state cross-bridge cycle

In Fig.1.2, first, ATP connects to the myosin head, causing the cross-bridge to separate, then in the second stage, ATP is hydrolyzed to ADP and Pi (inorganic phosphate), which puts the myosin back in the "cocked" position. The myosin head is linked to the actin filaments once Pi is released. The actin filaments are pulled into the center of the sarcomere by the myosin head during the final stage, which is referred to as the "power stroke." The myosin head and actin join together to create a cross-bridge after a power stroke.

A. F. Huxley created the first mathematical representation of this hypothesis in 1957 [4]. This study, which establishes the cross-bridge theory's fundamentals and pioneers the field of muscle mechanics research, is recognized as a classic work in the field. It aids in determining the mechanism of muscle contraction. The fundamental concept behind the cyclic association between the two primary contractile proteins

actin and myosin hasn't changed, though. For a very long time, it was believed that the traditional cross-bridge model, which included the interaction of the two filaments, was an all-purpose instrument for explaining and simulating the contractile activity and energy characteristics of muscle. The Zahalak energetic model, often known as the distribution-moment model [9], is one of the most popular and well-known research based on Huxley's writings. Since the main goal of the current thesis work is to find an energetic strategy for cross-bridge mechanisms by applying statistical thermomechanics, this model is quite important. The distribution moment model proposed by Zahalak is based on the cross-bridge theory of Huxley with two sliding filaments. His 1980s-era model has been put forth to more accurately characterize the reaction to muscular stretch. Additionally, Zahalak took into account the impact of  $Ca^{++}$  ions, which is crucial to this work because we assert that the cross-bridge mechanism is entropic and is primarily regulated by the release of  $Ca^{++}$  ions. Numerous papers are cited for the reader [9, 13]. We must first comprehend the structure, function, and interaction of actin and myosin in order to properly comprehend the events that are taking place in the cross-bridge process and to build a probabilistic strategy. According to our research in this regard, myosin and actin proteins serve as the building blocks of a general mechanism for generating cell motion, of which muscle contraction is a specific case [14]. Actin proteins, which have anisotropic distributions in cells that often have asymmetric forms, perform a contractile and cytoskeletal role in the cells, according to numerous studies [15]. Actin filaments are created when G actin monomers polymerize [16]. Cell mobility, cell shape alterations, and cell division are frequently accompanied by modifications in intracellular actin distribution. Actin polymerization generates the available energy that powers the actions of the cell, according to Boal's citation [15]. In this way, we took a cue from Boal and used a truss system to represent the interplay between actin and microtubules in cell movement. Microtubules are intracellular filamentous structures that control numerous cellular motions. In the final of three studies using our cell model, we also looked at actin polymerization and demonstrated how it affects cell motility. This model is explained in greater depth in section 3. The Aim of the Study, Analysis, and Future Work Plan are covered in Sections 2, 4, and 5, respectively.



## 1.2 THE CELL AND CYTOSKELETAL STRUCTURES

The cell is the basic unit of all living organisms [17]. It is a complex but highly organized entity separated from the outside by a cell membrane. Two general cell types can be distinguished: prokaryotic and eukaryotic. Prokaryotes are single-celled organisms and comprise a single membrane-limited compartment. With few exceptions [18], a cell wall surrounds prokaryotic cells, providing structural support and protection. Eukaryotes comprise all members of the animal, plant and fungi kingdoms. Eukaryotic cells are more complex and typically much larger than that of prokaryotes. Unlike prokaryotes, eukaryotic cells also contain internal membranes and they are composed of different organelles, such as the endoplasmic reticulum, Golgi apparatus, mitochondria, lysosomes, etc., each one in charge of a specific and indispensable function. The structure of an eukaryotic cell is shown in Fig. 1.3

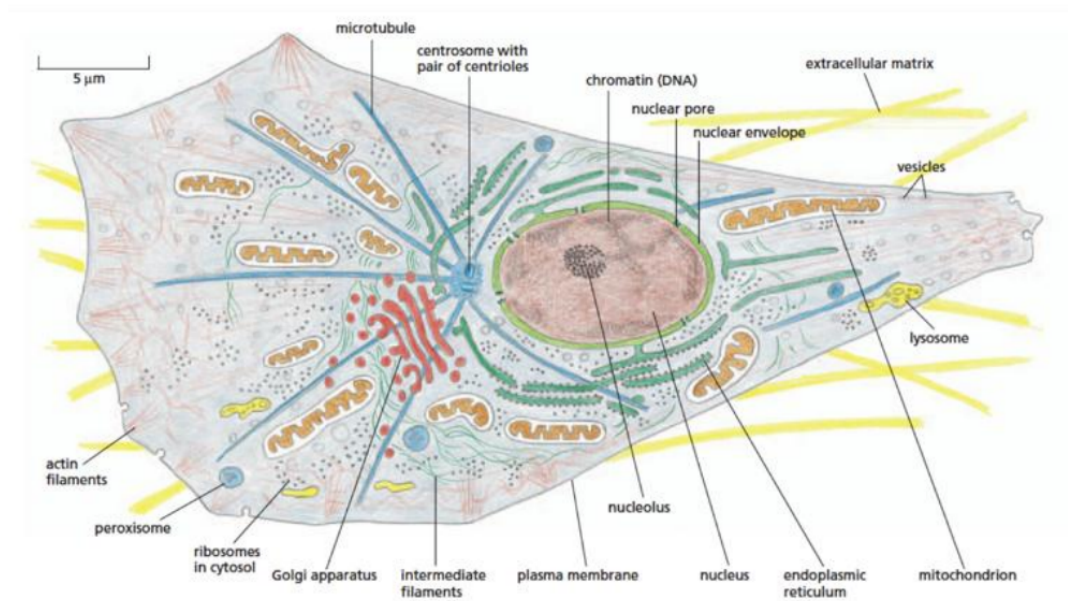


Figure 1.3: Structure of an eukaryotic cell [19].

One of the most important components of eukaryotic cells is the nucleus, which stores the genetic information required for cellular activities and in particular for cell division. All these organelles are confined by a lipid bilayer, a selective barrier that isolates the organelles from the cytoplasm and allows for a different soluble protein content, ionic strength, pH, among other features. Alongside, the cell itself is enclosed in a lipid bilayer or plasma membrane. This membrane acts as a barrier between the cytoplasm

and the exterior, but also enables external communication thanks to its permeability, transmembrane channels, and transmembrane or membrane-associated proteins. The organelles are embedded in the cytoplasm, a gel-like component (70-90% composed of water) that fills the cells [19]. The cytoplasm also contains the cytoskeleton, which is the cell scaffold. The cytoskeleton is a conglomerate of different types of filaments, which from the engineering standpoint may be seen as structural elements of a biopolymer network defining the architecture of the cell. Cells interestingly show material properties characteristic of both solids and liquids; they are able to elastically maintain their shape and yet plastically adapt it to the changing environment. Furthermore, cell response to external deformations may be highly non-linear [20, 21]. The cytoskeleton and plasma membrane together are thought to define the viscoelastic properties of cells [22, 23], which may also depend on the degree of internal stresses as well as on the mechanical properties of the extracellular milieu and the structure of cytoskeleton is shown in Fig.1.4 [24].

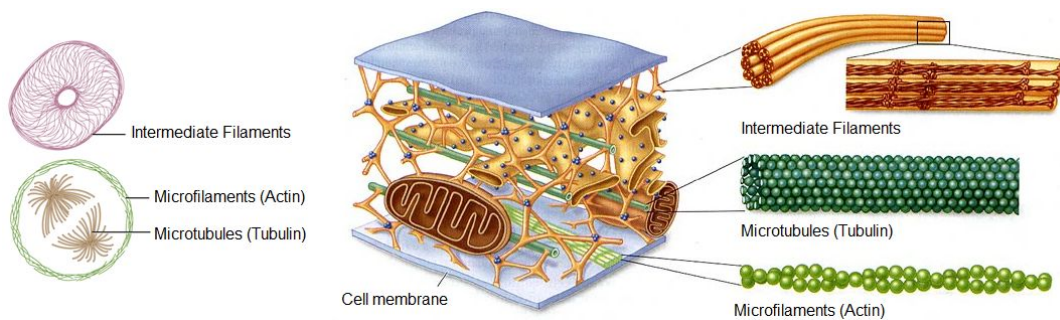


Figure 1.4: Structure of Cytoskeleton

The cytoskeleton is composed of three classes of fibers: microtubules, built of polymers of the protein tubulin; intermediate filaments, built of one or more rod-shaped protein subunits; and microfilaments, which are also called actin filaments. A schematic picture of these is shown in Fig.1.5.

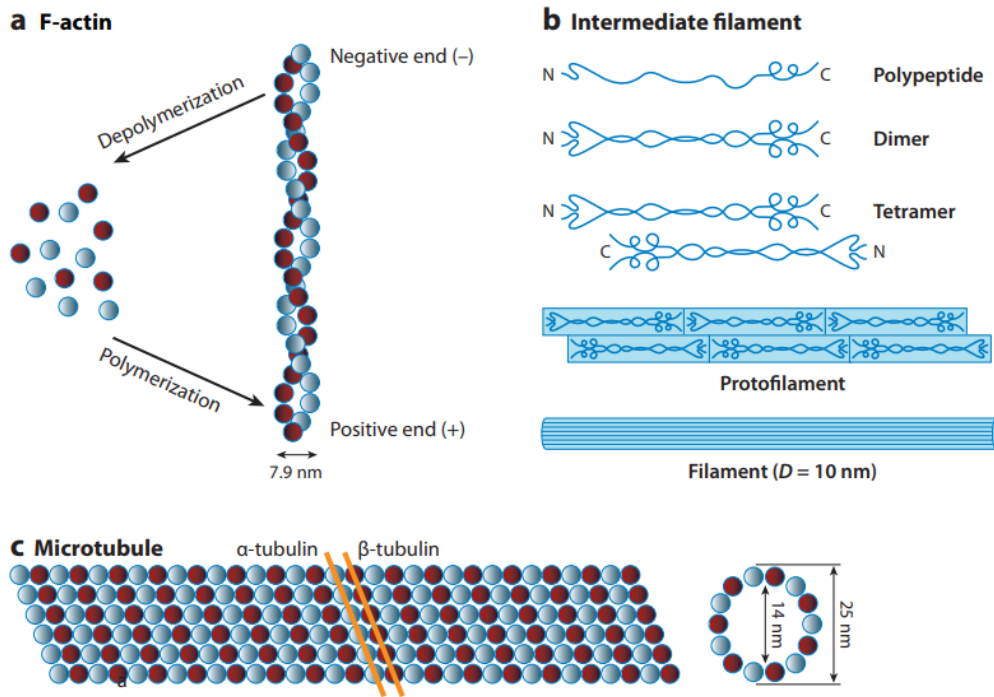


Figure 1.5: Cytoskeletal Filaments. Image reproduced from [25]

Actin is well-studied, abundant and found in every type of cell, responsible for a multitude of tasks. Actin filaments are formed by globular actin (G-actin) polymerizing into filaments (F-actin), a helical structure with a diameter of approximately 6nm. Lengths in the cell is typically on the order of a micron, although their contour length in vitro is typically on the order of their persistence length 10-17  $\mu\text{m}$  [26, 27], i.e. they behave as semiflexible polymers [27, 28, 29]. Actin is one of the main providers of stiffness for the cell and it is found in numerous forms in the cell, for example the densely cross-linked F-actin network below the plasma membrane (cortical actin), the distributed lattice throughout the cytoplasm, the dense meshwork in the leading edge of the cell (lamellipodium) and bundles of filaments termed stress fibres. Stress fibres are formed from focal adhesions and provide the actin cytoskeleton through integrins with a connection to the ExtraCellular Matrix (ECM). An important aspect in the formation of F-actin networks is their propensity to assemble into various types of cross-linked networks [30] by cross-linking proteins, or Actin Binding Proteins (ABPs). Examples of such proteins are the rod-like  $\alpha$ -actinin, found at focal adhesions, in stress fibres and cortical actin, and filaman, a hinge-like protein that binds filaments at orthogonal angles into a gel [19, 28] Actin filaments are dynamic, con-

tinuously polymerizing and depolymerizing, resulting in a machinery able to adapt to biochemical and mechanical signals. Intermediate filaments are a family of various proteins of which the expression depends on the type of cell and function. For example, endothelial cells express different kinds of keratin, and vimentin is prominent in mesenchymal cells such as fibroblasts [31]. These filaments are more flexible than actin, and often have a highly curved appearance when observed in the cell [33], probably due to their shorter persistence length  $\sim 1 \mu\text{m}$  [28, 31, 33, 34]. They are further more resistant to high salt concentrations, and much more stable, than actin filaments or microtubules [28, 31]. They have been proposed to be responsible for enabling the cell to withstand larger forces, as entangled networks typically exhibit strong strain hardening, and single filaments can be stretched far beyond their original length, unlike actin filaments which break at smaller strains [31, 35]. Intermediate filaments connect to the nuclear envelope through lamins, and radiate towards the surface of the cell where they through interaction with plectins might provide a connection to the ECM and other cells [31, 36, 37, 39]. Improper expression of intermediate filaments is known to greatly affect physiological function. For example, in mice, knocking out the vimentin gene in mice demonstrated that vimentin regulates the mechanical response to blood flow and pressure in arteries [31]. Further, cancer cells have been shown to exhibit a disrupted intermediate filament network, collapsed around the nucleus, along with distinctly different mechanical properties [40, 41]. Microtubules, the third type of cytoskeletal filaments is formed from tubulin into a hollow cylinder with an outer diameter of roughly 25nm and consequently a far higher bending stiffness than that of either actin or intermediate filaments [28]. Their persistence length is thus far greater, about 6mm [26, 28]. With a high bending stiffness and rod-like appearance, they are useful in aiding the formation of long slender structures. Microtubules are often found in an arrangement in which they radiate from the center of the cell [19], and perturbation of the microtubule network has been observed to collapse the intermediate filament network in turn, suggesting a role in keeping this open and stabilizing it against compression [31, 40, 42]. Microtubules are highly dynamic, allowing for remodeling and adaptation of cell structure and response in a matter of minutes [28]. Thus, microtubules being resistant to compressive stresses while actin and intermediate filaments carrying tensile forces constitute a coherent network of tensegrity in the continuous media of the cell unity [88]. The actomyosin-

based contractile machinery of the cell generates the stabilizing prestress actively in the simplest form of the cellular tensegrity model [89, 90], while the extracellular matrix adhesions of the cell passively distend the cell.

### **1.3 MECHANISMS OF CELL MOTILITY**

Cell movement is a complex and dynamic process that causes changes in cell morphology by reorganizing the actin cytoskeleton and modulating cell adhesions. For directional cell migration, cells must continuously receive the polarized environmental signals and transmit the polarized intracellular signals from a fixed direction, which orient protrusion of the leading edge. Cell crawling involves a coordinated cycle of movements, which can be viewed in three stages as it can be shown in Fig. 1.6 and Fig. 1.7. In the first stage, protrusions such as pseudopodia, lamellipodia, or microspikes must be extended from the leading edge of the cell and this extension of the leading edge involves the polymerization and crosslinking of actin filaments. For example, inhibition of actin polymerization blocks the formation of cell surface protrusions. Actin polymerization is expressed in detail in chapter 1.3.1. The regulated turnover of actin filaments leads to the extension of processes such as filopodia and lamellipodia at the leading edge of the cell. Unconventional myosins may also participate in the extension of processes at the leading edge. Second, these extensions must attach to the substratum across which the cell is migrating. For slow-moving cells, such as fibroblasts, attachment involves the formation of focal adhesions. Cells moving more rapidly, such as amoebas or white blood cells, form more diffuse contacts with the substratum, the molecular composition of which is not known. Finally, in the third stage of cell crawling, retraction of the trailing edge, is the least understood. The attachments of the trailing edge to the substratum are broken, and the rear of the cell recoils into the cell body. The process appears to require the development of tension between the front and rear of the cell, generating contractile force that eventually pulls the rear of the cell forward.

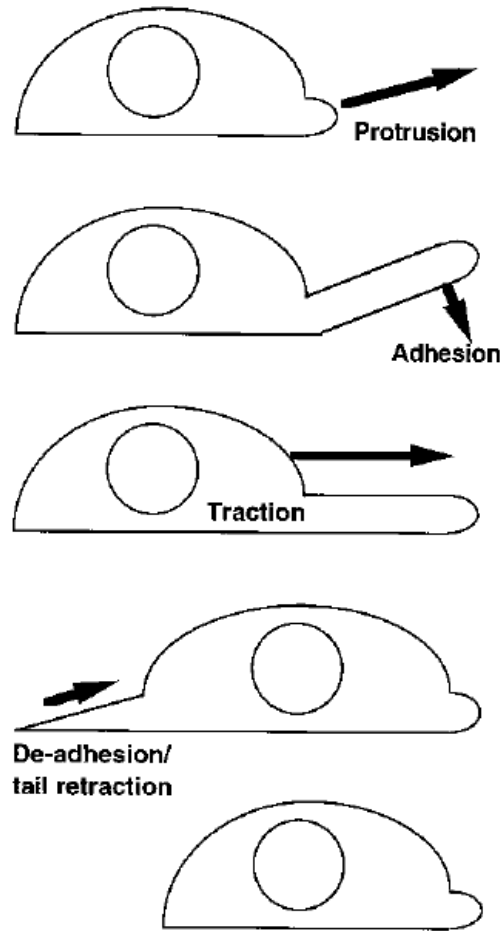


Figure 1.6: A single cell moving across a two-dimensional [43]

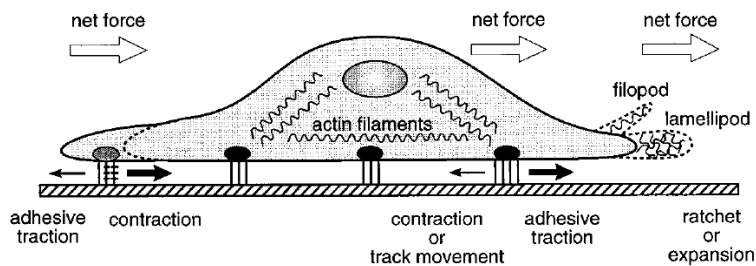


Figure 1.7: Illustration of filopod and lamellipod in cell migration [43]

### 1.3.1 ACTIN POLYMERIZATION

According to many researchers actin filaments and microtubules are also responsible for cellular motion and actin proteins are the basic engines for the cell locomotion and these proteins have anisotropic distributions in the cell which generally have an

asymmetric shape [46]. Changes in intracellular actin distribution which is called actin polymerization controls protrusion of the cell in the current paradigm for cell migration [47]. Actin polymerization is powered by ATP. Each actin monomer contains a bound ATP molecule, which is hydrolyzed after polymer formation. The half time of hydrolysis following the assembly of an ATP-bound actin subunit to the filament is two seconds. Further, the half time for release of inorganic phosphate from the actin fibril is about six minutes. These slow rates are relevant for the transient rearrangements of the actin cytoskeleton since many actin binding proteins involved exhibit binding affinities that depend on the nucleotide state in the filament. After hydrolysis of ATP in the fibril, the critical concentration for binding of the ADP-bound protomers increases significantly. The weaker binding results in instability of the filaments and increases disassembly.

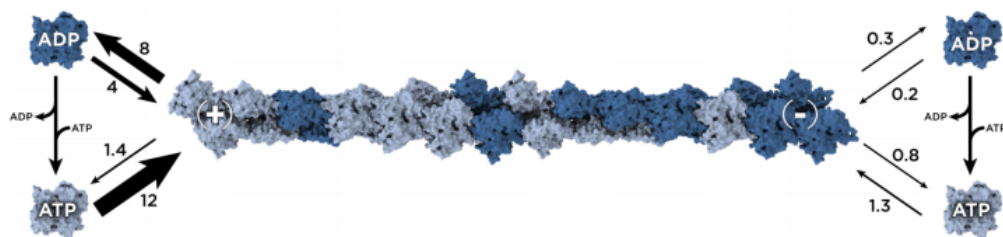


Figure 1.8: Rates of association and dissociation of actin monomers at the pointed (-) and barbed (+) end of the filament [43].

Actin filaments exhibit structural and functional polarity based on the head to-tail orientation of the subunits. The two ends are dramatically different in the components that bind to them (Fig. 1.8). This includes actin subunits that polymerize much faster onto one end (the (+) or barbed end) than they do on the other (the (-) or pointed end). Generally, subunits that polymerize on the (+) end are more likely to contain ATP than on the (-) end. Therefore, the (-) end is most likely to have an ADP-bound subunit and depolymerize. The dissociating ADP-actin molecules are recharged, often mediated by profilin, which also delivers the ATP-bound actin subunits to the (+) end, thus closing the nucleotide-facilitated polymerization cycle of actin (Fig.1.9). When the ATP-actin concentration is between the critical concentration for the (+) and (-) ends, the filament grows at the (+) end while actin subunits disassemble from the other end. The overall length of the filament remains constant and subunits that

polymerize on the barbed end travel through the filament to the pointed end as if on a treadmill. At the leading edge of migrating cells, treadmilling is believed to be the responsible mechanism for turnover of actin filaments, with actin monomers added to filaments near the leading edge of the cell and lost from the other end toward the rear. This is just one example of how the directed assembly and disassembly of individual filaments driven by ATP produce the complex rearrangements of the actin cytoskeleton that are required for actin-based motility allowing for remodeling and adaptation of cell structure and response in a matter of minutes [28].

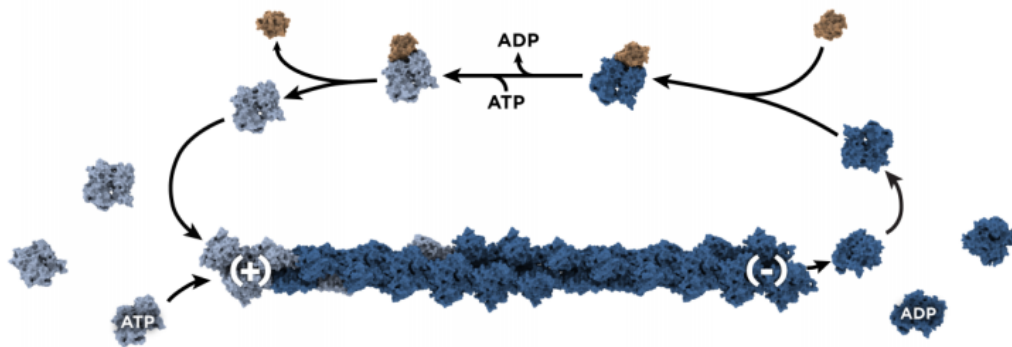


Figure 1.9: Regulation of actin filament polymerization and treadmilling [43].

#### 1.4 DEFINITION OF THE SUBJECT AND ITS IMPORTANCE

Cell motility is necessary for the survival of all living species and is a fundamental process, from simple, uni-cellular organisms such as amoeba, to complex multi-cellular organisms such as mammals [43]. Cell motility has primary significance for such biological processes as the embryo development, wound healing, cancer metastasis, and immune response [44]. Thereby, a sound understanding of the foundation of the cell motility is central in order to explain the functioning of all organisms. At a very early stage of human embryo development, invasion and migration of trophoblasts into maternal uterus epithelium is critical for blastocyst implantation [45]. Healing and immunity is also critically dependent on cell motility. Fibroblasts and endothelial cells migrate to wound to secrete collagen and generate new blood vessels respectively to regenerate the damaged tissue. Meanwhile, keratinocytes migrate and proliferate over the newly produced collagen to generate new epithelium to cover the wound. Just shortly after injury, immune cells, namely neutrophils and macrophages,



move to the site of injury to clean up pathogens and debris. While migration of immune cells is required, it is not restricted to wound healing. Infection of microbes also triggers inflammatory response. In response to the infection, leukocytes originated from bone marrow migrate to the site and kill the invading microbes. This innate immunity forms the first line of defense against pathogens. Cell migration is clearly critical to physiology; however, it also contributes to cancer metastasis. While solid primary tumors can often be surgically removed, motile cancer cells invade surrounding tissue stroma, and can invade to other distal organs to establish metastasis.

## **1.5 LITERATURE REVIEW OF RELEVANT RESEARCH**

Anthony van Leeuwenhoek used a glass bead as a crude microscope and moved it near to a pool-taken drop of water in 1674 to record the first observation of cell movement. The motion of these animalcules in the water was so rapid and varied, above, downwards, and all around, that it was fascinating to witness, the man later remarked. [49]. The creatures he observed were presumably ciliated protozoa, which are unicellular, non-photosynthetic eukaryotic organisms that are less than one millimeter in length. They may be identified by the agitated, coordinated movement of hundreds to thousands of these organisms' surface hairlike cilia. Despite this very early observation, it has taken relatively recent developments in microscopy, molecular biology, and biochemistry to enable the discovery of the fundamental molecular mechanisms by which cells are able to feel their environment, exert forces, and move in a directed manner in search of nutrients or any other task they need to perform. H. E. Huxley and J. Hanson made the first observation of the cytoskeleton in 1953 when they used electron microscopy to identify the double array of filaments in cross-striated muscles [50, 52]. The cytoskeleton is defined as the system of protein filaments that allows the cell to maintain its structural integrity and morphology, exert forces, and produce motion. The "sliding-filament model," which describes muscular contraction by the relative sliding of two different types of filaments, originally dubbed "thick" and "thin" filaments, was published the next year concurrently with A. F. Huxley and R. Niedergerke but independently [53, 54]. This established the beginning of a scientific knowledge of the subcellular processes underlying cell motility, which was

further established with the aid of other genetic, biochemical, and crystallographic research. Along with characterizing the biochemical makeup and arrangement of these subcellular structures, significant developments in the last 20 years in physical micro-manipulation and fluorescence imaging methods have made it possible to characterize the mechanisms at work in great detail. On the one hand, one may define the forces that cells can exert as well as their reactions to applied stimuli with the use of micro-pipettes, atomic force microscopes, and optical tweezers. The microscopic movements of individual molecules *in vivo* are, nevertheless, shown by fluorescence-microscopy methods. Finally, these approaches have made it possible to examine simpler systems where some particular features of the processes involved may be defined independently. This has been made possible by the combination of biochemistry, gene-expression control, and the micro-fabrication of bio-mimetic artificial systems in *in-vitro* experiments. Understanding the general principles that underlie cell motility required an integrated approach in addition to these biochemical and behavioral characterizations to explain how this sophisticated molecular machinery may self-organize and result in a coherent, intentional movement at the cellular level. An eukaryotic cell is the best example of a complex system since it combines the coordinated interaction of more than ten thousand distinct protein types, totaling millions and making up 60% of its dry mass [48]. Numerous distinct molecular actors make up the cytoskeletal system. For instance, actin, one of the key biopolymers involved in cell structure and dynamic activity, was discovered to bind to roughly 160 proteins in 2003 [55]. By referring to the most recent data on the various databases, it is possible to understand the continually changing complexity of this biomolecular machinery, which is still a subject of active research [63]. Therefore, biophysical investigations, both on experimental and theoretical grounds, helped to establish the general principles underlying cell motility and describe how this complexity is integrated at the cellular level. First, at the molecular level, the conversion of chemical energy held in covalent bonds into mechanical work depends on out-of-equilibrium thermodynamic principles and the asymmetrical properties, or polarity, of the structures involved, and takes place in a highly fluctuating environment of Brownian particles [56, 57]. The development of coordinated motion in large protein collections depends on collective processes, self-organization, and dynamical symmetry breakings over longer time scales [58]. On even longer length scales, swimming of microbes has long caught the

interest of physicists [59, 60], while morphogenesis and pattern forms in biological tissues depend on self-organization events, as initially envisioned by Turing in 1952 [61, 62]. In light of this, various theoretical physics disciplines, including the theory of stochastic processes, statistical physics, out-of-equilibrium thermodynamics, hydrodynamics, nonlinear dynamics, and pattern formation, have contributed to and continue to do so in order to further our understanding of cell motility.

Numerous models [66, 67] that focus on mimicking cells as separate units in the tissue can be found. First, tracking cell information and calculating cell interactions are made simple by center-based and simple particle models [68, 70]. These techniques, however, scarcely capture the shapes of the cells within a monolayer and the tissue morphology. Another popular modeling technique to simulate epithelial tissues is the vertex-based model, which addresses some of the drawbacks of the earlier kind of models [71, 73]. For instance, cell-cell interfaces are precisely defined and cell representation is more accurate. They do, however, not come without drawbacks. Careful consideration must be given to cell rearrangements and cell proliferation, as well as the explicit handling of changes in cell number of vertices and surrounding cells. The modeling capabilities of both approaches have recently been expanded by an intriguing center-based and vertex-based model combination [74, 76]. Recently, some writers have concentrated their efforts on creating systems for 3D deformable cells [77, 78]. Nevertheless, their application to biomechanical processes involving several cells is still exceedingly laborious and expensive in terms of computing. In contrast, even when simulating a large number of cells, Potts models are typically quite adaptable and effective [79, 80]. Although they are frequently viewed by many authors as being overly phenomenological, they have actually been effectively used to simulate the mechanical behavior of cells and tissues. The basis of collective movement in epithelial layers has also been discussed using sub-cellular and molecular-based models [87, 81, 82]. These models are particularly beneficial for simulating and researching extremely particular chemical mechanisms. They can only imitate a small number of cells and a limited number of concurrent biological activities. In contrast, several researchers take the other tack and use continuum models to replicate multicellular systems [83, 86]. The finite element method (FEM) can be used to handle the mechanical difficulty posed by the migration of epithelial tissue, for instance, by modeling it

as a continuum medium [84, 86]. Unfortunately, this kind of model does not take into account the shape and behavior of individual cells in the tissue, despite the fact that it scales quite well for vast cell layers. Additionally, this modeling approach struggles to incorporate several biophysical phenomena.

## 1.6 AIM OF THE STUDY

Cell motility plays a vital role in physiology. Therefore, it is essential to understand the molecular mechanism underlying cell motility, which is based on a tensegrity network of the contractile proteins (actin carrying tensile forces) in interaction with the load bearing proteins (basically tubulin under compression). The latter is also the universal mechanism observed in the processes such as cell locomotion, division, adhesion, and differentiation to different types of tissue. The basic protein for cell locomotion is the actin molecule that demonstrates an anisotropic distribution within the cell with asymmetric shapes, working together with filamentous intracellular structures (microtubules) that are responsible for establishing the cytoskeleton and various kinds of movements within the cell. A change in the intracellular distribution of actin often accompanies cell movement and/or deformation in the cell shape and is one of the key factors triggering cell division. The molecular mechanism/motor (principal actuator) is actin polymerization where the driving energy is generated through ATP-hydrolysis. Developing a mathematical model to understand cell motility in detail is the main subject of this study. To this end, we present two models for cell locomotion by using truss systems, which incorporates the microtubules and the elastic (contractile) actin molecules' interaction. In the first model we simulated three different mechanisms of movement through the cell model, namely the friction-induced cell motion in the preferred direction (Case 2, much entropic) and the cell motion triggered by actin polymerization (Case 3, more energetic). In the first case, however, we examined the stationary state of our truss model. In this study, three different cell motility mechanisms (entropic versus energetic and stationary) are handled and these cases examine the specific physics of cell movement. In the second model, which based on the facts that the cytoskeleton plays a primary role for cell motility and that the cytoplasm is viscoelastic. To this end, we present a viscoelas-

tic model for cell locomotion by using a hexagonal truss system, which incorporates the threshold element, the viscous elements and finally the elastic (contractile) actin molecules'. In our discussion we simulated three different mechanisms of movement through the cell model, namely the fully elastic model, friction-induced cell motion by using threshold and elastic actin elements and the third one is friction-induced cell motion by using threshold, viscous elements and elastic actin elements. In the second model of this study, first of all, we modeled our cell motility model as a hexagonal cell model differently from other cell models and we considered internal stimulus providing movement as a nature of cell as internal threshold which is applied to the element 1 as a displacement input. So that our cell could start its movement without an external force and we created a preferred direction by applying friction force to the amoebae's feet. In the next case, we used viscous elements in order to model the cytoplasm, which is the liquid between the cell membrane and the nucleus to express a more realistic and physiological amoeboid cell. In this work, we have presented a study of 2D truss and hexagonal models proposed to simulate cell motility. We have seen that using the friction force, we can move the cell until the effect of the force is over (a passive phenomenon), where the cell moved towards the side where the coefficient of friction is larger (decreasing the motility on that side). Thanks to the difference of kinetic friction coefficients (effected force), through which a "preferred direction" has been introduced to the cell. In 2D truss model in Case 2, we proved that the cell can gain a preferred direction through treadmilling mechanism, actin polymerization, which has been simulated by time-dependent mass varying functions at the two ends of the polymer realized actively (energetic dominant case).

## 1.7 2D CELL MOTILITY MODEL

This work deals with the modeling of cell locomotion and the truss system shown in Fig.1.10 is used to model the cell structure. This model is symmetric and geometrically nonlinear, whereas the material is linear in the Lagrangian setting. In Fig.1.10, there are three truss elements. While Elements 2 and 3 have the same moduli of elasticity, Element 1 is more compliant, in other words,  $E_2 = E_3 > E_1$ . In Fig.3,  $L_1$  symbolizes the actin filament length and  $L_2, L_3$  denote microtubulus lengths, further-

more,  $m_1$ ,  $m_2$  and  $m_3$  represent masses applied to Nodes 1,2, and 3, respectively and have a relation  $m_1 = m_2 < m_3$ .  $\mathbf{W}$  is the weight generated by  $m_3$  and it is equal to  $m_3\mathbf{g}$ , where  $\mathbf{g}$  stands for the gravitational acceleration.

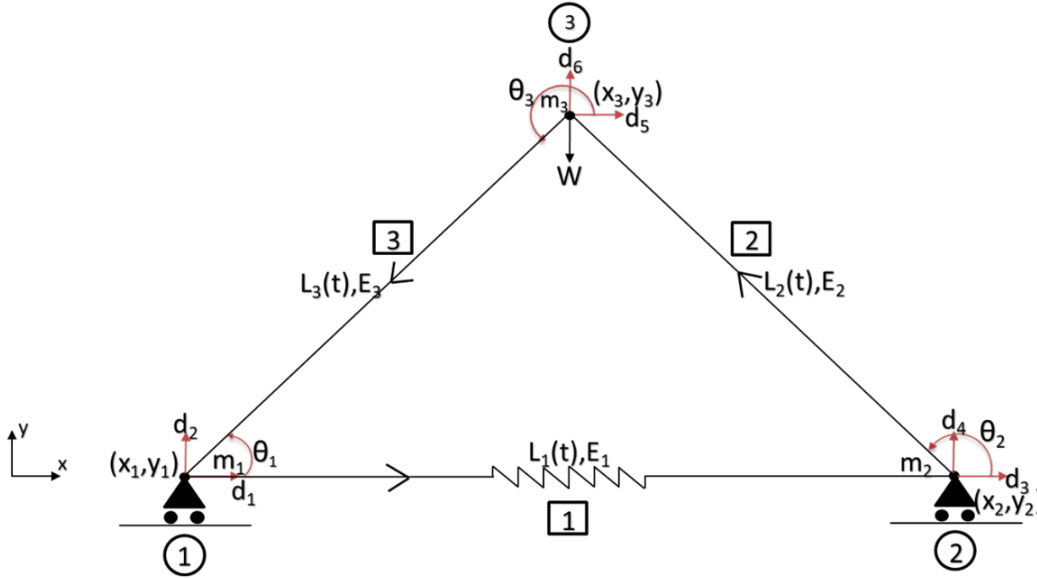


Figure 1.10: Cell motility model

The general system of equations used to describe nonlinear dynamic systems is given as follows:

$$\mathbf{M}\ddot{\mathbf{d}} + \mathbf{F}_{int}(\mathbf{d}) = \mathbf{F}_{ext} \quad (1.1)$$

The terms  $\mathbf{M}$ ,  $\ddot{\mathbf{d}}$ ,  $\mathbf{F}_{int}(\mathbf{d})$ ,  $\mathbf{F}_{ext}$  represent the global mass matrix, global acceleration vector, global internal force vector, and global external force vector, respectively. We discretize the Equation (1.1) in space by using the Finite Element Method, [92]. In this study, we have only one external force applied to Node 3 in -y direction, which is  $\mathbf{W}$ . Hence, the global external force vector and the global displacement vector take the form:

$$F_{ext} = \begin{bmatrix} 0 \\ 0 \\ 0 \\ 0 \\ 0 \\ -m_3g \end{bmatrix} \quad d = \begin{bmatrix} d_1 \\ d_2 \\ d_3 \\ d_4 \\ d_5 \\ d_6 \end{bmatrix}$$

and the lumped mass matrix is

$$M = \begin{bmatrix} m_1 & 0 & 0 & 0 & 0 & 0 \\ 0 & m_2 & 0 & 0 & 0 & 0 \\ 0 & 0 & m_3 & 0 & 0 & 0 \\ 0 & 0 & 0 & m_4 & 0 & 0 \\ 0 & 0 & 0 & 0 & m_5 & 0 \\ 0 & 0 & 0 & 0 & 0 & m_6 \end{bmatrix}$$

The system is discretized into  $n_{el}$  line elements. For the system at hand there are three elements which satisfy the following condition:

$$B = \bigcup_{e=1}^{n_{el}} B_e \quad (1.2)$$

In the following part, the derivations are provided to obtain the element stiffness matrix and element internal force vector in earnest.

In Fig.1.11,  $B_0$  represents the stress-free initial configuration,  $B$  the current configuration,  $N_0^e$  element normal force in the initial configuration and  $N^e$  element normal force in the current configuration. In this notation  $e$  represents the element index. The local coordinates in undeformed and deformed configurations are  $X_a^e, Y_a^e$  and  $x_a^e, y_a^e$  respectively. In this notation,  $a$  is the node number of each element,  $a=1,2$ . The element internal force vector is defined as follows:

$$\mathbf{F}_{int}^e(\mathbf{d}^e) = \frac{\partial U^e}{\partial \mathbf{d}^e} \quad (1.3)$$

where  $U^e$  is the element strain energy. The element stress for current configuration is

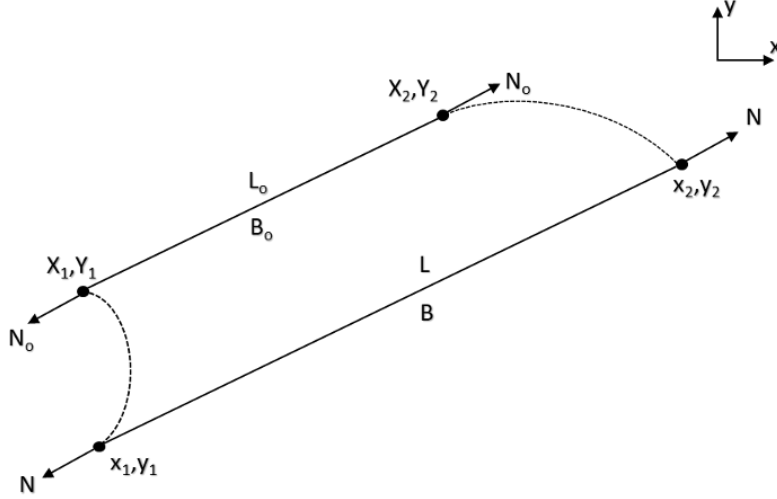


Figure 1.11: Initial and current body configurations

$$\sigma^e = E^e \varepsilon_{GL}^e \quad (1.4)$$

with  $\varepsilon_{GL}^e$  being the element Green-Lagrange strain measure which is equal to  $\varepsilon_{GL}^e = \frac{1}{2}((\lambda^e)^2 - 1)$ , where the element stretch is defined as  $\lambda^e = \frac{L^e}{L_0^e}$ . Element normal forces for initial and current bodies are as follows

$$\begin{aligned} N^e &= E^e \varepsilon_{GL}^e \lambda^e A^e \\ &= E^e A^e \frac{(L^e)^2 - (L_0^e)^2}{2(L_0^e)^2} \frac{L^e}{L_0^e} \\ &= E^e A^e \frac{(L^e)^3 - L^e (L_0^e)^2}{2(L_0^e)^3} \end{aligned} \quad (1.5)$$

After tedious simplifications the element internal energy term is derived as follows;

$$U^e = \frac{1}{2} E^e (\varepsilon_{GL}^e)^2 A_0^e L_0^e \quad (1.6)$$

Equation (1.3) is used to calculate the element internal force vector. Therefore, in order to solve this equation, chain rule is applied as follows:

$$\mathbf{F}_{int}^e(\mathbf{d}^e) = \frac{\partial U^e}{\partial \mathbf{d}^e} = \underbrace{\frac{\partial U^e}{\partial \varepsilon_{GL}^e}}_{1^{st} \text{ derivative}} \underbrace{\frac{\partial \varepsilon_{GL}^e}{\partial \mathbf{d}^e}}_{2^{nd} \text{ derivative}} \quad (1.7)$$



The 1<sup>st</sup> derivative is equal to

$$\frac{\partial U^e}{\partial \varepsilon_{GL}^e} = L_0^e N^e \quad (1.8)$$

and for the 2<sup>nd</sup> derivative another chain rule is applied

$$\frac{\partial \varepsilon_{GL}^e}{\partial \mathbf{d}^e} = \underbrace{\frac{\partial \varepsilon_{GL}^e}{\partial L^e}}_{3^{rd} \text{ derivative}} \underbrace{\frac{\partial L^e}{\partial \mathbf{d}^e}}_{4^{th} \text{ derivative}} \quad (1.9)$$

where

$$\frac{\partial \varepsilon_{GL}^e}{\partial L^e} = \frac{L^e}{(L_0^e)^2} \quad (1.10)$$

In order to calculate the 4<sup>th</sup> derivative, element length is needed

$$L^e = \sqrt{(L_x^e)^2 + (L_y^e)^2} \quad (1.11)$$

Here,  $L_x^e$  and  $L_y^e$  are the projected element lengths and these lengths are equal to

$$L_x^e = x_2^e - x_1^e = (X_2^e + u_2^e) - (X_1^e + u_1^e) \quad (1.12)$$

$$L_y^e = y_2^e - y_1^e = (Y_2^e + v_2^e) - (Y_1^e + v_1^e) \quad (1.13)$$

If Equation (1.12) and Equation (1.13) are substituted into Equation (1.11), one can find  $L$  and then, the 4<sup>th</sup> derivative takes the following form

$$\frac{\partial L^e}{\partial \mathbf{d}^e} = \begin{bmatrix} \partial L^e / \partial u_1^e \\ \partial L^e / \partial v_1^e \\ \partial L^e / \partial u_2^e \\ \partial L^e / \partial v_2^e \end{bmatrix} = \frac{1}{L^e} \begin{bmatrix} -L_x^e \\ -L_y^e \\ L_x^e \\ L_y^e \end{bmatrix} = \widehat{\mathbf{L}}^e \quad (1.14)$$

After finding all the derivatives, the element internal force vector can be written in the following compact form

$$\mathbf{F}_{int}^e(\mathbf{d}^e) = L_0^e N^e \frac{\partial \varepsilon_{GL}^e}{\partial L^e} \frac{\partial L^e}{\partial \mathbf{d}^e} = N^e \frac{L^e}{L_0^e} \widehat{\mathbf{L}}^e \quad (1.15)$$

The element stiffness matrix is given as

$$\mathbf{K}^e(\mathbf{d}^e) = \frac{\partial \mathbf{F}_{int}^e(\mathbf{d}^e)}{\partial \mathbf{d}^e} = \frac{\partial}{\partial \mathbf{d}^e} \left( L_0^e N^e \frac{\partial \varepsilon_{GL}^e}{\partial L^e} \frac{\partial L^e}{\partial \mathbf{d}^e} \right) \quad (1.16)$$

$$\begin{aligned} \mathbf{K}^e(\mathbf{d}^e) = L_0^e \left( \underbrace{\frac{\partial N^e}{\partial \mathbf{d}^e}}_{5^{th} \text{ derivative}} \quad \frac{\partial \varepsilon_{GL}^e}{\partial L^e} \left( \frac{\partial L^e}{\partial \mathbf{d}^e} \right)^T + N^e \underbrace{\frac{\partial^2 \varepsilon_{GL}^e}{\partial L^e \partial \mathbf{d}^e}}_{6^{th} \text{ derivative}} \left( \frac{\partial L^e}{\partial \mathbf{d}^e} \right) \right. \\ \left. + N^e \frac{\partial \varepsilon_{GL}^e}{\partial L^e} \underbrace{\frac{\partial^2 L^e}{\partial (\mathbf{d}^e)^2}}_{7^{th} \text{ derivative}} \right) \end{aligned} \quad (1.17)$$

The 5<sup>th</sup>, 6<sup>th</sup> and 7<sup>th</sup> derivatives are determined by the use of chain rule again

$$\begin{aligned} \frac{\partial N^e}{\partial \mathbf{d}^e} &= \frac{\partial N^e}{\partial L^e} \frac{\partial L^e}{\partial \mathbf{d}^e} \\ \frac{\partial N^e}{\partial \mathbf{d}^e} &= E^e A^e \frac{3(L^e)^2 - (L_0^e)^2}{2(L_0^e)^3} \widehat{\mathbf{L}}^e \end{aligned} \quad (1.18)$$

$$\begin{aligned} \frac{\partial^2 \varepsilon_{GL}^e}{\partial L^e \partial \mathbf{d}^e} &= \frac{\partial}{\partial L^e} \left( \frac{\partial \varepsilon_{GL}^e}{\partial \mathbf{d}^e} \right) \\ &= \frac{\partial^2 \varepsilon_{GL}^e}{\partial (L^e)^2} \frac{\partial L^e}{\partial \mathbf{d}^e} + \frac{\partial \varepsilon_{GL}^e}{\partial L^e} \frac{\partial^2 L^e}{\partial \mathbf{d}^e \partial L^e} \\ &= \frac{1}{(L_0^e)^2} \widehat{\mathbf{L}}^e \end{aligned} \quad (1.19)$$

$$\begin{aligned}
\frac{\partial^2 L^e}{\partial(\mathbf{d}^e)^2} &= \frac{1}{L^e} \left( \underbrace{\begin{bmatrix} 1 & 0 & 1 & 0 \\ 0 & 1 & 0 & 1 \\ 1 & 0 & 1 & 0 \\ 0 & 1 & 0 & 1 \end{bmatrix}}_{\widehat{\mathbf{I}}^e} - \underbrace{\frac{\partial L^e}{\partial \mathbf{d}^e}}_{\widehat{\mathbf{L}}^e} \underbrace{\left( \frac{\partial L^e}{\partial \mathbf{d}^e} \right)^T}_{\widehat{\mathbf{L}}^{eT}} \right) \\
&= \frac{1}{L^e} \left( \widehat{\mathbf{I}}^e - \widehat{\mathbf{L}}^e \widehat{\mathbf{L}}^{eT} \right)
\end{aligned} \tag{1.20}$$

After simplifications the result is obtained as ;

$$\mathbf{K}^e(\mathbf{d}^e) = \underbrace{E^e A^e \frac{3(L^e)^3 - L^e (L_0^e)^2}{2(L_0^e)^4} \widehat{\mathbf{L}}^e \widehat{\mathbf{L}}^{eT}}_{\mathbf{K}_m^e(\mathbf{d}^e)} + \underbrace{\frac{N^e}{L_0^e} \widehat{\mathbf{I}}^e}_{\mathbf{K}_g^e(\mathbf{d}^e)} \tag{1.21}$$

where  $\mathbf{K}_m^e$  and  $\mathbf{K}_g^e$  are element material and element geometric stiffness matrices respectively.

In order to obtain the global stiffness matrix, global internal force vector and displacement vector, the element stiffness matrices, element internal force vectors and element displacement vectors should be assembled as follows:

$$\mathbf{K}_{IJ} = \mathbb{A}_{e=1}^{n_{el}} \mathbf{K}_{ij}^e \tag{1.22}$$

$$\mathbf{F}_{int_I} = \mathbb{A}_{e=1}^{n_{el}} \mathbf{F}_{int_i}^e \tag{1.23}$$

$$\mathbf{d}_I = \mathbb{A}_{e=1}^{n_{el}} \mathbf{d}_i^e \tag{1.24}$$

where the operator  $\mathbb{A}$  symbolizes the assembly of all element contributions of the degrees of freedom  $i, j = 1, \dots, edof$  to the global degrees of freedom  $I, J = 1, \dots, gdof$ . For our system, there are 6 global degrees of freedom and 4 degrees of freedom per each element.

In order to solve the non-linear problem [93] by using the Newton's method, we first need to specify the residual which is:

$$\mathbf{R}(\mathbf{d}) = M\ddot{\mathbf{d}} + \mathbf{F}_{int}(\mathbf{d}) - \mathbf{F}_{ext} \quad (1.25)$$

For the time discretization of the second order differential equation the Newmark- $\beta$  method is used [94]. According to this method, the displacements can be updated as follows:

$$\mathbf{d} = \mathbf{d}_n + \Delta t \dot{\mathbf{d}}_n + (\Delta t)^2 \left( \frac{1}{2} - \beta \right) \ddot{\mathbf{d}}_n + (\Delta t)^2 \beta \ddot{\mathbf{d}} \quad (1.26)$$

Here,  $\beta$  is a constant parameter of the Newmark- $\beta$  method. Furthermore,  $\Delta t$  represents the selected time step and subscript  $n$  represents the known quantities from the preceding time step  $t_n$ . If we rearrange Equation (1.26) to get a predictor and corrector scheme, following equations are obtained:

$$\tilde{\mathbf{d}} = \mathbf{d}_n + \Delta t \dot{\mathbf{d}}_n + (\Delta t)^2 \left( \frac{1}{2} - \beta \right) \ddot{\mathbf{d}}_n \quad (1.27)$$

$$\mathbf{d} = \tilde{\mathbf{d}} + (\Delta t)^2 \beta \ddot{\mathbf{d}}_n \quad (1.28)$$

We can rewrite Equation (1.28) to obtain the updated acceleration term:

$$\ddot{\mathbf{d}} = \frac{\mathbf{d} - \tilde{\mathbf{d}}}{(\Delta t)^2 \beta} \quad (1.29)$$

Then, Equation (1.29) is implemented into Equation (1.25), and we can represent the residual term only as a function of the global displacement vector, which is given as:

$$\mathbf{R}(\mathbf{d}) = \frac{1}{(\Delta t)^2 \beta} \mathbf{M} - (\mathbf{d} - \tilde{\mathbf{d}}) + \mathbf{F}_{int}(\mathbf{d}) - \mathbf{F}_{ext} \quad (1.30)$$

In order to obtain the consistent tangent matrix  $\mathbf{A}$ , the residual vector is differentiated with respect to the displacement vector:

$$\frac{\partial \mathbf{R}(\mathbf{d})}{\partial \mathbf{d}} = \frac{1}{(\Delta t)^2 \beta} \mathbf{M}(\mathbf{d} - \tilde{\mathbf{d}}) + \mathbf{F}_{int}(\mathbf{d}) - \mathbf{F}_{ext} \quad (1.31)$$

Finally, the following update equation of the Newton's method is used until a certain convergence criterion is satisfied:

$$\mathbf{d} \leftarrow \mathbf{d}_k - \mathbf{A}_k^{-1} \mathbf{R}_k \quad (1.32)$$

In this notation, subscript  $k$  represents the iteration number of the Newton loop at each time step. In Fig.1.12, the algorithmic framework of the numerical formulation is shown in detail.

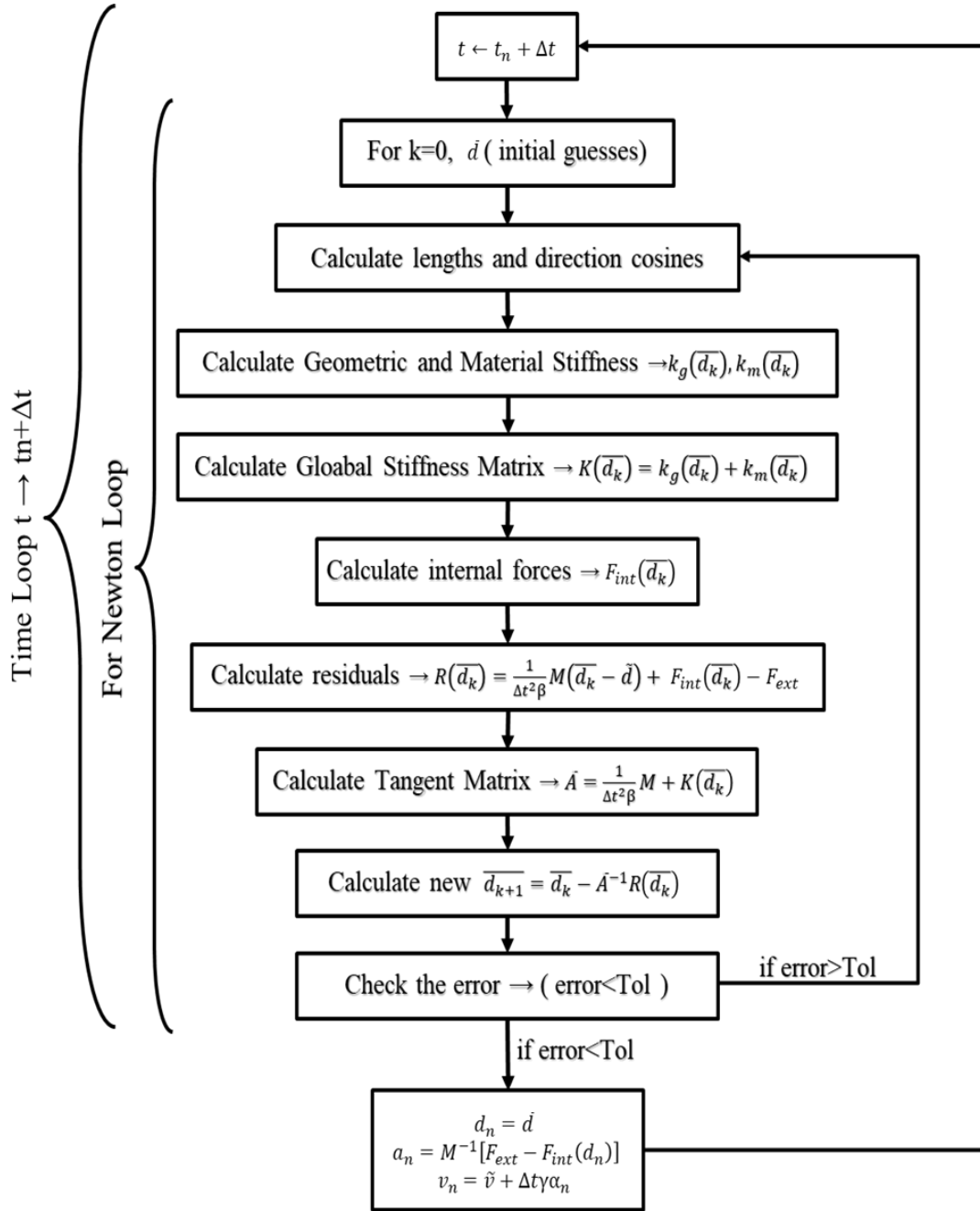


Figure 1.12: Algorithmic Flow Chart

## 1.8 ANALYSIS

In this study, three different cases have been examined. In all the cases  $E_2 = E_3 = 10000 \text{ N/m}^2$  and  $E_1 = 2000 \text{ N/m}^2$ ,  $L_2 = L_3 = 2\sqrt{2} \text{ m}$  and  $L_1 = 1 \text{ m}$ . In case 1 and case 2,  $m_1 = m_2 = 4 \text{ kg}$  and  $m_3 = 12 \text{ kg}$ . In case 3, while  $m_1$  and  $m_2$  are denoted as time-dependent functions,  $m_3 = 12 \text{ kg}$ .

### 1.8.1 Case 1

In the first case, the system is considered symmetric as it can be shown in Fig.6. Roller supports are assigned joints on both ends of the system thus the system is free to translate along the horizontal surface.

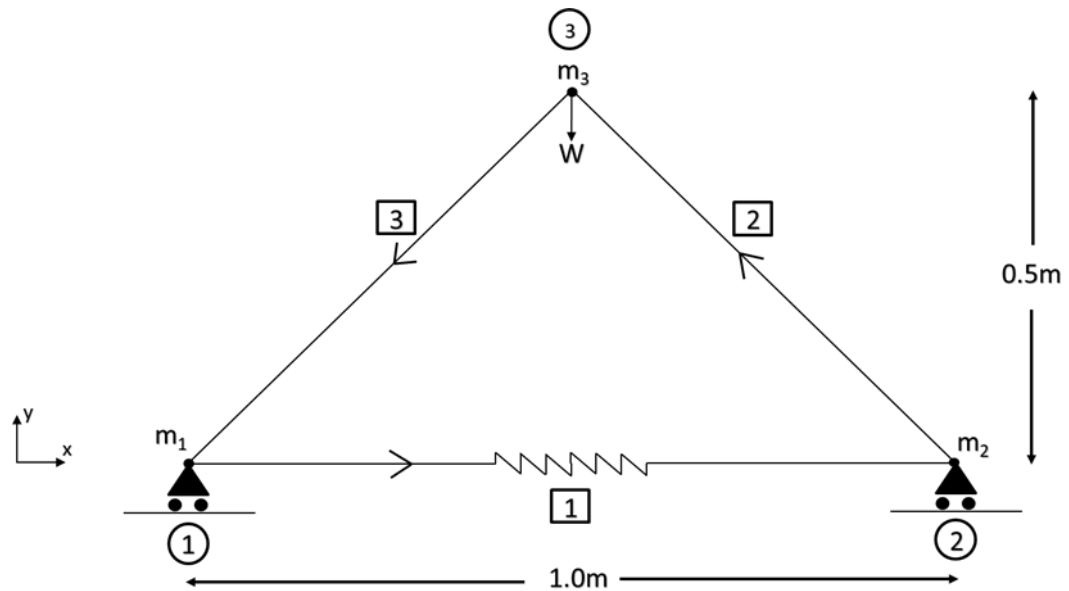


Figure 1.13: Symmetric model for case 1

This symmetric system, however, can not be expected to move only with the mass  $m_3$  as it is seen in Fig.1.13. As it is illustrated in Fig.1.16,  $x$  and  $y$  coordinates of the centre of mass of the truss system move only in  $y$ -axis but a movement in the  $x$ -direction is not observed and the changes of  $x$  and  $y$  coordinates of the centre of mass with respect to time are shown in Fig.1.14 and Fig.1.15

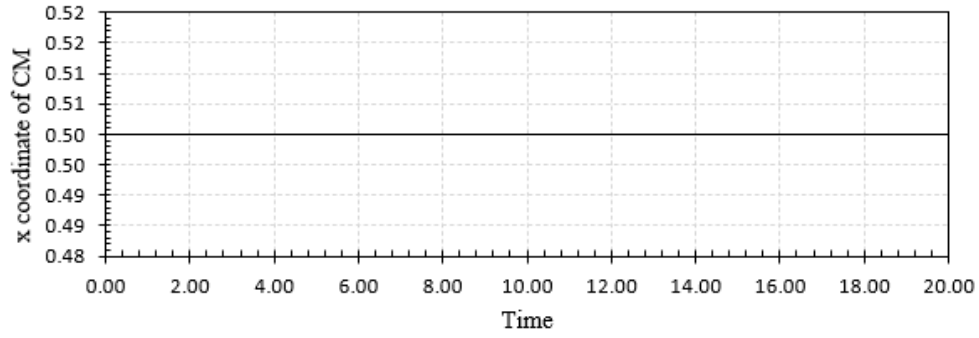


Figure 1.14: The change in x coordinate of the centre of mass of the symmetric truss model with respect to time for case 1

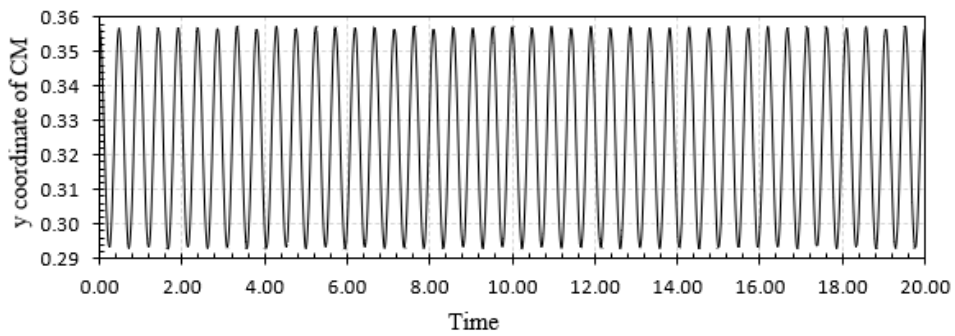


Figure 1.15: The change in y coordinate of the centre of mass of the symmetric truss model with respect to time for case 1

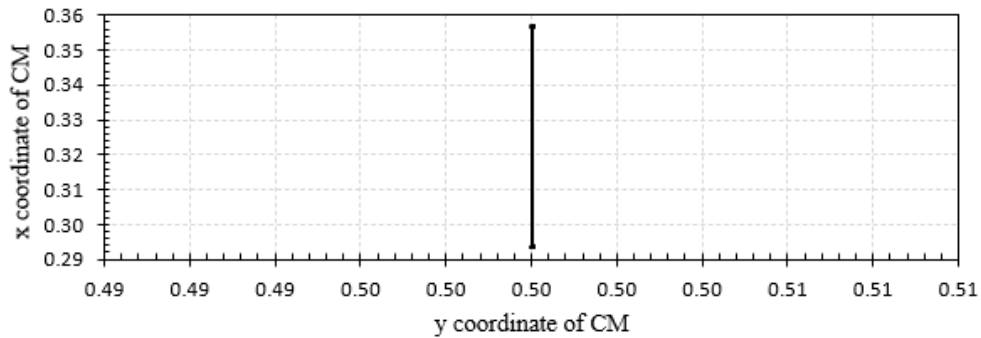


Figure 1.16: The change in x and y coordinates of the center of mass of the symmetric truss model for case 1



### 1.8.2 Case 2

As it is mentioned in the first case, the symmetry of the truss system has to be eliminated in order to gain a locomotion to cell model. In the second case, symmetry is removed by using friction force. Friction acts in a direction opposite to the direction of motion. That's why, to move the cell model in  $+x$  direction, the value of the reaction force of Node 2 which is denoted by  $R_4$  should be multiplied by the kinetic friction constant where  $\mu=0.4$ . This friction force is applied in  $-x$  direction as it is shown in Fig.1.17

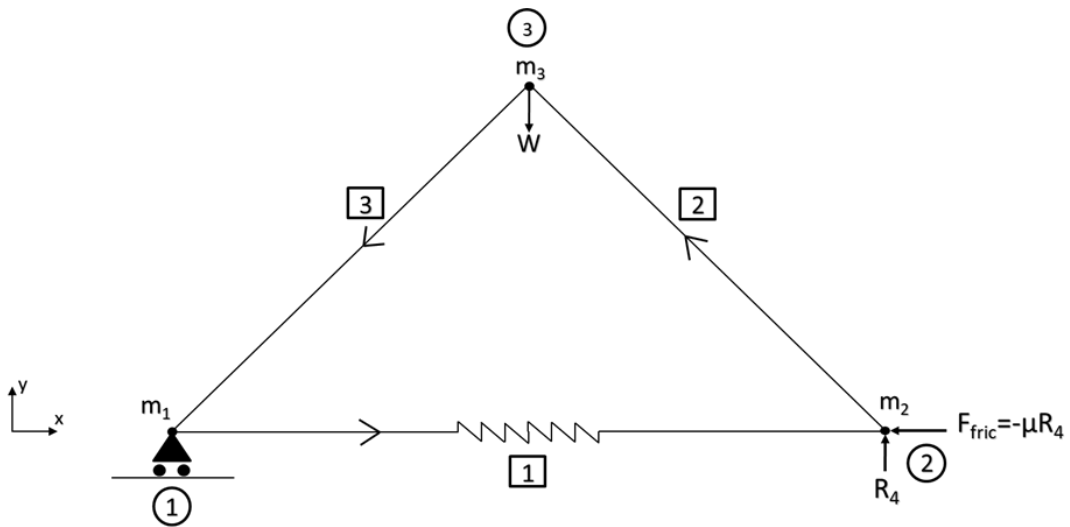


Figure 1.17: Non-symmetrical model for case 2 (Symmetry is removed by using friction force)

Therefore, while our cell is moving  $+x$  direction, its movement in  $-x$  direction becomes minimum. As can be understood from Fig.1.20, the centre of mass of the truss system has started to move both in  $+x$  and  $y$  directions. In Fig.1.18 and Fig.1.19, the change in  $x$  and  $y$  coordinates of the centre of mass with respect to time are represented respectively. These graphs prove that the cell has started its movement.

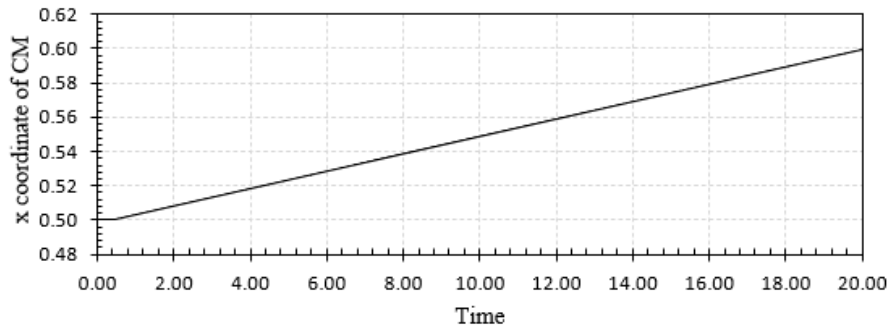


Figure 1.18: The change in x coordinate of the centre of mass of the non-symmetric truss model with respect to time for case 2

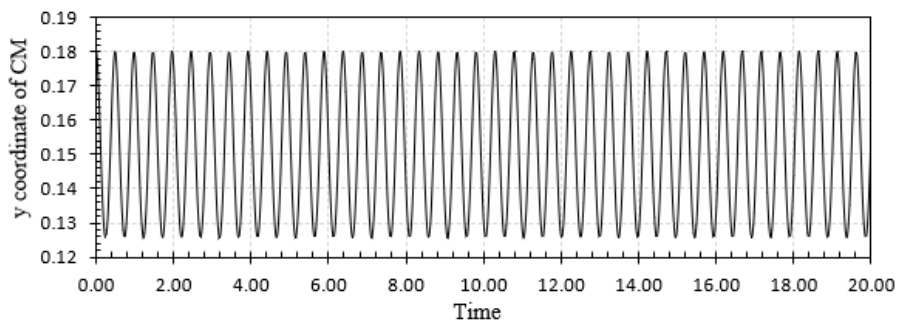


Figure 1.19: The change in y coordinate of the centre of mass of the non-symmetric truss model with respect to time for case 2

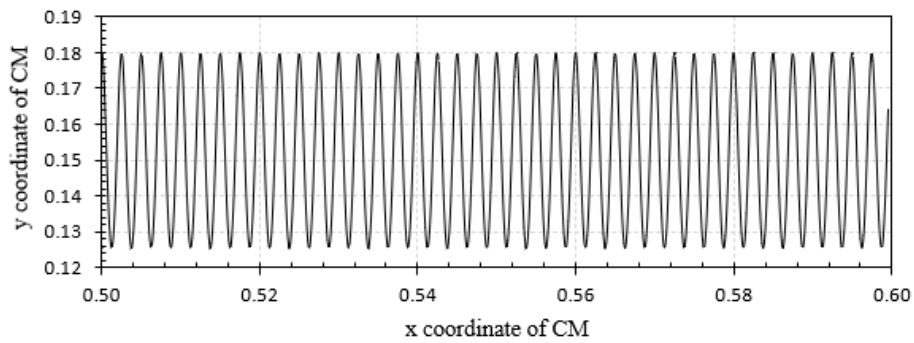


Figure 1.20: The change in x and y coordinates of the center of mass of the non-symmetric truss model for case )

### 1.8.3 Case 3

In the last case,  $m_1$  and  $m_2$  are formulated as time-dependent functions, which is shown in Fig.1.21.

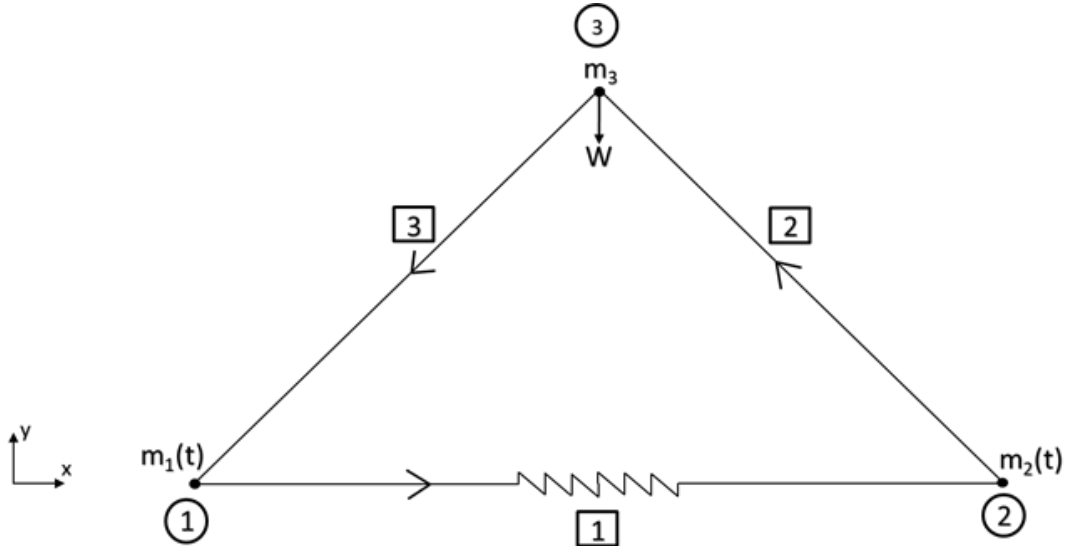


Figure 1.21: Non-symmetrical model for case 3 (Symmetry is removed by polymerizing actin)

When we change the masses depending on the time, Element 1, which is actin, is polarized. As David Boal mentioned in Chapter 11 [15], monomers can be captured and released by actin filaments and they are represented as capture (which has + sign) or barbed end and release (which has - sign) or pointed end as it is shown in Fig.1.22 [15].

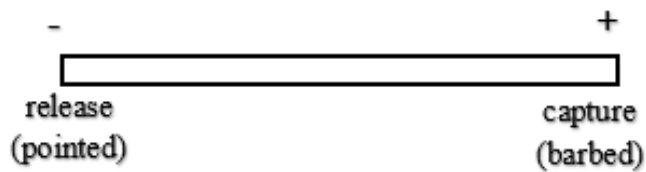


Figure 1.22: Monomer capturing and releasing

In Fig.1.22,  $m_1$  and  $m_2$  are expressed as time-dependent sinusoidal functions which are  $8 - 4 * \sin(2000 * t / \pi)$  and  $8 + 4 * \sin(2000 * t / \pi)$  respectively. As mass function applied to the first node decreases in time, mass function applied to the second node increases thereby, the symmetry is removed and the cell starts to move in the  $+x$

direction. In physiology it is called the treadmilling, in which when the concentration of free actin monomers falls below a certain level, the barbed end will continue to increase in length but the pointed end will decrease in length. The Movement in actin filament is restricted by giving mass decreasing in time which is  $m_1$  and it denotes the pointed end, whereas actin element gains the ability to by giving mass increasing in time which is  $m_2$  and it represents the barbed end. In Fig.1.23 and Fig.1.24, the changes of  $x$  and  $y$  coordinates of the centre mass of the cell body with respect to time and in the Fig.1.25 the change in  $x$  and  $y$  coordinates of the centre of mass are presented.

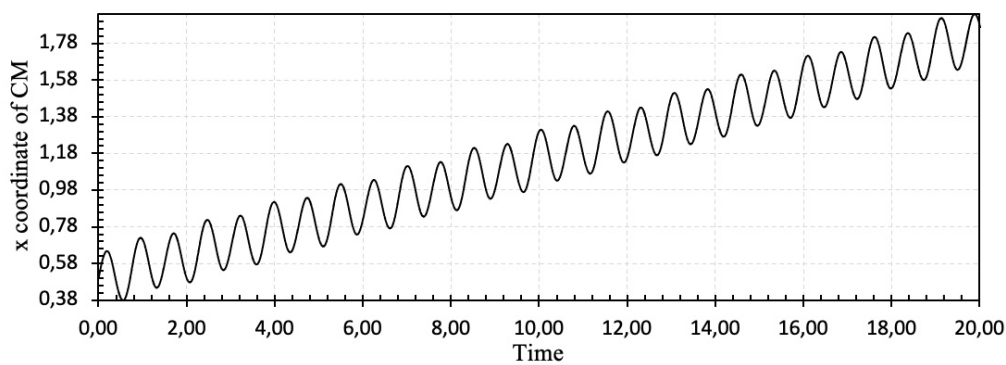


Figure 1.23: The change in  $x$  coordinate of the center of mass of the non-symmetric truss model with respect to time for case 3

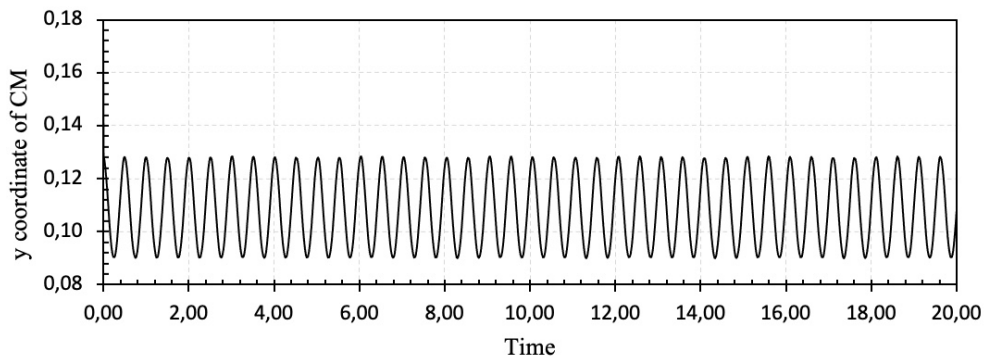


Figure 1.24: The change in  $y$  coordinate of the center of mass of the non-symmetric truss model with respect to time for case 3

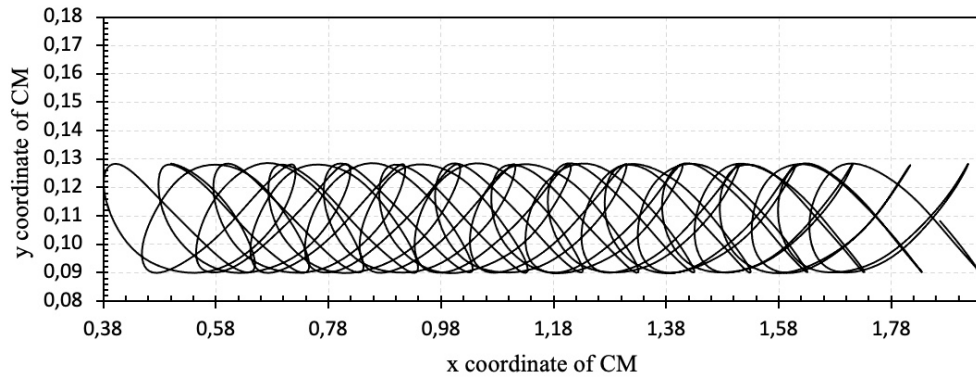


Figure 1.25: The change in x and y coordinates of the center of mass of the non-symmetric truss model for case 2

## 1.9 HEXAGONAL CELL MOTILITY MODEL

This work deals with the modeling of cell locomotion and the hexagonal truss system shown in Fig.1.26 is used to model the cell structure. This model is symmetric and geometrically nonlinear, whereas the material is linear in the Lagrangian setting. In Fig.1.26, there are 36 truss elements and all Elements have the same moduli of elasticity.  $m$  represent the mass and masses applied to all 16 nodes are equal. In our model Element 1 represent the threshold which is denoted as red line in Fig.1.26 and Element 6, Element 11, Element 16, Element 21 and Element 26 are the viscous elements and they are symbolized as blue lines and all the remaining black elements are the elastic elements.

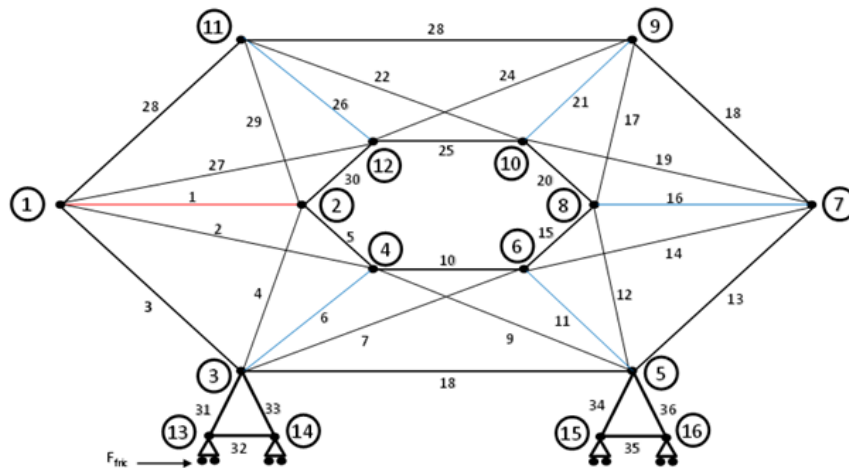


Figure 1.26: Hexagonal Cell motility model

The general system of equations used to describe nonlinear dynamic systems is given

as follows:

$$M\ddot{\mathbf{d}} + \mu\dot{\mathbf{d}} + \mathbf{F}_{int}(\mathbf{d}) = \mathbf{F}_{ext} \quad (1.33)$$

The terms  $M, \dot{\mathbf{d}}, \mu, \mathbf{d}, \mathbf{F}_{int}(\mathbf{d}), \mathbf{F}_{ext}$  represent the global mass matrix, global acceleration vector, viscosity constant, global velocity vector, global internal force vector, and global external force vector, respectively. We discretize the Equation 1.33 in space by using the Finite Element Method, [32]. In this study, we do not have any external force vector so the Equation 1.33 takes the form like this,

$$M\ddot{\mathbf{d}} + \mu\dot{\mathbf{d}} + \mathbf{F}_{int}(\mathbf{d}) = \mathbf{0} \quad (1.34)$$

The element internal force vector is defined as follows:

$$\mathbf{F}_{int}^e(\mathbf{d}^e) = \frac{\partial U^e}{\partial \mathbf{d}^e} \quad (1.35)$$

where  $U^e$  is the element elastic energy and has the following Neo-Hookean form;

$$U^e = \frac{E}{2} \left( (\lambda^e)^2 + 2\frac{1}{\lambda^e} - 3 \right) \quad (1.36)$$

where the element stretch is equal to  $\lambda^e = \frac{L^e}{L_0^e}$  where  $L_0^e$  represents the initial length and for viscous materials  $\lambda^e$  can be described also in this form

$$\lambda^e = \lambda_v^e \lambda_e^e \quad (1.37)$$

Where  $\lambda_v^e$  and  $\lambda_e^e$  denote the viscous and elastic parts of the stretch respectively. If we substitute the Equation 1.37 into the Equation 1.36 we can obtain the elastic free energy function as follow;

$$U^e = \frac{E}{2} \left[ (\lambda^e \lambda_v^{e-1})^2 + 2(\lambda^e \lambda_v^{e-1})^{-1} - 3 \right] \quad (1.38)$$

Equation 1.35 is used to calculate the element internal force vector. Therefore, in order to solve this equation, chain rule is applied as follows:

$$\mathbf{F}_{int}^e(\mathbf{d}^e) = \frac{\partial U^e}{\partial \mathbf{d}^e} \underbrace{\frac{\partial U^e}{\partial \lambda^e}}_{1^{st} \text{ derivative}} \underbrace{\frac{\partial \lambda^e}{\partial L^e}}_{2^{nd} \text{ derivative}} \underbrace{\frac{\partial L^e}{\partial \mathbf{d}^e}}_{3^{rd} \text{ derivative}} \quad (1.39)$$

The 1<sup>st</sup> derivative is equal to First Piola-Kirchoff stress which is symbolized as  $\mathbf{P}^e$

$$\mathbf{P}^e = \frac{\partial U^e}{\partial \lambda^e} = \frac{E}{2} \left[ \lambda^e \lambda_v^{e-1} \cdot \lambda_v^{e-1} - 2 (\lambda^e \lambda_v^{e-1})^{-2} \lambda_v^{e-1} \right] \quad (1.40)$$

and for the 2<sup>nd</sup> derivative another chain rule is applied

$$\frac{\partial \lambda^e}{\partial L^e} = \frac{1}{L_0^e} \quad (1.41)$$

In order to calculate the 3<sup>rd</sup> derivative, element length is needed

$$L^e = \sqrt{(L_x^e)^2 + (L_y^e)^2} \quad (1.42)$$

Here,  $L_x^e$  and  $L_y^e$  are the projected element lengths and these lengths are equal to

$$L_x^e = x_2^e - x_1^e = (X_2^e + u_2^e) - (X_1^e + u_1^e) \quad (1.43)$$

$$L_y^e = y_2^e - y_1^e = (Y_2^e + v_2^e) - (Y_1^e + v_1^e) \quad (1.44)$$

If Equation 1.43 and Equation 1.44 are substituted into Equation 1.42, one can find  $L$  and then, the derivative of  $L^e$  with respect to  $\mathbf{d}^e$  takes the following form

$$\frac{\partial L^e}{\partial \mathbf{d}^e} = \begin{bmatrix} \partial L^e / \partial u_1^e \\ \partial L^e / \partial v_1^e \\ \partial L^e / \partial u_2^e \\ \partial L^e / \partial v_2^e \end{bmatrix} = \frac{1}{L^e} \begin{bmatrix} -L_x^e \\ -L_y^e \\ L_x^e \\ L_y^e \end{bmatrix} = \widehat{\mathbf{L}}^e \quad (1.45)$$

After finding all the derivatives, the element internal force vector can be written in the following compact form

$$\mathbf{F}_{int}^e(\mathbf{d}^e) = E^e \left( \frac{\lambda^e}{\lambda_v^e{}^2} - \frac{\lambda_v^e}{\lambda^{e2}} \right) \frac{1}{L_0^e} \widehat{\mathbf{L}}^e \quad (1.46)$$

The element stiffness matrix is given as

$$\mathbf{K}^e(\mathbf{d}^e) = \frac{\partial \mathbf{F}_{int}^e(\mathbf{d}^e)}{\partial \mathbf{d}^e} = \frac{\partial}{\partial \mathbf{d}^e} \left( P^e \frac{1}{L_0^e} \widehat{\mathbf{L}}^e \right) \quad (1.47)$$

And after tedious simplifications the element stiffness matrix is determined as;

$$\begin{aligned} \mathbf{K}^e(\mathbf{d}^e) = & \underbrace{\frac{E^e}{L_0^{e2}} \left( \frac{\lambda^e}{\lambda_v^e{}^2} - \frac{\lambda_v^e}{\lambda^{e2}} \right) \widehat{\mathbf{L}}^e \widehat{\mathbf{L}}^{eT}}_{\mathbf{K}_m^e(\mathbf{d}^e)} + \frac{E^e}{L_0^{e2}} \left( \frac{1}{\lambda^e} \right) \left( \frac{1}{\lambda_v^e{}^2} - 2 \frac{\lambda_v^e}{\lambda^{e3}} \right) \widehat{\mathbf{L}}^e \widehat{\mathbf{L}}^{eT} \\ & + \underbrace{\frac{E}{L_0 L} \left( \frac{1}{\lambda^e} \right) \left( \frac{\lambda^e}{\lambda_v^e{}^2} - \frac{\lambda_v^e}{\lambda^{e2}} \right) (\widehat{\mathbf{I}}^e - \widehat{\mathbf{L}}^e \widehat{\mathbf{L}}^{eT})}_{\mathbf{K}_g^e(\mathbf{d}^e)} \end{aligned} \quad (1.48)$$

where  $\mathbf{K}_m^e$  and  $\mathbf{K}_g^e$  are element material and element geometric stiffness matrices respectively.

In order to obtain the global stiffness matrix, global internal force vector and displacement vector, the element stiffness matrices, element internal force vectors and element displacement vectors should be assembled as follows:

$$K_{IJ} = \mathbb{A}_{e=1}^{nel} K_{ij}^e \quad (1.49)$$

$$F_{int_I} = \mathbb{A}_{e=1}^{nel} F_{int_i}^e \quad (1.50)$$

$$d_I = \mathbb{A}_{e=1}^{nel} d_i^e \quad (1.51)$$



where the operator  $\mathbb{A}$  symbolizes the assembly of all element contributions of the degrees of freedom  $i, j = 1, \dots, edof$  to the global degrees of freedom  $I, J = 1, \dots, gdoof$ . For our system, there are 24 global degrees of freedom and 4 degrees of freedom per each element.

In order to solve the non-linear problem [95] by using the Newton's method, we first need to specify the residual which is:

$$\mathbf{R}(\mathbf{d}) = \mathbf{M}\ddot{\mathbf{d}} + \mathbf{F}_{int}(\mathbf{d}) + \boldsymbol{\mu}\dot{\mathbf{d}} - \mathbf{F}_{ext} \quad (1.52)$$

For the time discretization of the second order differential equation the Newmark- $\beta$  method is used [96]. According to this method, the displacements can be updated as follows:

$$\mathbf{d} = \mathbf{d}_n + \Delta t \dot{\mathbf{d}}_n + (\Delta t)^2 \left( \frac{1}{2} - \beta \right) \ddot{\mathbf{d}}_n + (\Delta t)^2 \beta \ddot{\mathbf{d}} \quad (1.53)$$

Here,  $\beta$  is a constant parameter of the Newmark- $\beta$  method. Furthermore,  $\delta t$  represents the selected time step and subscript  $n$  represents the known quantities from the preceding time step  $t_n$ . If we rearrange Equation 1.53 to get a predictor and corrector scheme, following equations are obtained:

$$\tilde{\mathbf{d}} = \mathbf{d}_n + \Delta t \dot{\mathbf{d}}_n + (\Delta t)^2 \left( \frac{1}{2} - \beta \right) \ddot{\mathbf{d}}_n \quad (1.54)$$

$$\mathbf{d} = \tilde{\mathbf{d}} + (\Delta t)^2 \beta \ddot{\mathbf{d}}_n \quad (1.55)$$

We can rewrite Equation 1.55 to obtain the updated acceleration term:

$$\ddot{\mathbf{d}} = \frac{\mathbf{d} - \tilde{\mathbf{d}}}{(\Delta t)^2 \beta} \quad (1.56)$$

Then, Equation 1.56 is implemented into Equation 1.52, and we can represent the residual term only as a function of the global displacement vector, which is given as:

$$\mathbf{R}(\mathbf{d}) = \frac{1}{(\Delta t)^2 \beta} \mathbf{M} - (\mathbf{d} - \tilde{\mathbf{d}}) + \mathbf{F}_{int}(\mathbf{d}) - \mathbf{F}_{ext} \quad (1.57)$$

In order to obtain the consistent tangent matrix  $\mathbf{A}$ , the residual vector is differentiated with respect to the displacement vector:

$$\frac{\partial \mathbf{R}(\mathbf{d})}{\partial \mathbf{d}} = \frac{1}{(\Delta t)^2 \beta} \mathbf{M}(\mathbf{d} - \tilde{\mathbf{d}}) + \mathbf{F}_{int}(\mathbf{d}) - \mathbf{F}_{ext} \quad (1.58)$$

Finally, the following update equation of the Newton's method is used until a certain convergence criterion is satisfied:

$$\mathbf{d} \leftarrow \mathbf{d}_k - \mathbf{A}_k^{-1} \mathbf{R}_k \quad (1.59)$$

In this notation, subscript  $k$  represents the iteration number of the Newton loop at each time step. In Fig.1.12, the algorithmic framework of the numerical formulation is shown in detail.

## 1.10 ANALYSIS

In this study, three different cases have been examined. In all the cases  $E=100000 \text{ N/m}^2$  and mass ( $m$ ) which is applied all the nodes is 1 kg.

### 1.10.1 Case 1

In the first case, the system is considered fully elastic and symmetric as it can be shown in Fig.1.27. Roller supports are assigned joints on both ends of the system thus the system is free to translate along the horizontal surface.

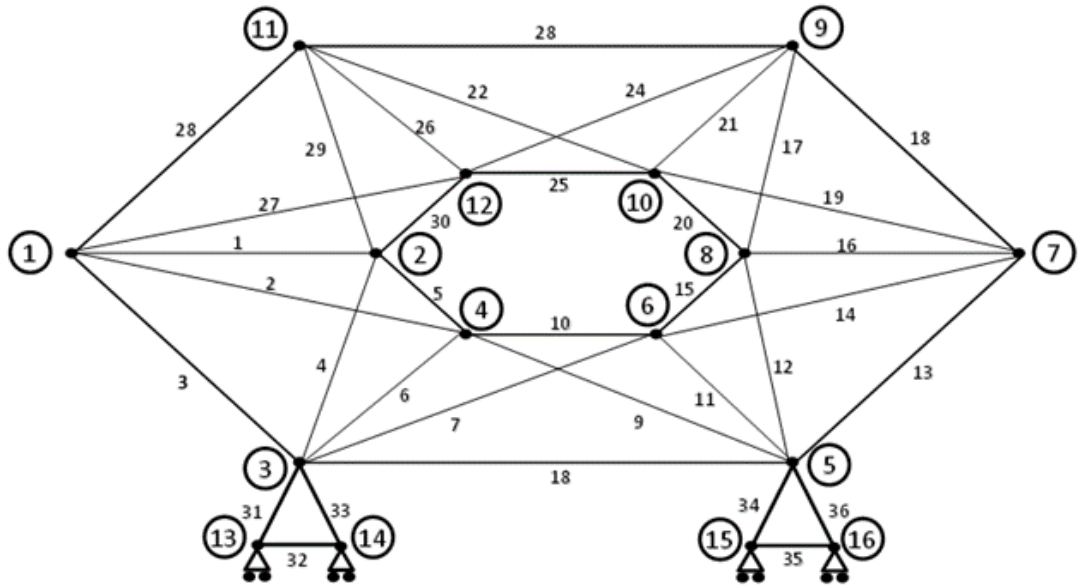


Figure 1.27: Fully elastic model for case 1

In this case we do not apply any internal force to this fully elastic system so we cannot observe any movement. As it is illustrated in Fig.1.28 and Fig. 1.29,  $x$  and  $y$  coordinates of the centre of mass with respect to time of the hexagonal truss system do not move in both directions.

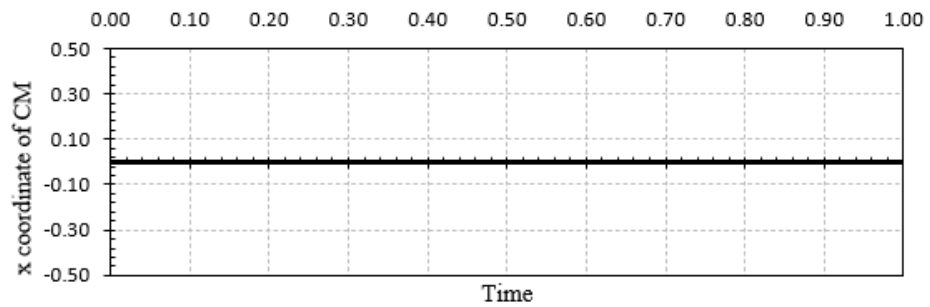


Figure 1.28: The change in  $x$  coordinate of the centre of mass of the fully elastic hexagonal truss model with respect to time for case 1

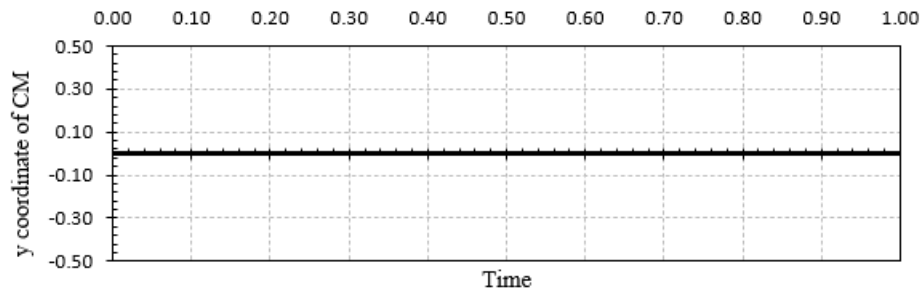


Figure 1.29: The change in  $y$  coordinate of the centre of mass of the fully elastic hexagonal truss model with respect to time for case 1

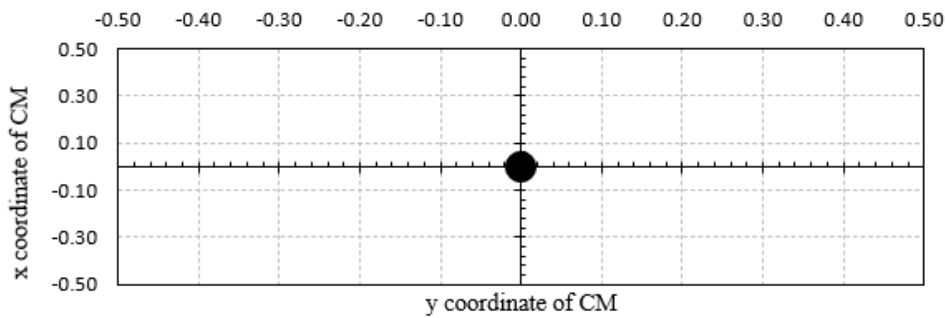


Figure 1.30: The change in  $x$  and  $y$  coordinates of the center of mass of the fully elastic hexagonal truss model for case 1

### 1.10.2 Case 2

In the second case, internal force which is also called threshold is applied to the first element. Threshold is denoted as red line as it is seen in Fig. 1.31. As mentioned in the first case our symmetry condition is removed by using friction force. Friction acts in a direction opposite to the direction of motion. That's why, to move the cell model in  $-x$  direction, the value of the reaction force of Node 13 should be multiplied by the kinetic friction constant where  $\mu=0.02$ . This friction force is applied in  $+x$  direction as it is shown in Fig.1.31.

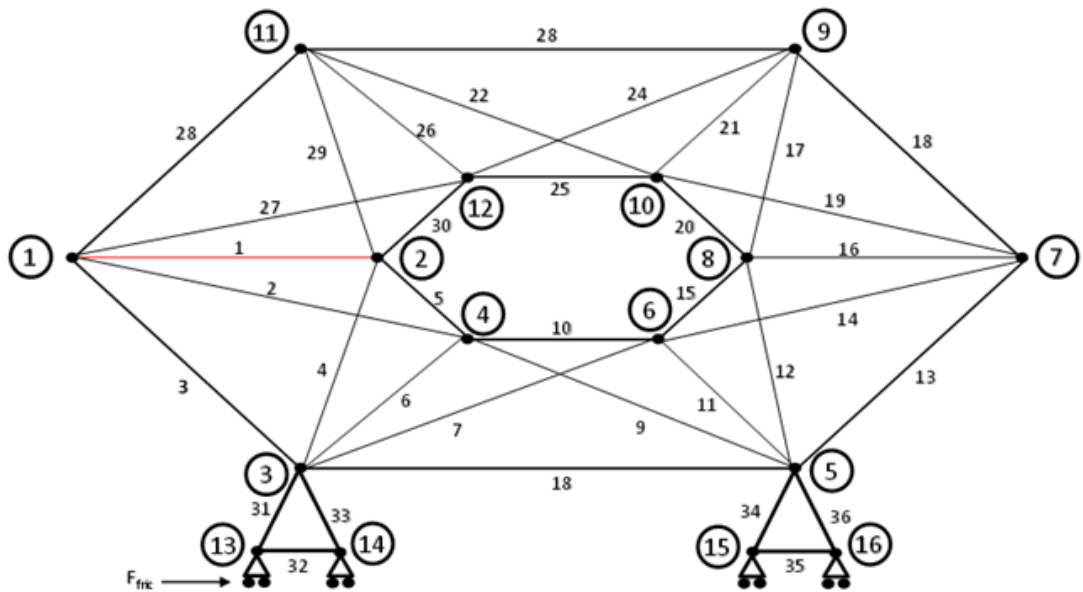


Figure 1.31: Elastic elements with threshold for case 2 (Symmetry is removed by using friction force)

As can be understood from Fig.1.34, the center of mass of the truss system has started to move both in  $+x$  and  $y$  directions. In Fig.1.32 and Fig.1.33, the change in  $x$  and  $y$  coordinates of the centre of mass with respect to time are represented respectively. These graphs prove that the cell has started its movement.

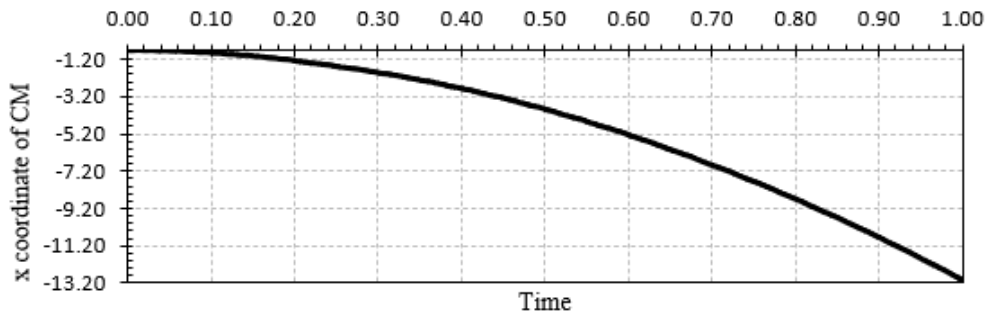


Figure 1.32: The change in  $x$  coordinate of the centre of mass of the non-symmetric truss model with respect to time for case 2

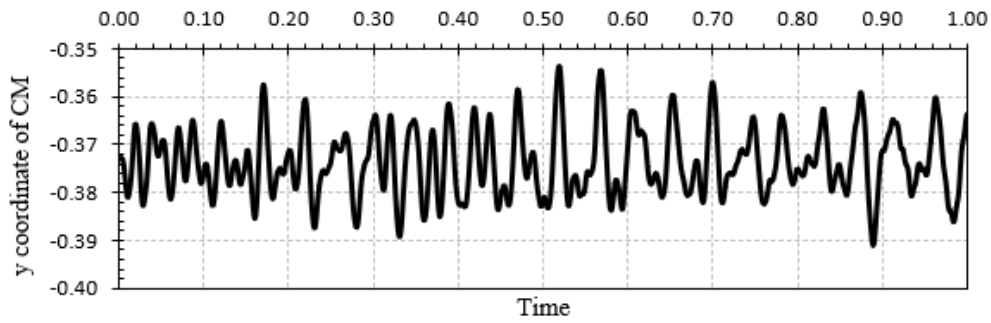


Figure 1.33: The change in  $y$  coordinate of the centre of mass of the non-symmetric truss model with respect to time for case 2

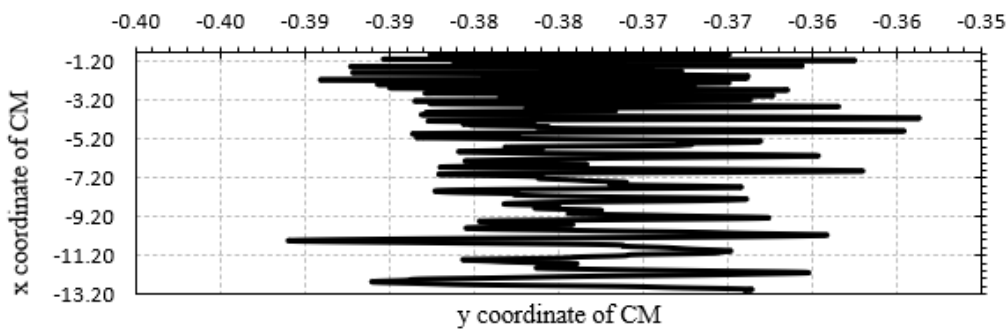


Figure 1.34: The change in  $x$  and  $y$  coordinates of the center of mass of the non-symmetric truss model for case

### 1.10.3 Case 3

In the last case in order to model the cytoplasm mathematically we use the viscous elements. These elements are illustrated as blue lines in Fig. 1.35. Elements 6, 11, 16, 21 and 22 were modeled as viscous material by using Maxwell Model. By this way, the region between two hexagonal represent the cytoplasm. Our hexagonal cell model begins its movement as a result of threshold (internal force) and friction force which is applied as in Case 2.

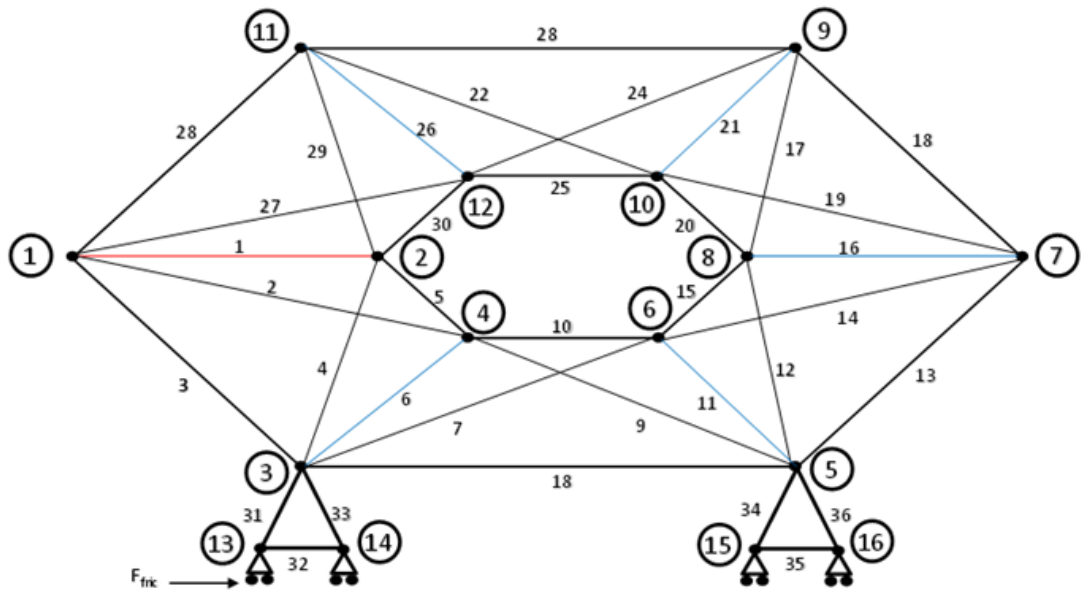


Figure 1.35: Non-symmetrical model for case 3 (Symmetry is removed by polymerizing actin)

In Fig.1.37 and Fig.1.38, the changes of  $x$  and  $y$  coordinates of the centre mass of the cell body with respect to time and in the Fig.1.35 the change in  $x$  and  $y$  coordinates of the centre of mass are presented.

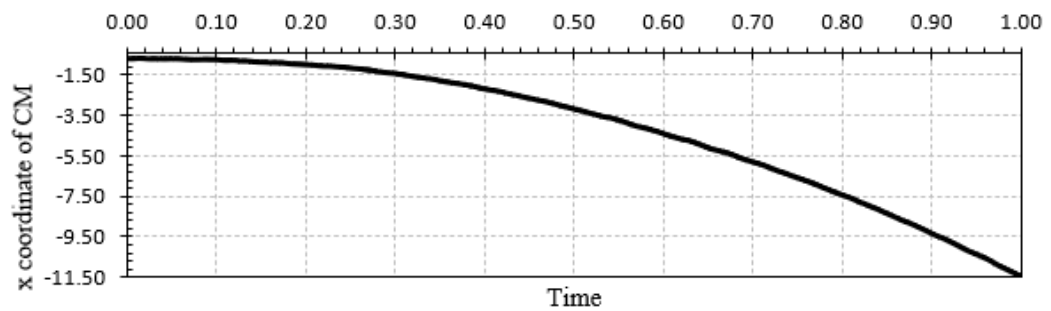


Figure 1.36: The change in  $x$  coordinate of the center of mass of the non-symmetric truss model with respect to time for case 3

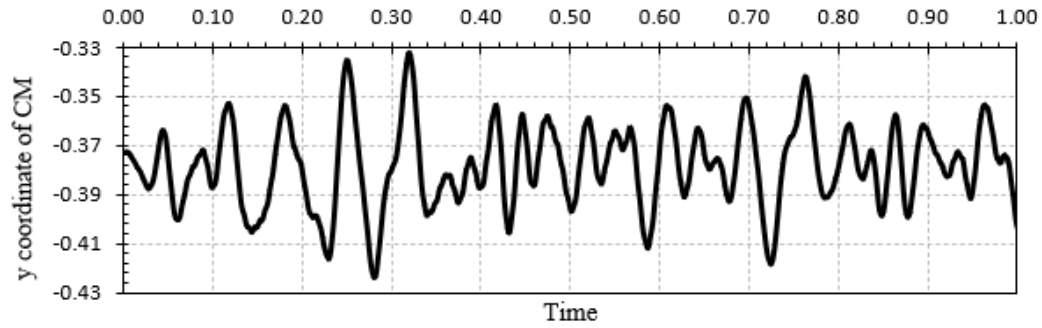


Figure 1.37: The change in  $y$  coordinate of the center of mass of the non-symmetric truss model with respect to time for case 3

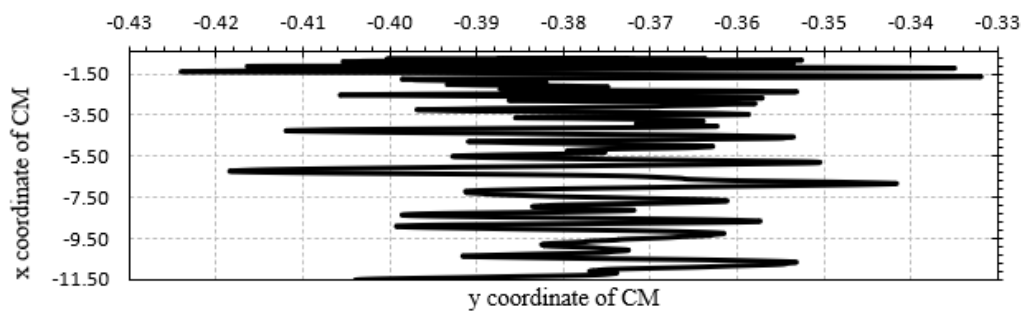


Figure 1.38: The change in  $x$  and  $y$  coordinates of the center of mass of the non-symmetric truss model for case 2



## CHAPTER 2

### PROBABILISTIC MODELS

#### 2.1 INTRODUCTION

In this thesis, we aim to develop formalism of statistical mechanics and statistical thermodynamics that can be used for biological applications. When we first started the thesis, we studied the classical mechanics part before statistical mechanics. As we presented in the previous thesis progress reports, we dealt with several Newtonian mechanic's models and accomplished this part. Now, it is time to start studying the Statistical mechanics part. Statistical mechanics is a tool, that describes the macroscopic behavior of a system through the analysis of its microscopic components. Therefore, statistical mechanics is a framework to move from a probabilistic, high-dimensional description of a system to its macroscopic description through space distributions. By using this approach, we can write the probability of many different microscopic states [97] Fluids flow, boil, freeze, and evaporate. Solids melt and deform. Oil and water do not mix. Metals and semiconductors conduct electricity. Crystals grow. Chemicals react and rearrange, take up heat, and give it off. Rubber stretches and retracts. Proteins catalyze biological reactions [98]. Using the tools of statistical thermodynamics, the driving forces of these processes can be found. Stochastic thermodynamics is a modern paradigm for treating small systems in thermodynamic environments [99]. In order to express the statistical thermodynamics, first of all, we need to know the definitions of entropy, the distribution function, energy, enthalpy, free energy, and the partition function to explain the behaviors of molecules in physical, chemical, and biological systems [98]. Therefore, as a motivation and introduction to what follows, let us quickly go through the titles before formulating our research question. Let us begin with entropy.

### 2.1.1 Entropy

More precisely, the assumption of an equilibrium distribution for the medium allows for a definition of the thermodynamic entropy of an observable state. Entropy is one of the most fundamental concepts in statistical thermodynamics. It describes the tendency of matter toward disorder [98]. Ludwig Boltzmann's celebrated equation defines entropy as  $S=k_B \ln W$ . He explained that isolated systems naturally develop from less probable macroscopic states to more probable ones. Boltzmann's achievement has been honored with the inscription of this equation on his tombstone. Entropy establishes a connection between the micro and macrostates. Boltzmann's equation can be expressed as follows term by term where  $S$  is a macroscopic quantity and called entropy. The symbol  $W$  denotes the German word *Wahrscheinlichkeit*, which means 'probability.'  $W$  is the multiplicity factor and defines the number of microstates. Moreover  $k_B$  is Boltzmann's constant, and it is equal to  $1.380662 \times 10^{-23} \text{ JK}^{-1}$ . The entropy concept that we introduce in this part, the distribution function, the partition function, multiplicity, and averages, provide a foundation for describing entropy and these definitions are given in detail in section 2.1.3. Now we continue with energy, enthalpy and free energy definitions.

### 2.1.2 Energy, Enthalpy and Free Energy

Energy describes the capacity of a system to perform work. Energy is a conserved quantity, which means that it flows. Hence this capacity to perform work can be moved from one place to another [98]. The First Law of Thermodynamics describes the conservation of energy and the interchangeability of heat and different types of work. The internal energy of an isolated system is constant. It is experimentally observed that energy can be neither created nor destroyed [101]. Enthalpy is the heat content of a system and is denoted by  $H$ . As we all know, the heat can go in or out of the system. If this system is a chemical reaction, the change of heat is called enthalpy change. Knowing if the system's enthalpy increases or decreases during a chemical reaction is a crucial factor in understanding whether that reaction can happen. The change in the enthalpy of the system during a chemical reaction is defined as the change in its internal energy plus the change in the product of the pressure times the

volume of the system which is formulated as

$$H = E + PV \quad (2.1)$$

Free energy, in thermodynamics, is energy-like property or state function of a system in thermodynamic equilibrium. Free energy has the dimensions of energy, and its value is determined by the state of the system and not by its history. Free energy is used to determine how systems change and how much work they can produce. It is expressed in two forms: the Helmholtz free energy  $A$ , sometimes called the work function, and the Gibbs free energy  $G$  and the free energy expressions are expressed as;

$$A = E - TS \quad (2.2)$$

and

$$G = H - TS \quad (2.3)$$

### 2.1.3 Probability Theory

$p_A$ , the formula for the probability of result  $p_A$ , is  $p_A = \frac{n_A}{N}$  if  $N$  is the total number of potential outcomes and  $n_a$  of those possibilities fall into set A. Probabilities are numbers with a range of zero to one. Deterministic outcomes are those in which there is just one conceivable result and their probability is one [102]. We regard the system to be a part of the canonical ensemble. The term "canonical ensemble" refers to a group of systems where each identical system in the ensemble has a fixed volume, fixed temperature, and fixed number of particles ( $N, V, T$ ). The isothermal walls that encircle each of the systems are impenetrable. Although there is no interchange of particles between the systems, the isothermal wall permits energy to do so [103]. The probability of discovering a certain microstate with energy  $E_i$  for the canonical ensemble is represented by the density  $p(E_i)$  if a microscopic state  $i$  has the system

energy  $E_i$ . The likelihood of discovering the system in state  $i$  and having energy  $E_i$  is ;

$$p(E_i) = \frac{e^{-E_i/k_B T}}{Z} \quad (2.4)$$

where the partition function is  $Z$ . The partition function, which is a sum of terms representing the weighting factors of all the states [104], is connected to a specific thermodynamic variable. The partition function may be expressed as follows ;

$$Z = \sum_{i=1}^N e^{-E_i/k_B T} \quad (2.5)$$

Entropy is another way to represent the probability function. The relationship may be found by multiplying the logarithm of Equation 2.4 by  $p_i$  ;

$$-p_i \ln p_i = \beta p_i E_i + p_i \ln Z \quad (2.6)$$

or

$$-\sum_i p_i \ln p_i = \beta \langle E \rangle + \ln Z \quad (2.7)$$

where  $\beta = \frac{1}{k_B T}$  and  $\langle E \rangle = \sum_i p_i E_i$  is the mean energy. Thermodynamic relations can be found as; if we add up all the states,  $i$ .

$$S = -k_B (\beta \langle E \rangle + \ln Z) \quad (2.8)$$

Thus, we expect [105]

$$S = -k_B \sum_i p_i \ln p_i \quad (2.9)$$

The lattice model is the cornerstone of statistical mechanics [98]. The lattice model has a solution made up of several little compartments where the ligands can be scat-

tered. This straightforward theory is also known as ligand-receptor binding. In this context, we refer to all possible arrangements of these  $L$  ligands in solution and on the receptor as microstates. There are two separate microstates depicted in In Fig. 2.1.

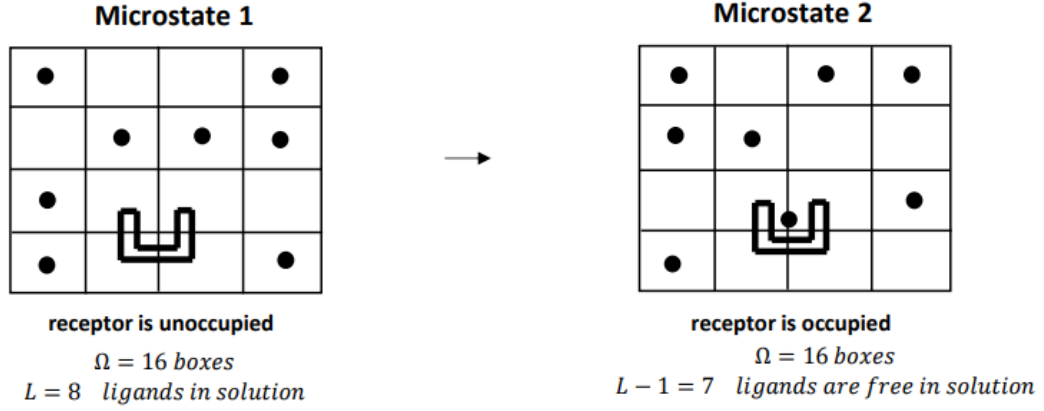


Figure 2.1: Lattice Model

The first microstate in this diagram has all the ligands free in solution, whereas the second microstate has a ligand occupying the receptor. We can get the bound probability using this model. It is bound probability.

$$p_{bound} = \frac{\text{weight when receptor occupied}}{\text{sum of weight when all ligands are free and when one of them is bound to the receptor}} \quad (2.10)$$

$$E_{unoccupied} = L\varepsilon_{sol} \quad (2.11)$$

where  $L$  is the number of ligands in the solution and  $\varepsilon_{sol}$  is the energy of a ligand in the solution. For the occupied microstate (Microstate 2), the energy formulation is

$$E_{unoccupied} = (L - 1)\varepsilon_{sol} \quad (2.12)$$

In this instance, the solution exclusively contains free  $L-1$  ligands (one ligand attached to the receptor). For Microstate 1 and Microstate 2, the multiplicity factors,

commonly known as the number of microstates or number of configurations, are symbolized by the  $W$  symbol and equal to

$$W_{unoccupied} = \frac{\Omega!}{L!(\Omega - L)!} \cong \frac{\Omega^L}{L!} \quad (2.13)$$

$$W_{unoccupied} = \frac{\Omega!}{(L - 1)!(\Omega - (L - 1))!} \cong \frac{\Omega^{L-1}}{(L - 1)!} \quad (2.14)$$

where the number of boxes in the lattice model is  $\Omega$ . The quantity of vacant boxes is denoted by  $\Omega - L$ . Because one ligand is joined to the receptor, the number of ligands drops by one, and  $L-1$  stands for the free ligands in the solution. This equation allows us to investigate the rivalry between binding energy and translational entropy in a variety of physiologically significant scenarios. The weight functions are

$$Weight_{unoccupied} = \frac{\Omega^L}{L!} e^{-\beta L \varepsilon_{sol}} \quad (2.15)$$

and

$$Weight_{unoccupied} = \frac{\Omega^{L-1}}{(L - 1)!} e^{-\beta[(L-1)\varepsilon_{sol} + \varepsilon_{bond}]} \quad (2.16)$$

where  $\varepsilon_{bond}$  is the ligand binding energy. If we substitute these weight functions into Equation 2.10 we obtain;

$$p_{bound} = \frac{\frac{\Omega^{L-1}}{(L - 1)!} e^{-\beta[(L-1)\varepsilon_{sol} + \varepsilon_{bond}]}}{\frac{\Omega^L}{L!} e^{-\beta L \varepsilon_{sol}} + \frac{\Omega^{L-1}}{(L - 1)!} e^{-\beta[(L-1)\varepsilon_{sol} + \varepsilon_{bond}]}} \quad (2.17)$$

After making some tedious simplifications, binding probability can be formulated as;

$$p_{bound} = \frac{(L/\Omega) e^{-\beta \Delta \varepsilon}}{1 + (L/\Omega) e^{-\beta \Delta \varepsilon}} \quad (2.18)$$

where  $\Delta \varepsilon = \varepsilon_{bond} - \varepsilon_{sol}$

## 2.2 AIM OF THE STUDY

In my thesis study until this point, two-dimensional truss, one-dimensional bar, and hexagonal cell motility models gained bias, and the movement with preferred direction emerged solely by asymmetric friction. Even though the preferred direction emerges with an asymmetric Newtonian force, it has to be established by means of statistical mechanics to develop a probabilistic approach. In the first part of my thesis available actin sites are represented with nodes on the 1D bar together with a myosin head as a point at the contact of the roller and the ground. The models of the first part, sliding filament theory is implemented to the models by using friction force analogous to the myosin head being attached to the actin-site. Now, after this point decision making (about being in the attached state) depends on probabilities. In the second part of my thesis, despite the friction force, symmetric and asymmetric decision boundaries on triangular probability distribution function are used to model correlated and uncorrelated dynamics of the bar. For the symmetric decision boundaries around mean, the dynamics of the bar will not be biased and it will not have a preferred direction according to the law of large numbers. Nonetheless, when asymmetric decision boundaries on triangular distribution are used where the mean is not zero, the bar will be actuated with a preferred direction. In the second part, which is discussed in detail in Appendix B, three boxes are defined to create the corresponding space array as indicated in Figure 2.2. Three arrows shown in the figure corresponds to all three possibilities of jumps such that jump to the left, jump to the right, and stand still.

Each box in the figure represents available actin sites for a point myosin head analogous to nodes in the preceding part (These parts have been presented in the previous thesis progress reports as 1D Bar Model, Truss Model and Hexagonal Model).<sup>2</sup>

The most important finding of this part is exerting the preferred direction to the system with probabilistic terms compared to the deterministic preferred direction induced by friction force in the first part. Using probabilistic terms to explain the dynamics, makes one be able to use tools of Statistical Mechanicals for the analysis.

Despite the acquired probabilistic perspective, the model is not capable of grasping

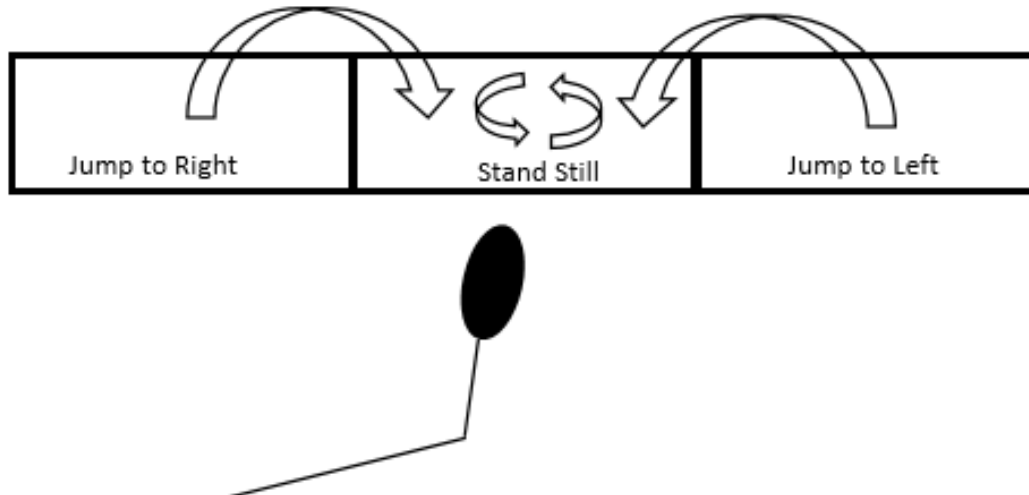


Figure 2.2: Active actin sites

the physical and physiological aspects of the dynamics since the decision makings are not based on probabilistic mechanisms/events, but they are induced manually. Therefore in the next part, mechanism-based decision-making is going to be introduced. For a discussion in greater depth, derivations, and analysis, please see Appendix B.

In the third part of my thesis (Third part is explained in detail in Appendix C), the decision-making procedure is to be changed to mechanism-based compared to manually determined probabilities in the last section, which is the second part. In the first part (1D Bar Model, 2D Truss Model and Hexagonal Model) preferred direction is imposed on the system with asymmetric friction force of Newtonian mechanics. After that in the second part, decision-making depends on manually imposed probabilities. Compared to Boltzmanian taste in the preceding part, decision making has to be mechanism-based. For that purpose, Newtonian dynamics and the spatial probability distributions are fused to reveal a spatiotemporal evolution equation. The master equation derived in this part evolves in time according to chosen arbitrary space probabilities denoted by  $p(x, t)$ . Through the use of the master equation, the faith of the system is determined in a mechanism-based sense.

1D bar model of the first part, friction forces are the reason behind the preferred direction of the walk. In the first part, the existence of symmetry determines whether the preferred direction exists or absent. In addition to the first part, probabilistic terms are used to investigate the dynamics in the second part. However, the relations



used in the second part are not mechanism-based but they are imposed on the system manually. Symmetric and asymmetric decision boundaries chosen determines the existence of the preferred direction of the myosin head in the second part. In part three, the rule-based master equation is stated and the terms are explained one by one in detail. Similar to other parts, the existence of the preferred direction has to be discussed separately for self-consistency. In the third part, unbiased random walk corresponds to symmetric friction force and symmetric decision boundaries in preceding parts. Likewise biased random walk is equivalent to asymmetric friction force and asymmetric decision boundaries where preferred direction exists. For the derivation of the master equation by using analytical and numerical methods and the derivation of the diffusion equation (heat equation) from the unbiased random walk, please see Appendix C.

### 2.3 THE MASTER EQUATION

The spatiotemporal evolution equation is defined as follows;

$$\begin{aligned}
 p(x, t + \Delta t) = & k_- \Delta t p(x + \Delta x, t) + k_+ \Delta t p(x - \Delta x, t) \\
 & + [1 - (k_- + k_+) \Delta t] p(x, t)
 \end{aligned}
 \tag{2.19}$$

In the relation,  $p(x, t)$  determines the probability of finding the particle (myosin head) at position  $x$  (refers to the actin site of interest) at a given time  $t$ . According to the laws of diffusion and probability theory  $k_-$  and  $k_+$  stand for the rate constants with units of frequency. Different statistical weights at a given instant can be imposed on the master equation by choosing different  $k$  values.

The first term in summation with a weight  $k_- \Delta t$  determines the probability of event; i.e., “the myosin head binded to the right available actin site then jumps to left in a single time interval  $\Delta t$ ” (see Figure 2.3) the second term  $k_+ \Delta t$  is the opposite of the first event. The third term in the relation guarantees the normalization of probabilities as subtracting other probabilities from the whole probability one and it is denoted as  $[1 - (k_- + k_+) \Delta t]$ . Since the unit of  $k$  is 1/sec, its product with  $\Delta t$  makes it a number which agrees with the dimensional analysis. All three events are visualized through

Figures 2.3 to 2.5 to make the understanding clear.

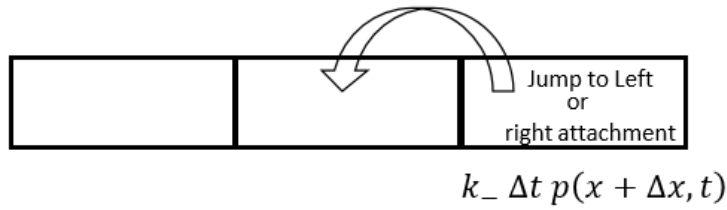


Figure 2.3: Jumping to the Left

As it can be seen from Fig.2.2,  $k_- \Delta t p(x - \Delta x, t)$  determines the probability of myosin head jumps to the left on actin and binds to next available actin site

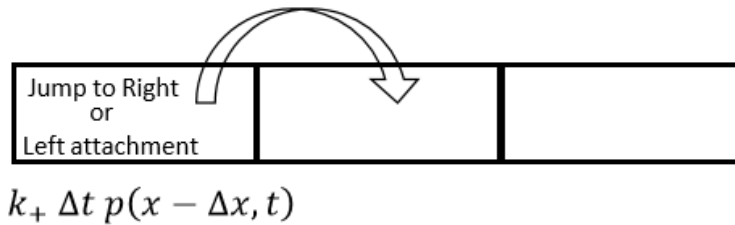


Figure 2.4: Jumping to the Right

Figure 2.4 shows a myosin head jumps to next available actin site on the right hand side with given probability

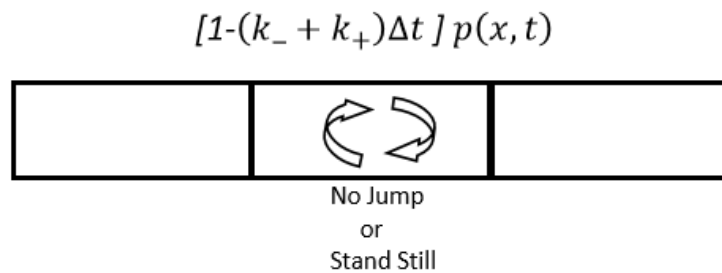


Figure 2.5: No Jump

Third and the final term (in Eqn 2.19 last term) determines the probability of stand still for the myosin which stays at the same actin site after time  $\Delta t$  passes (see Figure 2.5). Moreover, subtracting first and second terms from 1 in corresponding probability of “stand-still”  $[1 - (k_- + k_+) \Delta t] p(x, t)$  assures the normality of probabilities.

## 2.4 THE ONE-STATE MODEL

In the one-state model, as it can be understood from the name of the model, the myosin is attached to the actin without detachment freedom (there is only an attachment event, without detachment). For this reason, the movement of the myosin head on the actin filament is just like a train moving back and forth on the rails. In the literature of statistical mechanics, this model is called 1D random walk beside that it is called trinomial model in financial mathematics.

Our ambition is to write a set of rate equations that describe the time evolution of the probability distribution. The general form of the probability distribution function is defined as  $p_m(n, t)$  where the label  $m$  refers to the internal state,  $n$  refers to the position and  $t$  is time. In other words, the distribution function is equal to the probability of motor protein being at time  $t$ , in state  $m$ , at site  $n$ .

In this model due to restriction of one state, there is an ambiguity between states and sites. In other words there is no freedom for myosin head to detach from the actin. Therefore the applied constraint force drags the myosin head along the actin rather than detaching it away from the filament.

In the presence of external applied force, myosin head moves from one available actin site to the next with forward and backward rates  $k_+(F)$  and  $k_-(F)$  respectively [1]. Between the applied force and rate constants, there is an explicit relation. In our one state model, it is assumed that the applied force is in the backward negative direction which is shown in Figure 2.6.

In order to understand the treatment of site and state difference, we start our study with a very simple case and this case has no validity in real life. In reality, to produce

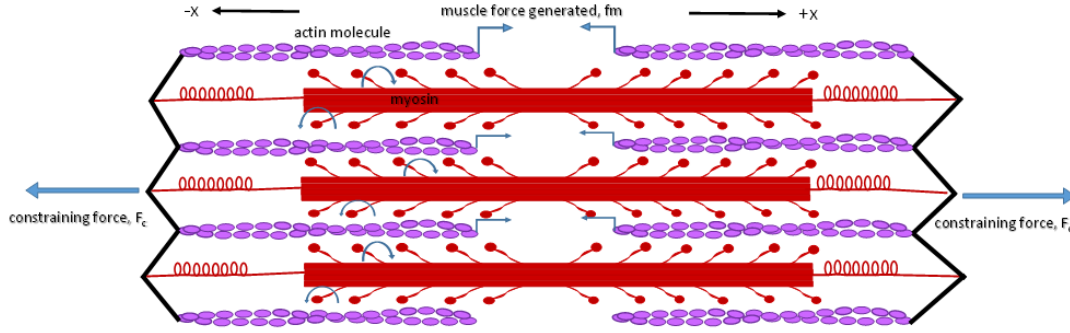


Figure 2.6: The free energy of a myosin head moving along an actin filament [97]

useful work there must be at least two states.

In equilibrium condition, there is no net flux from one state to the other. Therefore for neighboring sites  $n$  and  $n+1$ , the equilibrium constraint can be stated as;

$$k_+ P_n = k_- p_{n+1} \quad (2.20)$$

After that space probabilities can be defined as follows by using partition function and Boltzmann distribution where  $G_n$  represents the Gibbs free energy of given site  $n$ ;

$$p_n = \frac{e^{-\beta G_n}}{Z} \quad (2.21)$$

Similarly, the probability of attachment for the next site is then determined as;

$$p_{n+1} = \frac{e^{-\beta G_{n+1}}}{Z} \quad (2.22)$$

The given figure below (Fig. 2.7) shows the variation of Gibbs free energy all along the 1D space i.e. actin filament. Moreover associated Gibbs free energies of  $n^{th}$  and  $(n + 1)^{th}$  sites can be seen clearly.

If we substitute Equation 2.21 and Equation 2.22 into Equation 2.20, we obtain the following relation ;

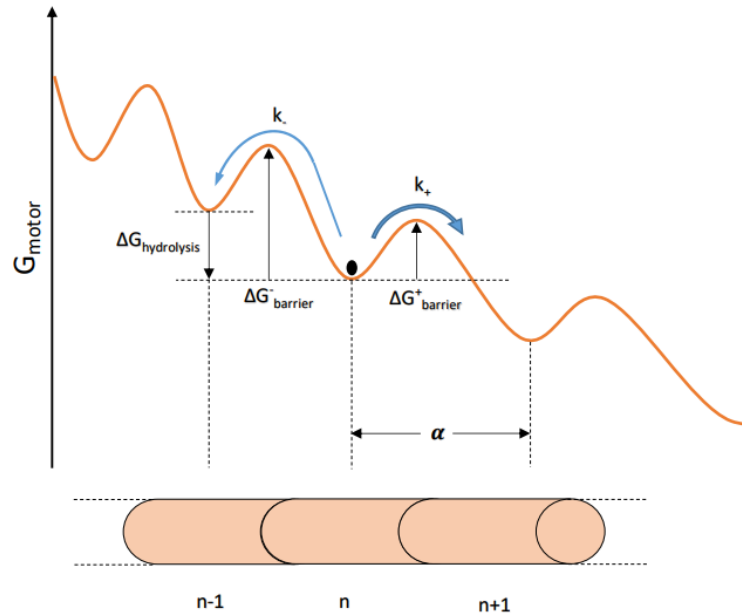


Figure 2.7: The free energy of a myosin head moving along an actin filament [97]

$$\frac{k_+}{k_-} = e^{-\beta\Delta G} \quad (2.23)$$

where  $\Delta G = G_{n+1} - G_n$

If a constraint force is applied in the negative  $x$ -direction, the corresponding free energy of the state which is at the left-hand side rises according to the relation  $G_n \rightarrow G_n + Fna$  as shown in Figure 2.8 below. In this relation  $a$  is the step size (in meter) in both directions. Please note that given  $F$  is a constraint force, rather than an external driving force which is shown in Figure 2.6 In the presence of constraint force, entropy of the system is decreased; in other words; it steals freedom from the entropy in order to give rise to the preferred direction. In conclusion, with the help of the constraint force movements in the direction of force is encouraged by decreasing probabilities for the opposite direction. Effects of a constraint force and resulting decrease in the system's entropy can be expressed analytically in terms of rate constant as follows. After the modifications, rate constants become a function of applied force together with its direction as a plus or minus sign given to the rate constants as shown in Equation 2.24.

$$\frac{k_+(F)}{k_-(F)} = e^{-\beta(\Delta G + Fa)} \quad (2.24)$$

Once again, please note that applied force changes barrier energies by modifying the energy landscape of the actin filament. Through those modifications associated rate constants changes since they are exponentially dependent on Gibbs free energy changes ( $\Delta G = G_{n+1} - G_n$ ). Moreover changing barrier energies does not only generate a preferred direction but also increases the transition rates between adjacent sites. The modification of energy landscape with applied constraint force is shown in Figure ?? to make the understanding clear.

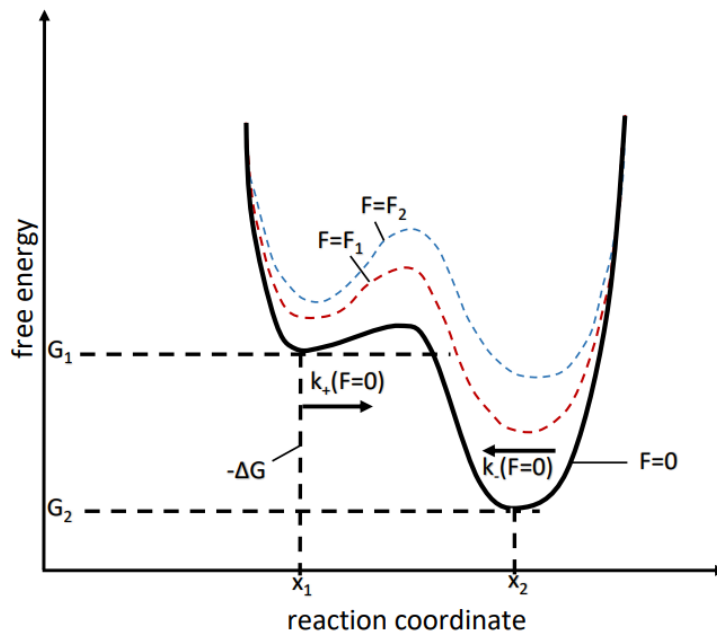


Figure 2.8: Energy landscape of a one-state model [1]

The solid line in Figure 2.8 shows the free energies in the absence of constraint force,  $F_c$  in Figure 2.6. If  $F_1$  and  $F_2$ , such that  $F_1 < F_2$ , is applied to the myosin head, corresponding free energies change to a different energy landscape shown by dash lines. Since both of the forces,  $F_1$  and  $F_2$  are in negative x-direction, they encourage the myosin head to move to the left by modifying barrier energies, in other words decreasing the probabilities of opposite events, which result in movement to the right side. Difference in changes of  $k_+$  and  $k_-$  in terms of humps can be seen clearly from the Figure 2.8. Moreover the figure shows the barrier energies and free energies of both sites apparently.

As it can be seen from the Figure 2.6, sarcomere has a symmetric geometry in positive and negative  $x$  directions. If you choose positive  $x$  directions from the center to the lateral ends, it causes sign nonlinearity on the sarcomere. After selecting this sign convention, both of the constraint forces in the Figure 2.6 becomes in positive directions for each side.

Particularly the myosins at the left side gain a preferred direction toward the left, which is local  $+x$ . Similarly, the myosins at the right side are encouraged to move toward the right side, away from the center, which is again local  $+x$  for right side of the sarcomere. Therefore, applied constraint force  $F_c$  behaves like  $2F_c$  due to the sign nonlinearity arising from the symmetric geometry of the sarcomere. In this model, the constraint force may depend on both  $k_+$  and  $k_-$ . We examine, however, the dependence of the force on  $k_+$  only since the opposite can be easily analyzed by following the steps mentioned above. In this case,  $k_+$  can be expressed in terms of free energies and constraint force as follows;

$$k_+ = k_- e^{-\beta(\Delta G + Fa)} \quad (2.25)$$

Additionally as we mentioned before in Appendix C,  $\Delta v = \Delta x(k_+ - k_-) = \Delta x k_+ - \Delta x k_-$ , where  $v$  denotes the velocity term. Moreover,  $\Delta x$  is our displacement term and is equal to step size  $a$  in meter, so the relation becomes

$$v = a(k_+ - k_-) = ak_+ - ak_- \quad (2.26)$$

Then if we substitute Equation 2.25 into Equation 2.26 force dependent velocity relation is found as;

$$v(F) = ak_- (e^{-\beta(\Delta G + Fa)} - 1) \quad (2.27)$$

Up to this point by using the master equation, the dynamics of the myosin head on the actin filament is modelled as a 1D random walk and the rate constants which are

$k_+$  and  $k_-$  are described as functions of constraint force. For the sake of reaching a more realistic model, we will try to express the rate constants as a function of the hydrolysis of ATP. Thus our model becomes much more meaningful in terms of its physical counterpart.

When Figure 2.7 is examined in a more detailed way, the particle or myosin head which stands in the pit at position  $n$ , associated free energy  $\Delta G_{barrier}$  is the amount of the energy required for the motor protein to overcome that hill. Similarly,  $\Delta G_{barrier}^+$  and  $\Delta G_{barrier}^-$  denote the required energy for the myosin head to attach to the adjacent available actin sites in both directions. The overall tilt of this figure ends up with a preferred direction to the right. The difference between the amount of energy that must be exceeded to attach to the right and left available actin sites is equal to the hydrolysis energy denoted by  $\Delta G_{hydrolysis}$ . To formulate the rate constants in terms of ATP, we assume  $k$  values in terms of the Arrhenius relation as a function of the height of the barrier between two adjacent sites. Therefore the relation can be written as

$$k = \Gamma e^{-\beta \Delta G_{barrier}} \quad (2.28)$$

where  $\Gamma$  is the frequency of attempts to go over the barrier.

In order to consider the effects of ATP on the dynamics, the lattice model has to be used which is shown in Figure 2.9. The figure shows the dissociation of a single ATP molecule into an ADP and an inorganic phosphate. As a result of hydrolysis the number of ATP molecules in the lattice decreases by one and the number of each the product molecules ADP and  $P_i$  increases by one.

### At Site $n$

The number of microstates which are shown in Fig. 2.9 together with energetics



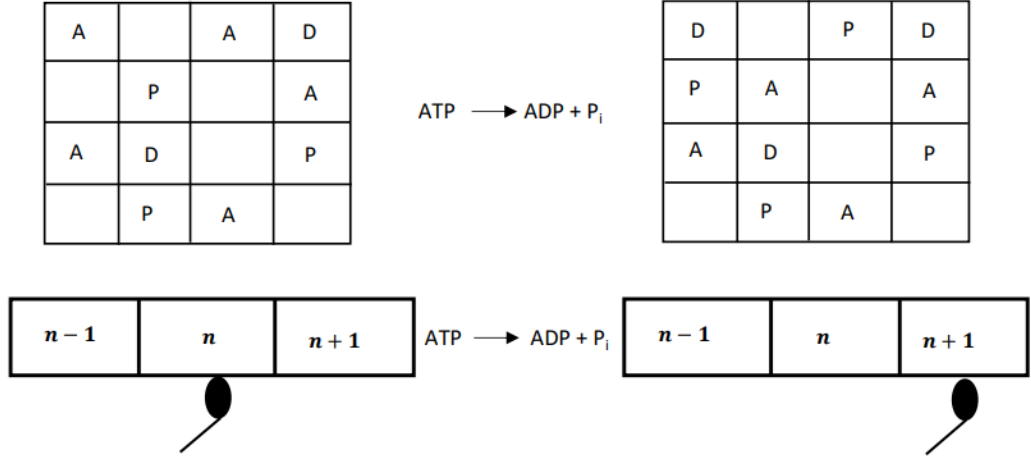


Figure 2.9: Lattice Model of ATP

corresponding to the macrostate where the myosine head is at  $n^{th}$  site shown in the left hand, is the associated weight function in Equation (29). The weight function is stated below (see page 4, figure 2.1 equation 2.10) by multiplying the number of microstates with exponential of ratio of the total bond energy to the thermal noise ( $\beta$ ).

$$W_n = \frac{\Omega!}{A!D!P!(\Omega - A - D - P)!} e^{-\beta A \varepsilon_{bond}} \quad (2.29)$$

where  $\Omega$  is the number of boxes and A, D and P stand for ATP, ADP and  $P_i$  molecules in solution respectively.  $\varepsilon_{bond}$  is the bond energy of a single ATP. After hydrolysis, the myosin head moves to the site indexed with  $n+1$  and one ATP molecule dissociated into an ADP and an inorganic phosphate  $P_i$ .

### At Site n+1

Similarly, the weight function after disassociation of a single ATP, myosin head moves to the right site  $n+1$ . Hence the new weight function can be expressed as;

$$W_{n+1} = \frac{\Omega!}{(A-1)!(D+1)!(P+1)! [\Omega - (A-1) - (D+1) - (P+1)]!} e^{-\beta(A-1)\varepsilon_{bond}} \quad (2.30)$$

A-1 indicates the number of ATP molecules remained after a dissociation of a single one, and D+1 and P+1 denote the increased ADP and  $P_i$  molecules by one in the

solution after the reaction.

The weight of the free energy difference between the position  $n$  and  $n+1$  is related to the ratio of the weight functions. The free energy difference between these sites are called  $\Delta G_{hydrolysis}$  and it can be formulated through the following relation;

$$\Delta G_{hydrolysis} = \Delta G_{barrier}^+ - \Delta G_{barrier}^- \quad (2.31)$$

Therefore;

$$e^{-\beta \Delta G_{hydrolysis}} = e^{-\beta(\Delta G_{barrier}^+ - \Delta G_{barrier}^-)} = \frac{e^{\beta \Delta G_{barrier}^+}}{e^{\beta \Delta G_{barrier}^-}} = \frac{W_{n+1}}{W_n} \quad (2.32)$$

We substitute Equation 2.29 and Equation 2.30 into Equation 2.32 and after making some simplifications, the following relation is reached;

$$e^{-\beta \Delta G_{hydrolysis}} = \frac{W_{n+1}}{W_n} = \frac{A}{DP} \Omega e^{\beta \varepsilon_{bond}} \quad (2.33)$$

Then, multiplying the logarithm of Equation 2.33, it becomes as follows;

$$\begin{aligned} -\beta \Delta G_{hydrolysis} &= \ln \left[ \frac{A}{DP} \Omega e^{\beta \varepsilon_{bond}} \right] \\ -\beta \Delta G_{hydrolysis} &= \ln \left( \frac{A}{DP} \Omega \right) + \ln \left( e^{\beta \varepsilon_{bond}} \right) \end{aligned} \quad (2.34)$$

where  $\beta = \frac{1}{k_B T}$  so;  $\ln$

$$\Delta G_{hydrolysis} = -\varepsilon_{bond} - \underbrace{k_B T \ln \left( \frac{A \Omega}{DP} \right)}_{k_B T [\ln(DP) - \ln(A \Omega)]} = -\varepsilon_{bond} + \underbrace{k_B T \ln \left( \frac{DP}{A \Omega} \right)}_{\ln \left( \frac{DP}{A \Omega} \right)} \quad (2.35)$$

$$\Delta G_{hydrolysis} = -\varepsilon_{bond} + k_B T \ln \left( \frac{DP}{A \Omega} \right)$$

If we multiply the ATP, ADP and Pi molecules with  $1/\Omega v$  we obtain the concentrations.  $v$  is the volume of a single box where  $\Omega v$  is the total volume covered by the lattice.

$$\Delta G_{hydrolysis} = -\varepsilon_{bond} + k_B T \ln \left( \frac{[D][P]}{[A]} v \right) \quad (2.36)$$

The ‘‘standard-state free energy’’ which is denoted by  $\Delta G_0$  is equal to  $-\varepsilon_{bond}$ . In this case; all boxes are occupied by A, D, P molecules so there is no extra freedom for ATP to break down to ADP and  $P_i$ , which will further change the entropy. The free energy of hydrolysis is a bond breaking energy.

So Equation 2.36 can be written as;

$$\Delta G_{hydrolysis} = \Delta G_{barrier}^+ - \Delta G_{barrier}^- = \Delta G_0 + k_B T \ln \left( \frac{[D][P]}{[A]} v \right) \quad (2.37)$$

And

$$\Delta G_{barrier}^+ = \Delta G_{hydrolysis} + \Delta G_{barrier}^- = \Delta G_0 + k_B T \ln \left( \frac{[D][P]}{[A]} v \right) + \Delta G_{barrier}^- \quad (2.38)$$

If we insert Equation 2.38 into Equation 2.28, the ATP dependent forward rate constant is obtained as follows;

$$k_+ = \Gamma_+ e^{-\beta \Delta G_{barrier}^+} = \Gamma_+ e^{-\beta (\Delta G_{hydrolysis} + \Delta G_{barrier}^-)} \quad (2.39)$$

$$k_+ = \Gamma_+ e^{-\beta \left[ \Delta G_0 + k_B T \ln \left( \frac{[D][P]}{[A]} v \right) + \Delta G_{barrier}^- \right]} \quad (2.40)$$

and the backward rate constant is ;

$$k_- = \Gamma_- e^{-\beta \Delta G_{barrier}^-} \quad (2.41)$$

So we calculate the forward and backward rate constants dependent on the ATP molecule.

## 2.5 ANALYSIS

In this study, three different cases have been examined. As we mentioned in Section 4, to evolve the master equation, first the rate constants have to be determined, which are the parameters of the process. The goal of the analysis is to find the binding probabilities of myosin heads to available actin sites. In all cases our space partition is between -30 and +30 values with space increment 0.1 so there are 601 boxes which are representing the available actin sites (In physiology, the actin molecule chains twisted around each other and the crossover points were about 360 angstroms apart [106]).  $k_B T$  value, which is in all our calculations is taken as  $4.1 \times 10^{-21}$  Joules at 300 K [97].  $k_B$  is Boltzmann's constant and T is temperature.  $a$  and F values which are illustrated in Equation 2.25 enter the calculations as 1 nm and  $2 \times 10^{-22}$  N respectively.

### 2.5.1 Case 1

In the first case, the forward and backward rate constants are selected asymmetric by giving different k values and create a preferred direction as a stationary process (rate constants are not functions of space and time). When we use the values  $k_+=0.5$  and  $k_-=0.3$  we observe that the right attachment/movement event is more probable (i.e. frequent) than the left and the system in the first case starts its motion in  $+x$  direction from position  $n$  to  $n+1$  as illustrated in Figure 2.10.

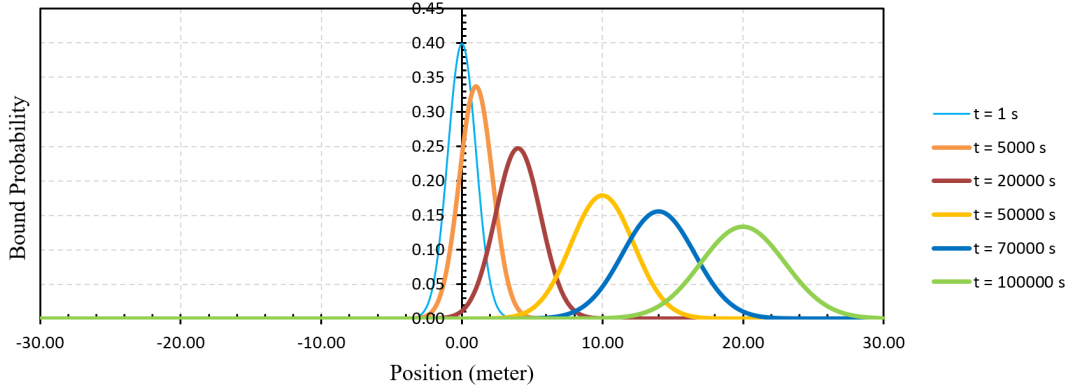


Figure 2.10: Binding Probabilities (Rate constants are selected constant values)

### 2.5.2 Case 2

In the second case, while a constraint force is applied to the actin-myosin system in the backward direction, which is explained in detail in Fig. 2.6, the probability of the myosin protein moving from the position  $n$  to the position  $n+1$  to the right is greater than the movement in the opposite direction.

The forward rate constant is expressed in Equation 2.25 depending on the force, and the backward rate constant is calculated according to Equation 2.23. After finding  $k_+(F)$  and  $k_-$ , we substitute these variables into Equation 2.19. Thus for this problem, we find the probabilities that myosin head binds to 601 available actin sites varying between -30 and +30.

When we compare this case with the first one, in both cases, the myosin head moves in the  $+x$  direction. Increasing the forward rate constant by applying the constraint force, accumulation rate of variance increases significantly since diffusion constant ( $D$ ) changes with  $\frac{a^2}{2}(k_+ + k_-)$  (see appendix C, Equation (C.28)). In other words, for a given time, we observe a greater variance for  $p(x,t)$ . Moreover, applied constraint force increases the velocity of mean,  $v$ , according to  $a(k_+ + k_-)$  (see Equation (26)). Therefore, the applied constraint force produces wider and more shifted  $p(x,t)$  curves at a given time by increasing  $k_+$  values which is represented in Figure 2.11.

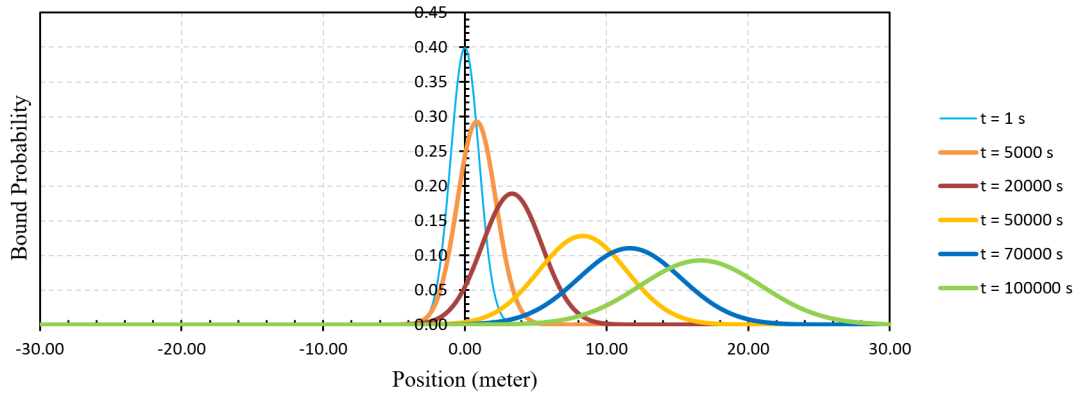


Figure 2.11: Binding Probabilities (Force dependent forward rate constant)

As shown in Figure 2.11, as Gaussian curves evolve towards right, which is  $+x$  direction, the detached myosin head and available actin sites become more probable to form a actomyosine complex. In other words, for a given time, binding probabilities increase. For a particular myosin head to progress, some actin sites must lose their probability to bind for the sake of conservation of normalization.

### 2.5.3 Case 3

In the last case, the forward rate constant is calculated depending on the ATP, ADP and  $P_i$  concentrations. The rates of rate constant values are obtained by using Equation 2.40 and Equation 2.41. In these formulations we have chosen ATP concentration as  $5 \times 10^{-3}$  mM, ADP concentration  $0.5 \times 10^{-3}$  mM,  $P_i$   $10 \times 10^{-3}$  mM and the standard state free energy  $\Delta G_0 \approx -20k_B T$  [97], the frequency of attempt is taken as 1/s.  $\Delta G_{barrier}^-$ , and  $\Omega$  values are selected as  $10^{-19}$  Joule and 1 1/s respectively. If we put rate constants which are based on ATP hydrolysis rather than force, into the master equation, we find the attachment probability of myosin head to available actin sites. As it can be seen in Figure 2.12, as in case 3, as time progresses, myosin head starts to move to the available actin sites on the right with the hydrolysis of ATP so it performs the muscle contraction.

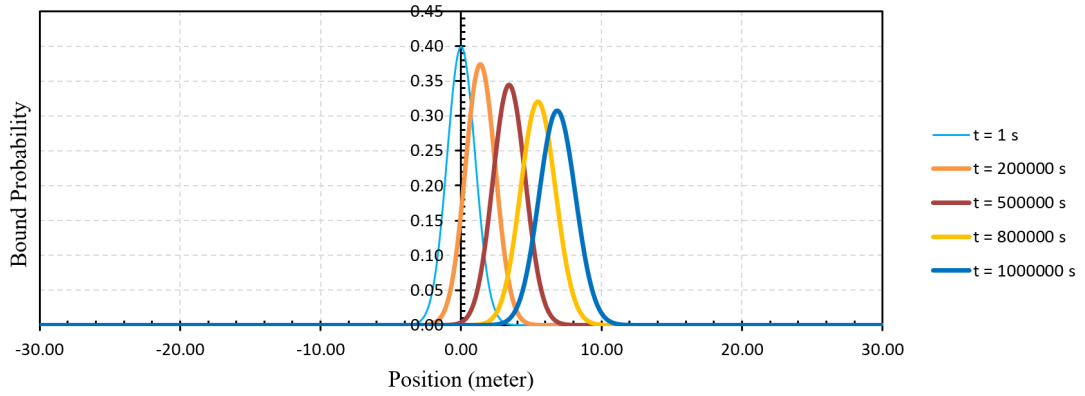


Figure 2.12: Binding Probabilities (  $[ATP] = 5 \times 10^{-3}$  mM )

Compared to the previous case (case 2), this time the existing preferred direction due to molecular asymmetry of actin filament ( $k_+ > k_-$ ) is further enhanced by ATP concentration. Effects of ATP concentration can be thought as a different cause behind the same macro observations of the second case where the preferred direction is enhanced by the constraint force.

If we further increase the ATP concentration in the sarcomere which is chosen  $15 \times 10^{-3}$  mM, it increases the forward rate constant more than the previous scenario. The more the forward rate constant increases, the greater  $D$  which is diffusion constant and discussed in more detail in Appendix C and  $v$  values (see Equation 2.26) drive the  $p(x,t)$ . In other words, we obtain a  $p(x,t)$  with a greater mean and variance for a given time since the mean is associated with  $vt$ , and the variance is given by  $2Dt$ . The effect of higher ATP concentration can be seen from the Figure 2.13 given below.

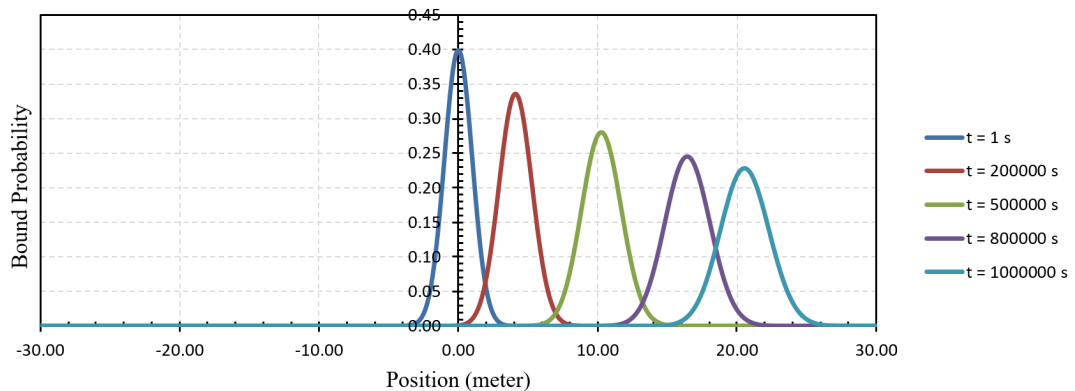


Figure 2.13: Binding Probabilities (  $[ATP] = 15 \times 10^{-3}$  mM )

## 2.6 THE TWO-STATE MODEL

As with our analysis of the one-state motor, our ambition is to write a set of rate equations that describe the time evolution of the probability distribution  $p_i(n, t)$ , where the label  $i$  refers to the internal state (either 0 or 1) and  $n$  refers to the position on the linear track. 0 and 1 represent the detached and attached states respectively.

Morphological characteristics for two-state cross-bridge model is shown in Figure 2.14 [111].

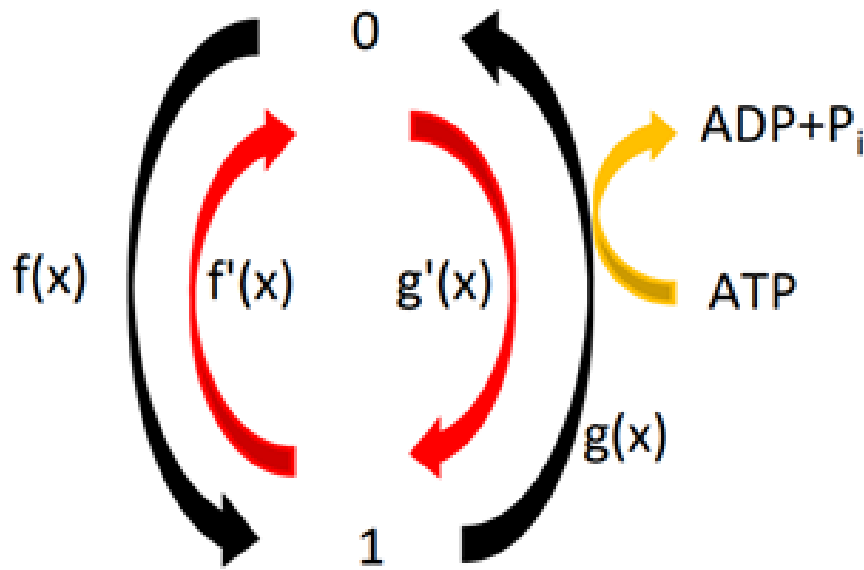


Figure 2.14: Kinetic diagram for a two-state cross-bridge model

In this figure  $f(x)$ ,  $f'(x)$ ,  $g(x)$  and  $g'(x)$  represent the rate constants and ATP hydrolysis occurs on unbound state via  $g$  path.

For example, if we interest ourselves in  $p_0(n, t)$ , we need to consider several different processes that result in the motor being at time  $t$  in state 0 at site  $n$ . In particular, the motor can come into this state from state 1 at position  $n-1$  with a rate  $k_A^+$ . In addition, we need to consider the processes in which the motor arrives in this state from state 1 at position  $n$  with a rate  $k_B^-$ . Finally, there is the uneventful situation where the motor stays put and remains in state 0 at position  $n$  during the time interval from  $t$  to  $t + \Delta t$ . This last microtrajectory occurs with probability  $1 - (k_A^- + k_B^+) \Delta t$ . Following a strategy similar to that we used in the case of the one state motor, we can write the time evolution of  $p_0(n, t)$  and  $p_1(n, t)$  as;



### 2.6.1 UNBOUND(DETACHED)

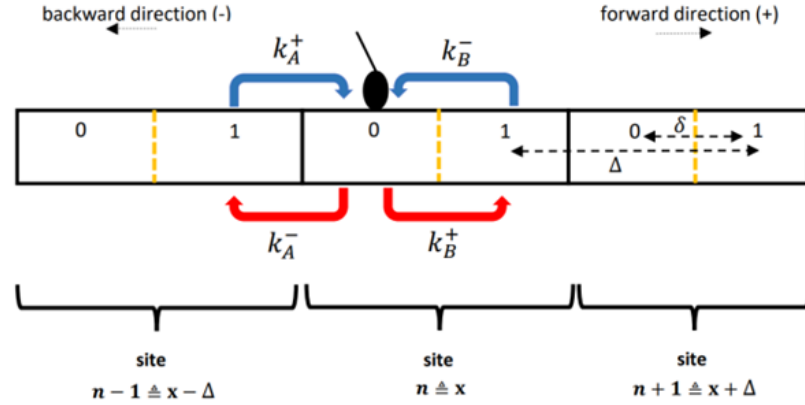


Figure 2.15: Two State Model for Unbound Case

We assume that in going from state 0 to state 1 at a given site, the distance traveled by the motor is  $\delta$  and in going from state 1 at one site to state 0 at the next site, the distance moved by the motor is  $\Delta - \delta$ , where  $\Delta$  is the periodicity of the cytoskeletal filament on which the motor moves.

$$p_0(n, t) = k_A^+ p_1(n-1, t) + k_B^- p_1(n, t) + [1 - (k_A^- + k_B^+) t] p_0(n, t) \quad (2.42)$$

This form is taken from Rob Phillips [111].

$$p_0(x, t + \Delta t) = k_A^+ p_1(x - (\Delta - \delta), t) \Delta t + k_B^- p_1(x + \delta, t) \Delta t + [1 - (k_A^- + k_B^+) \Delta t] p_0(x, t) \quad (2.43)$$

where  $\Delta \gg \delta$  so  $\Delta - \delta \cong \Delta$  then Eqn.2.43 becomes as follows;

$$p_0(x, t + \Delta t) = k_A^+ p_1(x - \Delta, t) \Delta t + k_B^- p_1(x + \delta, t) \Delta t + [1 - (k_A^- + k_B^+) \Delta t] p_0(x, t) \quad (2.44)$$

In Eqn. 2.44, expression  $k_B^- p_1(x + \delta, t) \Delta t$  represents the g path. This representation points out that by using ATP hydrolysis the two state cross bridge model becomes bound to unbound at the same state. Using the energy released as a result of ATP cleavage,  $k_A^+ p_1(x - \Delta, t) \Delta t$  term in Eqn.2.44 changes the state from unbound to

bound. This term is analogue with the f path in Figure 2.14 and this means that by using the expression  $k_A^+ p_1(x - \Delta, t) \Delta t$  the myosin head can both bound and takes a step from one site to other site.

If we write the time evolution of Eqn 2.44, we can obtain the following relation;

$$\frac{\partial p_0}{\partial t} = k_A^+ p_1(x - \Delta, t) + k_B^- p_1(x + \delta, t) - (k_A^- + k_B^+) p_0(x, t) \quad (2.45)$$

According to Taylor expansion,

$p_1(x - \Delta, t)$  and  $p_1(x + \delta, t)$  are determined as,

$$p_1(x - \Delta) = p_1(x) - \frac{\partial p_1}{\partial x} \Delta + \frac{1}{2} \frac{\partial^2 p_1}{\partial x^2} \Delta^2 + \text{HOT.} \quad (2.46)$$

And

$$p_1(x + \delta) = p_1(x) + \frac{\partial p_1}{\partial x} \delta + \frac{1}{2} \frac{\partial^2 p_1}{\partial x^2} \delta^2 + \text{HOT.} \quad (2.47)$$

Then Eqn 2.46 and Eqn. 2.47 are substituted into the Eqn. 2.45 so our relation becomes as follows;

$$\begin{aligned} \frac{\partial p_0}{\partial t} = & k_A^+ p_1 - k_A^+ \frac{\partial p_1}{\partial x} \Delta + k_A^+ \frac{1}{2} \frac{\partial^2 p_1}{\partial x^2} \Delta^2 + k_B^- p_1 + k_B^- \frac{\partial p_1}{\partial x} \delta + k_B^- \frac{1}{2} \frac{\partial^2 p_1}{\partial x^2} \delta^2 \\ & - (k_A^- + k_B^+) p_0 \end{aligned} \quad (2.48)$$

After making some simplifications;

$$\frac{\partial p_0}{\partial t} = p_1(k_A^+ + k_B^-) + \frac{\partial p_1}{\partial x} (k_B^- \delta - k_A^+ \Delta) + \frac{\partial^2 p_1}{\partial x^2} \frac{1}{2} (k_B^- \delta^2 - k_A^+ \Delta^2) - p_0(k_A^- + k_B^+) \quad (2.49)$$

## 2.6.2 BOUND (ATTACHED)

$$p_1(n, t) = k_A^- p_0(n + 1, t) t + k_B^+ p_0(n, t) t + [1 - (k_A^+ + k_B^-) t] p_1(n, t) \quad (2.50)$$

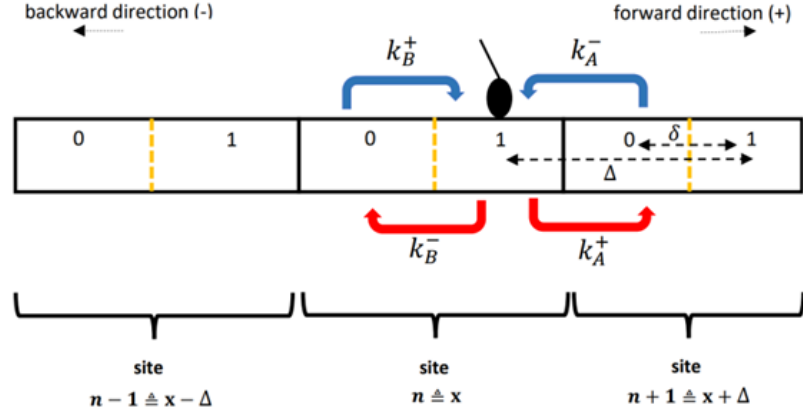


Figure 2.16: Two State Model for Bound Case

This form is taken from Rob Phillips [111].

$$p_1(x, t + \Delta t) = k_A^- p_0(x + (\Delta - \delta), t) \Delta t + k_B^+ p_0(x - \delta, t) \Delta t + [1 - (k_A^+ + k_B^-) \Delta t] p_1(x, t) \quad (2.51)$$

where  $\Delta \gg \delta$  so  $\Delta - \delta \cong \Delta$  then Eqn.2.51 becomes as follows;

$$p_1(x, t + \Delta t) = k_A^- p_0(x + \Delta, t) \Delta t + k_B^+ p_0(x - \delta, t) \Delta t + [1 - (k_A^+ + k_B^-) \Delta t] p_1(x, t) \quad (2.52)$$

If we write the time evolution of Eqn 2.52, we can obtain the following relation;

$$\frac{\partial p_1}{\partial t} = k_A^- p_0(x + \Delta, t) + k_B^+ p_0(x - \delta, t) - (k_A^+ + k_B^-) p_1(x, t) \quad (2.53)$$

According to Taylor expansion,  $p_0(x + \Delta, t)$  and  $p_0(x - \delta, t)$  are determined as,

$$p_0(x + \Delta) = p_0(x) - \frac{\partial p_0}{\partial x} \Delta + \frac{1}{2} \frac{\partial^2 p_0}{\partial x^2} \Delta^2 + HOT.. \quad (2.54)$$

and

$$p_0(x - \delta) = p_0(x) - \frac{\partial p_0}{\partial x} \delta + \frac{1}{2} \frac{\partial^2 p_0}{\partial x^2} \delta^2 + HOT.. \quad (2.55)$$

Then Eqn 2.54 and Eqn.2.55 are substituted into the Eqn.2.53, so our relation becomes as follows;

$$\begin{aligned} \frac{\partial p_1}{\partial t} = & k_A^- p_0 - k_A^- \frac{\partial p_0}{\partial x} \Delta + k_A^- \frac{1}{2} \frac{\partial^2 p_0}{\partial x^2} \Delta^2 + k_B^+ p_0 - k_B^+ \frac{\partial p_0}{\partial x} \delta + k_B^+ \frac{1}{2} \frac{\partial^2 p_0}{\partial x^2} \delta^2 \\ & - (k_A^+ + k_B^-) p_1 \end{aligned} \quad (2.56)$$

After making some simplifications;

$$\begin{aligned} \frac{\partial p_1}{\partial t} = & p_0(k_A^- + k_B^+) + \frac{\partial p_0}{\partial x} (k_A^- \Delta - k_B^+ \delta) + \frac{\partial^2 p_0}{\partial x^2} \frac{1}{2} (k_A^- \Delta^2 - k_B^+ \delta^2) \\ & - p_1(k_A^+ + k_B^-) \end{aligned} \quad (2.57)$$

## 2.7 THE FOUR-STATE MODEL

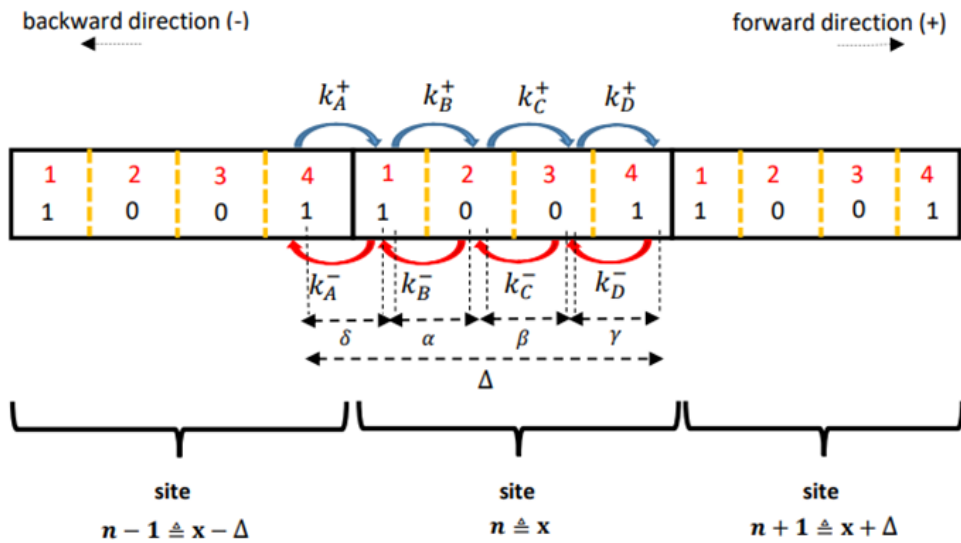


Figure 2.17: Four State Model

In Figure 2.17 black numbers show the attached and unattached states but red numbers denote the bound or unbound probabilities for convenience. Red 1 is bound probability from attached state at site  $n-1$  to state 1 at the next site  $n$  (which is shown by  $p_1$ ), red 2 is unbound probability from bound state to unbound state (which is shown by  $p_2$ ), red 3 is again unbound probability from unbound state to unbound state (which is shown by  $p_3$ ), and finally red 4 is bound probability from unbound state to bound state (which is shown by  $p_4$ ).

We assume that in going from state 1 to state 0, 0 to 0 and 0 to 1 at a given site, the distance traveled by the motor is represented by  $\alpha$ ,  $\beta$  and  $\gamma$  respectively and in going from state 1 at one site to state 1 at the next neighboring site, the distance moved by the motor is  $\delta$ .  $\Delta$  is the periodicity of the cytoskeletal filament on which the motor moves and is formulated by the sum of all the distances  $\Delta = \delta + \alpha + \beta + \gamma$ .

Before formulating the probability functions, this four state model is inspired from our four state cross bridge model which is shown in Figure 2.18 below.

The bound probability can be written in the following form.

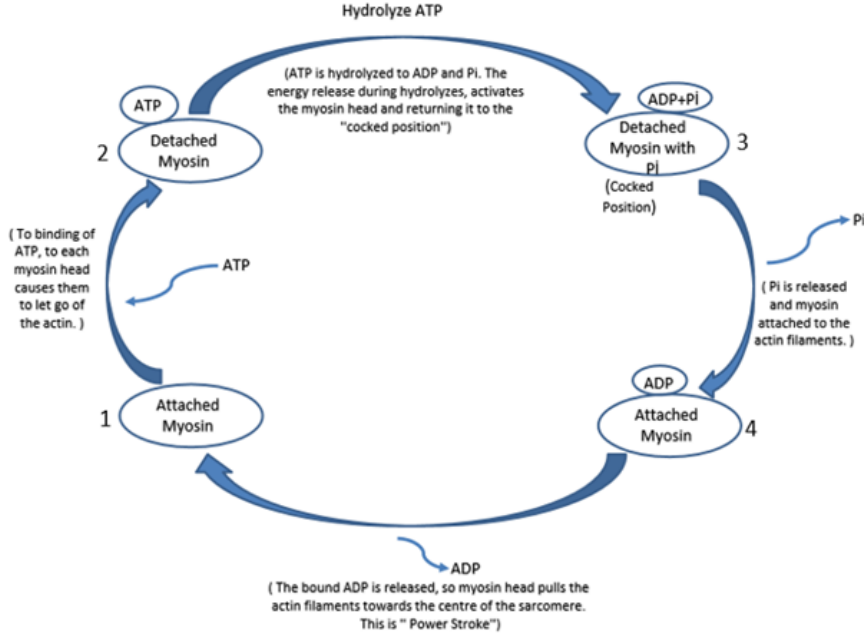


Figure 2.18: Four State Model

$$\begin{aligned}
 p_1(x, t + \Delta t) = & k_A^+ p_4(x - \delta, t) \Delta t + k_B^- p_2(x + \alpha, t) \Delta t \\
 & + [1 - (k_A^- + k_B^+) \Delta t] p_1(x, t)
 \end{aligned} \tag{2.58}$$

According to Taylor expansion,  $p_4(x - \delta, t)$  and  $p_2(x + \alpha, t)$  are determined as,

$$p_4(x - \delta) = p_4(x) - \frac{\partial p_4}{\partial x} \delta + \frac{1}{2} \frac{\partial^2 p_4}{\partial x^2} \delta^2 + \text{HOT.} \tag{2.59}$$

and

$$p_2(x + \alpha) = p_2(x) - \frac{\partial p_2}{\partial x} \alpha + \frac{1}{2} \frac{\partial^2 p_2}{\partial x^2} \alpha^2 + \text{HOT.} \tag{2.60}$$

Then Eqn 2.59 and Eqn. 2.60 are substituted into the Eqn. 2.58 and if we write the time evolution of Eqn 2.58, we can obtain the following relation;

$$\begin{aligned}
 \frac{\partial p_1}{\partial t} = & k_A^+ p_4 - k_A^+ \frac{\partial p_4}{\partial x} \delta + k_A^+ \frac{1}{2} \frac{\partial^2 p_4}{\partial x^2} \delta^2 + k_B^- p_2 + k_B^- \frac{\partial p_2}{\partial x} \alpha + k_B^- \frac{1}{2} \frac{\partial^2 p_2}{\partial x^2} \alpha^2 \\
 & - (k_A^- + k_B^+) p_1
 \end{aligned} \tag{2.61}$$

If we rewrite the Eqn. 2.61 with the help of Finite Difference Method (indicial form) we obtain the following relation;

$$\begin{aligned} \frac{p_{1j}^{n+1} - p_{1j}^n}{\Delta t} = & k_A^+ p_{4j}^n + k_B^- p_{2j}^n - (k_B^+ + k_A^-) p_{1j}^n - k_A^+ \delta \left( \frac{p_{4j+1}^n - p_{4j-1}^n}{2\Delta} \right) \\ & + k_B^- \alpha \left( \frac{p_{2j+1}^n - p_{2j-1}^n}{2\Delta} \right) + k_A^+ \frac{1}{2} \delta^2 \left( \frac{p_{4j+1}^n - 2p_{4j}^n + p_{4j-1}^n}{\Delta^2} \right) \\ & + k_B^- \frac{1}{2} \alpha^2 \left( \frac{p_{2j+1}^n - 2p_{2j}^n + p_{2j-1}^n}{\Delta^2} \right) \end{aligned} \quad (2.62)$$

After making some simplifications;

$$\begin{aligned} p_{1j}^{n+1} = & p_{1j}^n + \Delta t \left[ k_A^+ p_{4j}^n + k_B^- p_{2j}^n - (k_B^+ + k_A^-) p_{1j}^n - k_A^+ \delta \left( \frac{p_{4j+1}^n - p_{4j-1}^n}{2\Delta} \right) \right. \\ & + k_B^- \alpha \left( \frac{p_{2j+1}^n - p_{2j-1}^n}{2\Delta} \right) + k_A^+ \frac{1}{2} \delta^2 \left( \frac{p_{4j+1}^n - 2p_{4j}^n + p_{4j-1}^n}{\Delta^2} \right) \\ & \left. + k_B^- \frac{1}{2} \alpha^2 \left( \frac{p_{2j+1}^n - 2p_{2j}^n + p_{2j-1}^n}{\Delta^2} \right) \right] \end{aligned} \quad (2.63)$$

The probability of the second state which is the unbound probability and denoted by  $p_2$  can be formulated as;

$$\begin{aligned} p_2(x, t + \Delta t) = & k_B^+ p_1(x - \alpha, t) \Delta t + k_C^- p_3(x + \beta, t) \Delta t \\ & + [1 - (k_B^- + k_C^+ \Delta t)] p_2(x, t) \end{aligned} \quad (2.64)$$

According to Taylor expansion,  $p_1(x - \alpha)$  and  $p_3(x + \beta)$  are determined as,

$$p_1(x - \alpha) = p_1(x) - \frac{\partial p_1}{\partial x} \alpha + \frac{1}{2} \frac{\partial^2 p_1}{\partial x^2} \alpha^2 + \text{HOT..} \quad (2.65)$$

and

$$p_3(x + \beta) = p_3(x) - \frac{\partial p_3}{\partial x} \beta + \frac{1}{2} \frac{\partial^2 p_3}{\partial x^2} \beta^2 + \text{HOT..} \quad (2.66)$$

Then Eqn 2.65 and Eqn. 2.66 are substituted into the Eqn. 2.64 and if we write the time evolution of Eqn 2.64, we can obtain the following relation;

$$\begin{aligned} \frac{\partial p_2}{\partial t} = & k_B^+ p_1 - k_B^- \frac{\partial p_1}{\partial x} \alpha + k_B^+ \frac{1}{2} \frac{\partial^2 p_1}{\partial x^2} \alpha^2 + k_C^- p_3 + k_C^- \frac{\partial p_3}{\partial x} \beta + k_C^- \frac{1}{2} \frac{\partial^2 p_3}{\partial x^2} \beta^2 \\ & - (k_B^- + k_C^+) p_2 \end{aligned} \quad (2.67)$$

If we rewrite the Eqn. 2.67 with the help of Finite Difference Method (indicial form) we obtain the following relation;

$$\begin{aligned} \frac{p_{2j}^{n+1} - p_{2j}^n}{\Delta t} = & k_B^+ p_{1j}^n + k_C^- p_{3j}^n - (k_B^- + k_C^+) p_{2j}^n - k_B^+ \alpha \left( \frac{p_{1j+1}^n - p_{1j-1}^n}{2\Delta} \right) \\ & + k_C^- \beta \left( \frac{p_{3j+1}^n - p_{3j-1}^n}{2\Delta} \right) + k_A^+ \frac{1}{2} \alpha^2 \left( \frac{p_{1j+1}^n - 2p_{1j}^n + p_{1j-1}^n}{\Delta^2} \right) \\ & + k_C^- \frac{1}{2} \beta^2 \left( \frac{p_{3j+1}^n - 2p_{3j}^n + p_{3j-1}^n}{\Delta^2} \right) \end{aligned} \quad (2.68)$$

After making some simplifications;

$$\begin{aligned} p_{2j}^{n+1} = & p_{2j}^n + \Delta t \left[ k_B^+ p_{1j}^n + k_C^- p_{3j}^n - (k_B^- + k_C^+) p_{2j}^n - k_B^+ \alpha \left( \frac{p_{1j+1}^n - p_{1j-1}^n}{2\Delta} \right) \right. \\ & + k_C^- \beta \left( \frac{p_{3j+1}^n - p_{3j-1}^n}{2\Delta} \right) + k_A^+ \frac{1}{2} \alpha^2 \left( \frac{p_{1j+1}^n - 2p_{1j}^n + p_{1j-1}^n}{\Delta^2} \right) \\ & \left. + k_C^- \frac{1}{2} \beta^2 \left( \frac{p_{3j+1}^n - 2p_{3j}^n + p_{3j-1}^n}{\Delta^2} \right) \right] \end{aligned} \quad (2.69)$$

If we follow the same procedure as above, third and fourth states probabilities can be found in the following forms;

$$\begin{aligned} p_3(x, t + \Delta t) = & k_C^+ p_2(x - \beta, t) \Delta t + k_D^- p_4(x + \gamma, t) \Delta t \\ & + [1 - (k_C^- + k_D^+ \Delta t)] p_3(x, t) \end{aligned} \quad (2.70)$$

According to Taylor expansion,  $p_2(x - \beta)$  and  $p_4(x + \gamma)$  are determined as,



$$p_2(x - \beta) = p_2(x) - \frac{\partial p_2}{\partial x} \beta + \frac{1}{2} \frac{\partial^2 p_2}{\partial x^2} \beta^2 + \text{HOT..} \quad (2.71)$$

and

$$p_4(x + \gamma) = p_4(x) - \frac{\partial p_4}{\partial x} \gamma + \frac{1}{2} \frac{\partial^2 p_4}{\partial x^2} \gamma^2 + \text{HOT..} \quad (2.72)$$

Then Eqn 2.71 and Eqn. 2.72 are substituted into the Eqn. 2.70 and if we write the time evolution of Eqn 2.70, we can obtain the following relation;

$$\begin{aligned} \frac{\partial p_3}{\partial t} = & k_C^+ p_2 - k_C^+ \frac{\partial p_2}{\partial x} \beta + k_C^+ \frac{1}{2} \frac{\partial^2 p_2}{\partial x^2} \beta^2 + k_D^- p_4 + k_D^- \frac{\partial p_4}{\partial x} \gamma + k_D^- \frac{1}{2} \frac{\partial^2 p_4}{\partial x^2} \gamma^2 \\ & - (k_C^- + k_D^+) p_3 \end{aligned} \quad (2.73)$$

If we rewrite the Eqn. 2.73 with the help of Finite Difference Method (indicial form) we obtain the following relation;

$$\begin{aligned} p_{3_j}^{n+1} = & p_{3_j}^n + \Delta t \left[ k_C^+ p_{2_j}^n + k_D^- p_{4_j}^n - (k_C^- + k_D^+) p_{3_j}^n - k_C^+ \beta \left( \frac{p_{2_{j+1}}^n - p_{2_{j-1}}^n}{2\Delta} \right) \right. \\ & + k_D^- \gamma \left( \frac{p_{4_{j+1}}^n - p_{4_{j-1}}^n}{2\Delta} \right) + k_C^+ \frac{1}{2} \beta^2 \left( \frac{p_{2_{j+1}}^n - 2p_{2_j}^n + p_{2_{j-1}}^n}{\Delta^2} \right) \\ & \left. + k_D^- \frac{1}{2} \gamma^2 \left( \frac{p_{4_{j+1}}^n - 2p_{4_j}^n + p_{4_{j-1}}^n}{\Delta^2} \right) \right] \end{aligned} \quad (2.74)$$

And finally fourth state probability is as follows;

$$\begin{aligned} p_4(x, t + \Delta t) = & k_D^+ p_3(x - \gamma, t) \Delta t + k_A^- p_1(x + \delta, t) \Delta t \\ & + [1 - (k_D^- + k_A^+ \Delta t)] p_4(x, t) \end{aligned} \quad (2.75)$$

According to Taylor expansion,  $p_3(x - \gamma)$  and  $p_1(x + \delta)$  are determined as,

$$p_3(x - \gamma) = p_3(x) - \frac{\partial p_3}{\partial x} \gamma + \frac{1}{2} \frac{\partial^2 p_3}{\partial x^2} \gamma^2 + \text{HOT..} \quad (2.76)$$

and

$$p_1(x + \delta) = p_4(x) - \frac{\partial p_4}{\partial x} \delta + \frac{1}{2} \frac{\partial^2 p_4}{\partial x^2} \delta^2 + \text{HOT..} \quad (2.77)$$

Then Eqn 2.76 and Eqn. 2.77 are substituted into the Eqn. 2.75 and if we write the time evolution of Eqn 2.70, we can obtain the following relation;

$$\begin{aligned} \frac{\partial p_4}{\partial t} = & k_D^+ p_3 - k_D^+ \frac{\partial p_3}{\partial x} \gamma + k_D^+ \frac{1}{2} \frac{\partial^2 p_3}{\partial x^2} \gamma^2 + k_A^- p_1 + k_A^- \frac{\partial p_1}{\partial x} \delta + k_A^- \frac{1}{2} \frac{\partial^2 p_1}{\partial x^2} \delta^2 \\ & - (k_D^- + k_A^+) p_4 \end{aligned} \quad (2.78)$$

If we rewrite the Eqn. 2.78 with the help of Finite Difference Method (indicial form) we obtain the following relation;

$$\begin{aligned} p_{4_j}^{n+1} = & p_{4_j}^n + \Delta t \left[ k_D^+ p_{3_j}^n + k_A^- p_{1_j}^n - (k_D^- + k_A^+) p_{4_j}^n - k_D^+ \gamma \left( \frac{p_{3_{j+1}}^n - p_{3_{j-1}}^n}{2\Delta} \right) \right. \\ & + k_A^- \delta \left( \frac{p_{1_{j+1}}^n - p_{1_{j-1}}^n}{2\Delta} \right) + k_D^+ \frac{1}{2} \gamma^2 \left( \frac{p_{3_{j+1}}^n - 2p_{3_j}^n + p_{3_{j-1}}^n}{\Delta^2} \right) \\ & \left. + k_A^- \frac{1}{2} \delta^2 \left( \frac{p_{1_{j+1}}^n - 2p_{1_j}^n + p_{1_{j-1}}^n}{\Delta^2} \right) \right] \end{aligned} \quad (2.79)$$

## REFERENCES

- [1] Nigg, B. M., & Herzog, W. (1999). *Biomechanics of the musculo-skeletal system* (Vol. 2). New York: Wiley.
- [2] Herman, I. P. (2016). *Physics of the human body*. Springer.
- [3] Lieber, R. L. (2002). *Skeletal muscle structure, function, and plasticity*. Lippincott Williams & Wilkins.
- [4] Huxley, A. F. (1957). Muscle structure and theories of contraction. *Prog. Biophys. Biophys. Chem*, 7, 255-318.
- [5] Huxley, A. F. (2000). Cross-bridge action: present views, prospects, and unknowns. *Journal of Biomechanics*, 33(10), 1189-1195.
- [6] Huxley, A. F., & Simmons, R. M. (1971). Proposed mechanism of force generation in striated muscle. *Nature*, 233(5321), 533.
- [7] Huxley, H. E. (1969). The mechanism of muscular contraction. *Science*, 164(3886), 1356-1365.
- [8] Barclay, C. J., Woledge, R. C., & Curtin, N. A. (2010). Inferring crossbridge properties from skeletal muscle energetics. *Progress in Biophysics and Molecular Biology*, 102(1), 53-71.
- [9] Zahalak, G. I. (1981). A distribution-moment approximation for kinetic theories of muscular contraction. *Mathematical Biosciences*, 55(1-2), 89-114.
- [10] Zahalak, G. I. (1986). A comparison of the mechanical behavior of the cat soleus muscle with a distribution-moment model. *Journal of Biomechanical Engineering*, 108(2), 131-140.
- [11] Zahalak, G. I., & Ma, S. P. (1990). Muscle activation and contraction: constitutive relations based directly on cross-bridge kinetics. *Journal of Biomechanical Engineering*, 112(1), 52-62.

- [12] Zahalak, G. I. (2000). The two-state cross bridge model as a link between molecular and macroscopic muscle mechanics. *Skeletal Muscle Mechanics: from Mechanisms to Function*, John Wiley & Sons, Ltd., Chichester, UK, 95-124.
- [13] Zahalak, G. I., & Motabarzadeh, I. (1997). A re-examination of calcium activation in the Huxley cross-bridge model. *Journal of Biomechanical Engineering*, 119(1), 20-29.
- [14] Levitsky, D. I. (2004). Actomyosin systems of biological motility. *Biochemistry (Moscow)*, 69(11), 1177-1189.
- [15] Boal, D. (2012). *Mechanics of the Cell*. Cambridge University Press.
- [16] Wong, D. T., Gierke, S., Chang, V., & Taunton, J. (2007). Mechanism of actin network attachment to moving membranes: barbed end capture by N-WASP WH2 domains. *Cell*, 128(5), 901-913.
- [17] Rasnick, D., & Duesberg, P. H. (1999). How aneuploidy affects metabolic control and causes cancer. *Biochemical Journal*, 340(3), 621-630.
- [18] Golyshina, O. V., Pivovarova, T. A., Karavaiko, G. I., Kondratéva, T. F., Moore, E. R., Abraham, W. R., ... & Golyshin, P. N. (2000). *Ferroplasma acidiphilum* gen. nov., sp. nov., an acidophilic, autotrophic, ferrous-iron-oxidizing, cell-wall-lacking, mesophilic member of the *Ferroplasmaceae* fam. nov., comprising a distinct lineage of the Archaea. *International journal of systematic and evolutionary microbiology*, 50(3), 997-1006.
- [19] Alberts, B., Johnson, A., Lewis, J., Raff, M., Roberts, K., & Walter, P. (2007). *Molecular biology of the cell*. Garland science. New York, 1227-1242.
- [20] Trepap, X., Deng, L., An, S. S., Navajas, D., Tschumperlin, D. J., Gerthoffer, W. T., ... & Fredberg, J. J. (2007). Universal physical responses to stretch in the living cell. *Nature*, 447(7144), 592.
- [21] Kollmannsberger, P., Mierke, C. T., & Fabry, B. (2011). Nonlinear viscoelasticity of adherent cells is controlled by cytoskeletal tension. *Soft Matter*, 7(7), 3127-3132.

- [22] Kumar, S., Maxwell, I. Z., Heisterkamp, A., Polte, T. R., Lele, T. P., Salanga, M., ... & Ingber, D. E. (2006). Viscoelastic retraction of single living stress fibers and its impact on cell shape, cytoskeletal organization, and extracellular matrix mechanics. *Biophysical journal*, 90(10), 3762-3773.
- [23] Kasza, K. E., Rowat, A. C., Liu, J., Angelini, T. E., Brangwynne, C. P., Koenderink, G. H., & Weitz, D. A. (2007). The cell as a material. *Current opinion in cell biology*, 19(1), 101-107.
- [24] Tee, S. Y., Bausch, A. R., & Janmey, P. A. (2009). The mechanical cell. *Current Biology*, 19(17), R745-R748.
- [25] Mofrad, M. R. (2009). Rheology of the cytoskeleton. *Annual Review of Fluid Mechanics*, 41, 433-453.
- [26] Gittes, F., Mickey, B., Nettleton, J., & Howard, J. (1993). Flexural rigidity of microtubules and actin filaments measured from thermal fluctuations in shape. *The Journal of cell biology*, 120(4), 923-934.
- [27] Kasza, K. E., Broedersz, C. P., Koenderink, G. H., Lin, Y. C., Messner, W., Millman, E. A., ... & Weitz, D. A. (2010). Actin filament length tunes elasticity of flexibly cross-linked actin networks. *Biophysical journal*, 99(4), 1091-1100.
- [28] Mofrad, M. R., & Kamm, R. D. (Eds.). (2006). *Cytoskeletal mechanics: models and measurements in cell mechanics*. Cambridge University Press.
- [29] Xu, J., Tseng, Y., & Wirtz, D. (2000). Strain hardening of actin filament networks regulation by the dynamic cross-linking protein  $\alpha$ -actinin. *Journal of Biological Chemistry*, 275(46), 35886-35892.
- [30] Lieleg, O., Claessens, M. M., & Bausch, A. R. (2010). Structure and dynamics of cross-linked actin networks. *Soft Matter*, 6(2), 218-225.
- [31] Herrmann, H., Bär, H., Kreplak, L., Strelkov, S. V., & Aebi, U. (2007). Intermediate filaments: from cell architecture to nanomechanics. *Nature reviews Molecular cell biology*, 8(7), 562.

- [32] Ingber, D. E., Wang, N., & Stamenović, D. (2014). Tensegrity, cellular biophysics, and the mechanics of living systems. *Reports on Progress in Physics*, 77(4), 046603.
- [33] Rammensee, S., Janmey, P. A., & Bausch, A. R. (2007). Mechanical and structural properties of in vitro neurofilament hydrogels. *European Biophysics Journal*, 36(6), 661-668.
- [34] Mücke, N., Kreplak, L., Kirmse, R., Wedig, T., Herrmann, H., Aebi, U., & Langowski, J. (2004). Assessing the flexibility of intermediate filaments by atomic force microscopy. *Journal of molecular biology*, 335(5), 1241-1250.
- [35] Janmey, P. A., Euteneuer, U., Traub, P., & Schliwa, M. (1991). Viscoelastic properties of vimentin compared with other filamentous biopolymer networks. *The Journal of cell biology*, 113(1), 155-160.
- [36] Goldman, R. D., Goldman, A. E., Green, K. J., Jones, J. C., Jones, S. M., & Yang, H. Y. (1986). Intermediate filament networks: organization and possible functions of a diverse group of cytoskeletal elements. *J Cell Sci*, 1986(Supplement 5), 69-97.
- [37] Na, S., Chowdhury, F., Tay, B., Ouyang, M., Gregor, M., Wang, Y., ... & Wang, N. (2009). Plectin contributes to mechanical properties of living cells. *American Journal of Physiology-Cell Physiology*.
- [38] Wiche, G. (1989). Plectin: General Overview and Appraisal of its potential Role as a Subunit Protein of the Cytomatri. *Critical reviews in biochemistry and molecular biology*, 24(1), 41-67.
- [39] Svitkina, T. M., Verkhovsky, A. B., & Borisy, G. G. (1996). Plectin sidearms mediate interaction of intermediate filaments with microtubules and other components of the cytoskeleton. *The Journal of cell biology*, 135(4), 991-1007.
- [40] Rathje, L. S. Z., Nordgren, N., Pettersson, T., Rönnlund, D., Widengren, J., Aspenström, P., & Gad, A. K. (2014). Oncogenes induce a vimentin filament collapse mediated by HDAC6 that is linked to cell stiffness. *Proceedings of the National Academy of Sciences*, 111(4), 1515-1520.

- [41] Suresh, S., Spatz, J., Mills, J. P., Micoulet, A., Dao, M., Lim, C. T., ... & Seufferlein, T. (2005). Connections between single-cell biomechanics and human disease states: gastrointestinal cancer and malaria. *Acta biomaterialia*, 1(1), 15-30.
- [42] Maniotis, A. J., Chen, C. S., & Ingber, D. E. (1997). Demonstration of mechanical connections between integrins, cytoskeletal filaments, and nucleoplasm that stabilize nuclear structure. *Proceedings of the National Academy of Sciences*, 94(3), 849-854.
- [43] Mitchison, T. J., & Cramer, L. P. (1996). Actin-based cell motility and cell locomotion. *Cell*, 84(3), 371-379.
- [44] Ananthkrishnan, R., & Ehrlicher, A. (2007). The forces behind cell movement. *International journal of biological sciences*, 3(5), 303.
- [45] Pijnenborg, R., Bland, J. M., Robertson, W. A., & Brosens, I. (1983). Uteroplacental arterial changes related to interstitial trophoblast migration in early human pregnancy. *Placenta*, 4(4), 397-413.
- [46] Boal, D., & Boal, D. H. (2012). *Mechanics of the Cell*. Cambridge University Press.
- [47] Pollard, T. D., & Borisy, G. G. (2003). Cellular motility driven by assembly and disassembly of actin filaments. *Cell*, 112(4), 453-465.
- [48] B. Alberts, A. Johnson, J. Lewis, M. Raff, K. Roberts, and P. Walter, *Molecular Biology of the Cell* (Garland, New York, 2002), 4th ed., ISBN 0-8153-3218-1 ; 0-8153-4072-9.
- [49] D. Bray, *Cell Movements* (Garland, New York, 2001), 2nd ed., ISBN 0-8153-3282-3.
- [50] H. E. Huxley, *Proc. R. Soc. Lond. B Biol. Sci.* 141, 59 (1953).
- [51] J. Hanson and H. E. Huxley, *Nature* 172, 530 (1953).
- [52] H. E. Huxley, *Biochim Biophys Acta* 12, 387 (1953).
- [53] A. F. Huxley and R. Niedergerke, *Nature* 173, 971 (1954).

- [54] H. Huxley and J. Hanson, *Nature* 173, 973 (1954).
- [55] C. G. dos Remedios, D. Chhabra, M. Kekic, I. V. Dedova, M. Tsubakihara, D. A. Berry, and N. J. Nosworthy, *Physiol. Rev.* 83, 433 (2003).
- [56] R. D. Astumian, *Science* 276, 917 (1997).
- [57] P. Reimann, *Phys. Rep.* 361, 57 (2002).
- [58] F. Julicher, A. Ajdari, and J. Prost, *Rev. Mod. Phys.* 69, 1269 (1997).
- [59] G. I. Taylor, *Proc. R. Soc. A* 209, 447 (1951).
- [60] E. M. Purcell, *Am. J. Phys.* 45, 3 (1977).
- [61] A. M. Turing, *Phil. Trans. Roy. Soc. (Lond.)* 237, 37 (1952).
- [62] S. Kondo, *Genes Cells* 7, 535 (2002).
- [63] See, for example, <http://www.cytoskeletons.com/database.ph>
- [64] H. E. Huxley, *Eur. J. Biochem.* 271, 1403 (2004).
- [65] C. G. dos Remedios, D. Chhabra, M. Kekic, I. V. Dedova, M. Tsubakihara, D. A. Berry, and N. J. Nosworthy, *Physiol. Rev.* 83, 433 (2003)
- [66] P. Van Liedekerke, M.M. Palm, N. Jagiella, D. Drasdo, Simulating tissue mechanics with agent-based models: Concepts, perspectives and some novel results, *Comput. Part. Mech.* 2 (2015) 401–444. <http://dx.doi.org/10.1007/s40571-015-0082-3>.
- [67] .A. Camley, W.-J. Rappel, Physical models of collective cell motility: From cell to tissue, *J. Phys. D. Appl. Phys.* 50 (2017) 113002. <http://dx.doi.org/10.1088/1361-6463/aa56fe>.
- [68] E.A. Novikova, M. Raab, D.E. Discher, C. Storm, Persistence-driven durotaxis: Generic, directed motility in rigidity gradients, *Phys. Rev. Lett.* 118 (2017) 78103. <http://dx.doi.org/10.1103/PhysRevLett.118.078103>.
- [69] N. Sepúlveda, L. Petitjean, O. Cochet, E. Grasland-Mongrain, P. Silberzan, V. Hakim, Collective cell motion in an epithelial sheet can be quantitatively described by a stochastic interacting particle model, *PLoS Comput. Biol.* 9 (2013) e1002944. <http://dx.doi.org/10.1371/journal.pcbi.1002944>.



- [70] B. Smeets, R. Alert, J. Pešek, I. Pagonabarraga, H. Ramon, R. Vincent, Emergent structures and dynamics of cell colonies by contact inhibition of locomotion, *Proc. Natl. Acad. Sci.* 113 (2016) 14621–14626. <http://dx.doi.org/10.1073/pnas.1521151113>.
- [71] D. Bi, J.H. Lopez, J.M. Schwarz, M.L. Manning, A density-independent rigidity transition in biological tissues, *Nat. Phys.* 11 (2015) 1074–1079. <http://dx.doi.org/10.1038/nphys3471>.
- [72] A.J. Loza, S. Koride, G.V. Schimizzi, B. Li, S.X. Sun, G.D. Longmore, Cell density and actomyosin contractility control the organization of migrating collectives within an epithelium, *Mol. Biol. Cell.* 27 (2016) 3459–3470. <http://dx.doi.org/10.1091/mbc.E16-05-0329>.
- [73] J.-A. Park, J.H. Kim, D. Bi, J.A. Mitchel, N.T. Qazvini, K. Tantisira, C.Y. Park, M. McGill, S.-H. Kim, B. Gweon, J. Notbohm, R. Steward Jr., S. Burger, S.H. Randell, A.T. Kho, D.T. Tambe, C. Hardin, S.A. Shore, E. Israel, D.A. Weitz, D.J. Tschumperlin, E.P. Henske, S.T. Weiss, M.L. Manning, J.P. Butler, J.M. Drazen, J.J. Fredberg, Unjamming and cell shape in the asthmatic airway epithelium, *Nature Mater.* 14 (2015) 1040–1048. <http://dx.doi.org/10.1038/nmat4357>.
- [74] D. Bi, X. Yang, M.C. Marchetti, M.L. Manning, Motility-driven glass and jamming transitions in biological tissues, *Phys. Rev. X* 6 (2016) 1–12. <http://dx.doi.org/10.1103/PhysRevX.6.021011>.
- [75] D.L. Barton, S. Henkes, C.J. Weijer, R. Sknepnek, Active vertex model for cell-resolution description of epithelial tissue mechanics, *PLOS Comput. Biol.* 13 (2017) e1005569. <http://dx.doi.org/10.1371/journal.pcbi.1005569>.
- [76] P. Mosaffa, A. Rodríguez-Ferran, J.J. Muñoz, Hybrid cell-centred/vertex model for multicellular systems with equilibrium-preserving remodelling, (2017) 1–33. <http://dx.doi.org/10.1002/cnm.2928>.
- [77] T. Odenthal, B. Smeets, P. Van Liedekerke, E. Tjiskens, H. Van Oosterwyck, H. Ramon, Analysis of initial cell spreading using mechanistic contact formulations for a deformable cell model, *PLoS Comput. Biol.* 9 (2013) e1003267. <http://dx.doi.org/10.1371/journal.pcbi.1003267>.

- [78] A. Moure, H. Gomez, Phase-field model of cellular migration: Three-dimensional simulations in fibrous networks, *Comput. Methods Appl. Mech. Engrg.* 320 (2017) 162–197. <http://dx.doi.org/10.1016/j.cma.2017.03.025>.
- [79] A. Czirák, K. Varga, E. Méhes, A. Szabó, Collective cell streams in epithelial monolayers depend on cell adhesion, *New J. Phys.* 15 (2013) 75006. <http://dx.doi.org/10.1088/1367-2630/15/7/075006>.
- [80] M.M. Palm, R.M.H. Merks, Vascular networks due to dynamically arrested crystalline ordering of elongated cells, *Phys.Rev.E* 87 (2013). <http://dx.doi.org/10.1103/PhysRevE.87.012725>.
- [81] J. Escribano, M.T. Sánchez, J.M. García-Aznar, A discrete approach for modeling cell–matrix adhesions, *Comput. Part. Mech.* 1 (2014) 117–130. <http://dx.doi.org/10.1007/s40571-014-0006-7>.
- [82] T. Heck, B. Smeets, S. Vanmaercke, P. Bhattacharya, T. Odenthal, H. Ramon, H. Van Oosterwyck, P. Van Liedekerke, Modeling extracellular matrix viscoelasticity using smoothed particle hydrodynamics with improved boundary treatment, *Comput. Methods Appl. Mech. Engrg.* 322 (2017) 515–540. <http://dx.doi.org/10.1016/j.cma.2017.04.031>.
- [83] J.C. Arciero, Q. Mi, M.F. Branca, D.J. Hackam, D. Swigon, Continuum model of collective cell migration in wound healing and colony expansion, *Biophys. J.* 100 (2011) 535–543. <http://dx.doi.org/10.1016/j.bpj.2010.11.083>.
- [84] A. Ravasio, I. Cheddadi, T. Chen, T. Pereira, H.T. Ong, C. Bertocchi, A. Brugues, A. Jacinto, A.J. Kabla, Y. Toyama, X. Trepát, N. Gov, L. Neves de Almeida, B. Ladoux, Gap geometry dictates epithelial closure efficiency, *Nature Commun.* 6 (2015) 7683. <http://dx.doi.org/10.1038/ncomms8683>.
- [85] C. Valero, E. Javierre, J.M. García-Aznar, M.J. Gómez-Benito, Nonlinear finite element simulations of injuries with free boundaries: Application to surgical wounds, *Int. J. Numer. Method. Biomed. Eng.* 30 (2014) 616–633. <http://dx.doi.org/10.1002/cnm.2621>.
- [86] P. Moreo, J.M. García-Aznar, M. Doblaré, Modeling mechanosensing and its

- effect on the migration and proliferation of adherent cells, *Acta Biomater.* 4 (2008) 613–621. <http://dx.doi.org/10.1016/j.actbio.2007.10.014>.
- [87] R. Sunyer, V. Conte, J. Escribano, A. Elosegui-Artola, A. Labernadie, L. Valon, D. Navajas, J.M. Garcia-Aznar, J.J. Munoz, P. Roca Cusachs, X. Trepatal, Collective cell durotaxis emerges from long-range intercellular force transmission, *Science* (80) 353 (2016) 1157–1161. <http://dx.doi.org/10.1126/science.aaf7119>.
- [88] Pugh, A. (1976) *Introduction to Tensegrity* (Univ. of Calif. Press, Berkeley, CA).
- [89] Stamenovic ´, D., Fredberg, J. J., Wang, N., Butler, J. P. & Ingber, D. E. (1996) *J. Theor. Biol.* 181, 125–136.
- [90] Stamenovic ´, D. & Coughlin, M. F. (1999) *J. Theor. Biol.* 201, 63–74.
- [91] Siegelbaum, S. A., & Hudspeth, A. J. (2000). *Principles of neural science* (Vol. 4, pp. 1227-1246). E. R. Kandel, J. H. Schwartz, & T. M. Jessell (Eds.). New York: McGraw-Hill.
- [92] Hughes, T. J. (2012). *The finite element method: linear static and dynamic finite element analysis*. Courier Corporation.
- [93] Belytschko, T., Liu, W. K., Moran, B., & Elkhodary, K. (2013). *Nonlinear finite elements for continua and structures*. John Wiley & Sons
- [94] Newmark, N. M. (1959). A method of computation for structural dynamics. *Journal of the Engineering Mechanics Division*, 85(3), 67-94.
- [95] Janmey, P. A., Euteneuer, U., Traub, P., & Schliwa, M. (1991). Viscoelastic properties of vimentin compared with other filamentous biopolymer networks. *The Journal of cell biology*, 113(1), 155-160.
- [96] Goldman, R. D., Goldman, A. E., Green, K. J., Jones, J. C., Jones, S. M., & Yang, H. Y. (1986). Intermediate filament networks: organization and possible functions of a diverse group of cytoskeletal elements. *J Cell Sci*, 1986(Supplement 5), 69-97.
- [97] “Physical biology of the cell,” *Choice Reviews Online*, vol. 46, no. 09. pp. 46-5006-46–5006, 2009, doi: 10.5860/choice.46-5006.

- [98] K. A. Dill, S. Bromberg, and D. Stigter, *Molecular Driving Forces*. 2010.
- [99] U. Seifert, "Stochastic thermodynamics, fluctuation theorems and molecular machines," *Reports Prog. Phys.*, vol. 75, no. 12, 2012, doi: 10.1088/0034-4885/75/12/126001.
- [100] A. F. Huxley, "NoMuscle structure and theories of contraction. Prog.," *Biophys. Biophys. Chem*, vol. 7, pp. 255-318., 1957.
- [101] M. C. Atkins, P. W., & Symons, "Physical Chemistry," 2010.
- [102] C. Maes, "On the Origin and the Use of Fluctuation Relations for the Entropy," *Poincaré Semin*. 2003, vol. 2, pp. 145–191, 2004, doi: 10.1007/978–3–0348–7932–3<sub>8</sub>.
- [103] T. L. Hill, *An introduction to statistical thermodynamics*. 1986.
- [104] K. S. Schmitz, "Physical Chemistry: Multidisciplinary Applications in Society," Elsevier, 2018.
- [105] D. Boal, *Mechanics of the cell*, second edition. 2012.
- [106] H.E.Huxley, "The Mechanism of Muscular Contraction Author(s) Published by: Scientific American , a division of Nature America , vol. 213, no. 6, pp. 18–27, 1965
- [107] Gordon, A. M., Andrew F. Huxley, and F. J. Julian. "The variation in isometric tension with sarcomere length in vertebrate muscle fibres." *The Journal of physiology* 184.1 (1966): 170-192.
- [108] Huxley, Andrew F., and Ro M. Simmons. "Proposed mechanism of force generation in striated muscle." *Nature* 233.5321 (1971): 533-538.
- [109] Huxley, A. F. "Muscular contraction." *The Journal of physiology* 243.1 (1974): 1-43.
- [110] Walker, Sheppard M., and G. Randolph Schrodt. "I segment lengths and thin filament periods in skeletal muscle fibers of the Rhesus monkey and the human." *The Anatomical Record* 178.1 (1974): 63-81.

- [111] "Physical biology of the cell," Choice Reviews Online, vol. 46, no. 09. pp. 46-5006-46-5006, 2009, doi: 10.5860/choice.46-5006.
- [112] Zahalak, George I. "Modeling muscle mechanics (and energetics)." Multiple muscle systems. Springer, New York, NY, 1990. 1-23.
- [113] Kenney, W. L.; Wilmore, J. H. & Costill, D. L.: Physiology of sport and exercise. Human Kinetics 2012, 5 edn.
- [114] Watkins, J.: Structure and function of the musculoskeletal system. Human Kinetics 2010, 2 edn.
- [115] Nigg, B. M. & Herzog, W.: Biomechanics of the Muskulo-skeletal System. Wiley 2006, third edn.
- [116] MacIntosh, B. R.; Gardiner, P. F. & McComas, A. J.: Skeletal muscle: form and function. Human Kinetics 2006, 2 edn.
- [117] Flanagan, S. P.: Biomechanics: a case-based approach. Jones & Bartlett Learning 2014.
- [118] MacIntosh, B. R.; Gardiner, P. F. & McComas, A. J.: Skeletal muscle: form and function. Human Kinetics 2006, 2 edn.
- [119] Carlson, F. D. & Wilkie, D. R.: Muscle physiology. Prentice-Hall 1974
- [120] Gajdosik, R. L.: Passive extensibility of skeletal muscle: review of literature with clinical implications 16 (2001), 87-101.
- [121] Odegard, G. M. & Donahue, T. L. H.: Constitutive modeling of skeletal muscle tissue with an explicit strain-energy function. Journal of Biomechanical Engineering 130 (2008), 1 - 9, from CBM presentation topics.
- [122] Horowitz, R.: Passive force generation and titin isoforms in mammalian skeletal muscle 61 (1992), 392-398.
- [123] Rassier, D. E.; MacIntosh, B. R. & Herzog, W.: Length dependence of active force production in skeletal muscle. Journal of Applied Physiology 86 (1999), 1445-1457.

- [124] Best, T. M.; McElhanfy, J.; Jr, W. E. G. & Myers, B. S.: Characterization of the passive responses of live skeletal muscle using the quasi-linear theory of viscoelasticity 27 (1994), 170–192.
- [125] Horowitz, Robert, Koscak Maruyama, and Richard J. Podolsky. "Elastic behavior of connectin filaments during thick filament movement in activated skeletal muscle." *The Journal of cell biology* 109.5 (1989): 2169-2176.
- [126] Edman, K. A., G. Elzinga, and M. I. Noble. "Residual force enhancement after stretch of contracting frog single muscle fibers." *The Journal of General Physiology* 80.5 (1982): 769-784.
- [127] Rassier, Dilson E., and Walter Herzog. "Considerations on the history dependence of muscle contraction." *Journal of applied physiology* 96.2 (2004): 419-427.
- [128] Granzier, Henk, and Siegfried Labeit. "Structure–function relations of the giant elastic protein titin in striated and smooth muscle cells." *Muscle & Nerve: Official Journal of the American Association of Electrodiagnostic Medicine* 36.6 (2007): 740-755.
- [129] Kellermayer, Miklós SZ, et al. "Folding-unfolding transitions in single titin molecules characterized with laser tweezers." *Science* 276.5315 (1997): 1112-1116.
- [130] Woledge, Roger C., Nancy A. Curtin, and Earl Homsher. "Energetic aspects of muscle contraction." *Monographs of the physiological society* 41 (1985): 1-357

## Appendix A

### APPENDIX A

Table A.1: Table of units

<b>Geometry</b>	<b>Unit Name</b>	<b>Unit Symbol</b>	<b>Symbol</b>
Energy	Joule= $kgm^2s^{-2} = Nm = 10^7erg$	J	E
Force	Newton= $Jm^{-1} = kgmsec^{-2}$	N	F
Length	Meter= $10^{10}$ Angstrom ( $\text{\AA}$ ) = $10^9nm$	m	<i>a</i>
Pressure	Pascal= $N/m^2$	Pa	P
Volume	Cubic Meter	$m^3$	V
Entropy	$JouleKelvin^{-1}kilogram^{-1}$	S	S
Enthalpy	Joule= $kgm^2s^{-2} = 10^7erg$	J	H
Gibbs Free Energy	Joule= $kgm^2s^{-2} = 10^7erg$	J	G
Helmholtz Free Energy	Joule= $kgm^2s^{-2} = 10^7erg$	J	A
Thermodynamic Temperature	Kelvin= $^{\circ}C + 273.15=(^{\circ}F + 459.67) * (5/9)$	K	T
Time	Second	s	t

Table A.2: Table of constants

<b>Physical Quantity</b>	<b>Value</b>	<b>Symbol and Equivalences</b>
Gas constant	$8.31447 JK^{-1} mol^{-1}$	R
Boltzmann's constant	$1.3806526 \times 10^{-23} JK^{-1} = 0.138 pNmK^{-1}$	$k_B = R/N_A$
Avogadro's constant	$6.0221367 \times 10^{23} mol^{-1}$	$N_A$



## Appendix B

### TRIANGULAR PROBABILITY DISTRIBUTION FUNCTION

The probability distribution in Figure ?? determines the box which the myosin head will be attached at the next step.

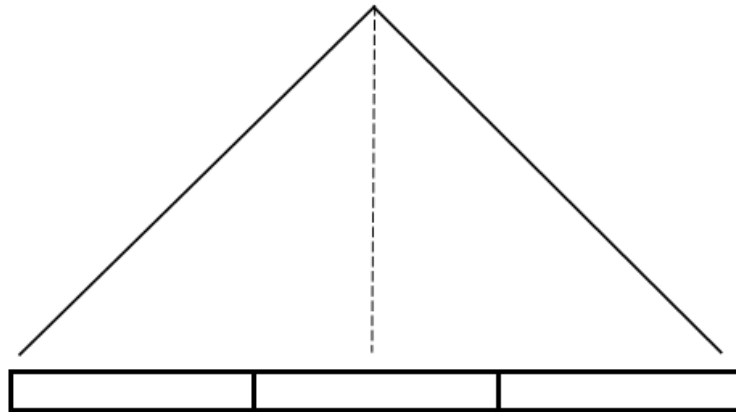


Figure B.1: Tent of the position distribution

The one-dimensional Triangular probability distribution with base  $2w$  looks like;

And the corresponding pdf of the tent is as follows;

$$P(x) = \frac{1 - \frac{|x|}{w}}{w} \quad (\text{B.1})$$

Where  $x$  is the position and the normality condition of pdf is

$$\int_{-\infty}^{+\infty} P(x) dx = 1 \quad (\text{B.2})$$

Which means the area under the triangle (in Figure B.2) must be equal to 1 so

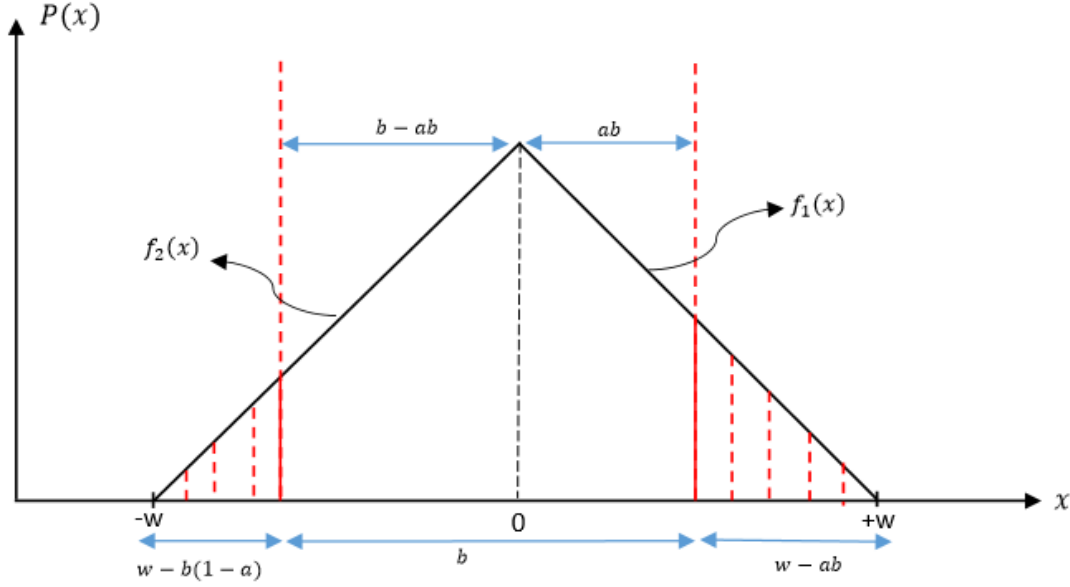


Figure B.2: 1D Triangular probability distribution

$$\text{Area of Triangle} = \frac{2wh}{2} = 1 \quad (\text{B.3})$$

where  $h$  is the height of the triangle and  $h = \frac{1}{w}$ . The functions of  $f_1(x)$  and  $f_2(x)$  are given as

$$f_1(x) = \frac{x}{w} + \frac{y}{\frac{1}{w}} = 1 \quad \rightarrow \quad y = \frac{1}{w} - \frac{1}{w^2}x \quad \text{where } x < 0 \quad (\text{B.4})$$

$$f_2(x) = \frac{x}{-w} + \frac{y}{\frac{1}{w}} = 1 \quad \rightarrow \quad y = \frac{1}{w} + \frac{1}{w^2}x \quad \text{where } x > 0 \quad (\text{B.5})$$

Then if we substitute the Equations B.4 and B.5 into the Equation B.1, the subsequent equation is reached.

$$\int_{-w}^{+w} P(x)dx = 1 \quad (\text{B.6})$$

$$\int_{-w}^0 \left( \frac{1}{w} + \frac{1}{w^2}x \right) dx + \int_0^w \left( \frac{1}{w} - \frac{1}{w^2}x \right) dx = 1 \quad (\text{B.7})$$

$$\left(\frac{1}{w}x + \frac{1}{w^2}\frac{x^2}{2}\right)\Big|_{-w}^0 + \left(\frac{1}{w}x - \frac{1}{w^2}\frac{x^2}{2}\right)\Big|_0^w = 1$$

$$\frac{1}{2} + \frac{1}{2} = 1$$
(B.8)

So the probability function takes the following form

$$P(x) = \frac{1}{w} - \frac{1}{w^2}|x| \quad \rightarrow \quad \{x = - \quad x < 0, \quad x = + \quad x > 0\} \quad (\text{B.9})$$

Then in order to calculate the mean, variance and standard deviation of the triangular probability distribution following procedures are exploited;

To find the mean value which is our expectation value can be found like this;

$$\mu = \langle x \rangle = Ex = \int_{-\infty}^{+\infty} xP(x)dx \quad (\text{B.10})$$

$$Ex = \int_{-w}^{+w} x \left( \frac{1}{w} - \frac{1}{w^2}|x| \right) dx \quad (\text{B.11})$$

$$Ex = \int_{-w}^0 x \left( \frac{1}{w} - \frac{1}{w^2}x \right) dx + \int_0^{+w} x \left( \frac{1}{w} - \frac{1}{w^2}x \right) dx \quad (\text{B.12})$$

$$Ex = \left( \frac{1}{w}\frac{x^2}{2} + \frac{1}{w^2}\frac{x^3}{3} \right)\Big|_{-w}^0 + \left( \frac{1}{w}\frac{x^2}{2} - \frac{1}{w^2}\frac{x^3}{3} \right)\Big|_0^w \quad (\text{B.13})$$

After simplifications the expectation of random variable x is obtained as

$$Ex = \mu = 0 \quad (\text{B.14})$$

Then the variance has the relation is,

$$\text{variance} = \langle x^2 \rangle = \sigma^2 = E[x^2] - (Ex)_{w=0}^2 = \int_{-\infty}^{\infty} x^2 P(x) dx - 0 \quad (\text{B.15})$$

$$E[x^2] = \int_{-\infty}^{\infty} x^2 P(x) dx \quad (\text{B.16})$$

if we substitute the Equation B.1 into the Equation B.15 and taking the integral, the following compact form can be written;

$$\begin{aligned}
E[x^2] &= \int_{-w}^w x^2 \left( \frac{1}{w} - \frac{1}{w^2} |x| \right) dx \\
&= \int_{-w}^0 \left( \frac{x^2}{w} + \frac{x^3}{w^2} \right) dx + \int_0^w \left( \frac{x^2}{w} - \frac{x^3}{w^2} \right) dx \\
&= \left( \frac{1}{w} \frac{x^3}{3} + \frac{1}{w^2} \frac{x^4}{4} \right) \Big|_{-w}^0 + \left( \frac{1}{w} \frac{x^3}{3} - \frac{1}{w^2} \frac{x^4}{4} \right) \Big|_0^w \\
\sigma^2 = \langle x^2 \rangle &= E[x^2] = \frac{w^2}{6}
\end{aligned} \quad (\text{B.17})$$

Finally to find the Standard deviation we take the square root of variance and the standard deviation is

$$\text{Standart deviation} = \sigma = \sqrt{\langle x^2 \rangle} = \sqrt{\frac{w^2}{6}} = \frac{w}{\sqrt{6}} \quad (\text{B.18})$$

Before starting our new model, by using Figure B. 3 we can find the probability of movement to the right and left by following the steps which are shown below.

$$\text{Probability of movement to the right} = \int_{ab}^w P(x) dx \quad (\text{B.19})$$

$$P_R = \int_{ab}^w \left( \frac{1}{w} - \frac{1}{w^2} |x| \right) dx \quad (\text{B.20})$$

$$P_R = \int_{ab}^w \left( \frac{1}{w} - \frac{x}{w^2} \right) dx \quad (\text{B.21})$$

$$P_R = \frac{1}{2} \frac{ab}{w} + \frac{(ab)^2}{2w^2} = \left( 1 - \frac{ab}{w} \right)^2 \frac{1}{2} \quad (\text{B.22})$$

And the probability of movement to the left is,

$$P_L = \int_{-w}^{b-ab} P(x)dx \quad (\text{B.23})$$

$$P_L = \int_{-w}^{b-ab} \left( \frac{1}{w} + \frac{1}{w^2}x \right) dx \quad (\text{B.24})$$

after making some simplifications the results is obtained as follow,

$$P_L = \frac{1}{2} + \frac{b-ab}{w} + \frac{(b-ab)^2}{2w^2} \quad (\text{B.25})$$

### 1-D RANDOM WALK

Before applying Brownian Motion to the model, random walk has to be defined with mathematical terms. For  $n$  many steps denoted by  $X_i$  which are i.i.d (independent identically distributed) a random walk is  $S_n = X_1 + \dots + X_n$ . In the model  $X_i$  can only take values from the set  $X_i = -1, 0, 1$  correspond to jump to left, jump to right and stand still. Different elements of the set  $X_i$  for each step are shown in Fig. 3 together with their physical interpretations.

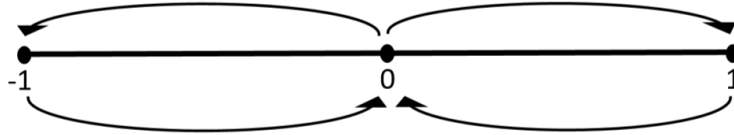


Figure B.3

In the definition above the indexes determines the time steps. Hence, for practical purposes the random walk can be denoted as

$$X(t_n) = \sum_{i=0}^{n-1} X(t_{i+1}) - X(t_i) \quad (\text{B.26})$$

In this equation  $n$  is the time step and  $i$  is the dummy variable and by using the Equation B.26 we calculate how many units traveled at the end of a certain period of time. In order to use this equation first of all we need to calculate the cumulative distribution (CD).

The example shown in Figure B.4 is whether an object or a person went right, left or kept the same position in the time interval from  $t_0$  to  $t_{10}$ .

A simulated path of random walk is shown below in Fig. B.4 for ten time steps.

1	0	1	1	-1	1	0	0	-1	1
$t_1$	$t_2$	$t_3$	$t_4$	$t_5$	$t_6$	$t_7$	$t_8$	$t_9$	$t_{10}$

Figure B.4

In order to determine the path of Brownian Motion, time steps has to be summed in a cumulative manner. The path is shown in Fig. B.5 and the related calculations are given as an example right below the figure.

1	1	2	3	2	3	3	3	2	3
$t_1$	$t_2$	$t_3$	$t_4$	$t_5$	$t_6$	$t_7$	$t_8$	$t_9$	$t_{10}$

Figure B.5: Brownian Path

The Fig. B.5 is our cumulative distribution array and by using the relation which is illustrated in Equation B.27 we can easily obtain the CD.

$$\begin{aligned}
 CD &= (1 + 0) + (0 + 1) + (1 + 1) + (2 + 1) + (3 + (-1)) + (2 + 1) \\
 &\quad + (3 + 0) + (3 + 0) + (3 + (-1)) + (2 + 1)
 \end{aligned}
 \tag{B.27}$$

After finding the CD (which is the Fig. B.5) we can use the Equation B.26;

$$X(t_n) = \sum_{i=0}^{n-1} X(t_{i+1}) - X(t_i)
 \tag{B.28}$$

$$\begin{aligned}
 X(t_{10}) &= (1 - 0) + (1 - 1) + (2 - 1) + (3 - 2) + (2 - 3) + (3 - 2) \\
 &\quad + (3 - 3) + (3 - 3) + (2 - 3) + (3 - 2) \\
 X(t_{10}) &= 3
 \end{aligned}
 \tag{B.29}$$

In this example the particle is moved total of 3 units in 10 time steps. Defining the Brownian Motion with analytical terms makes the model rule based. After stating the definition and solving the example, 1-D Brownian Motion can be used to model

the dynamics of myosin and actin. Main advantage of Brownian Motion is the existence of analytical solutions in space time. The relations mentioned above made the model rule-based for following analytical solutions and computer simulations. In the decision making model illustrated in Figure B.3, the boxes represented with -1 and +1 determine whether the myosin head attached to actin on the left or right hand side respectively. The third possibility in other words the box with 0, corresponds to stand still case which myosin does not change its position at that instant.

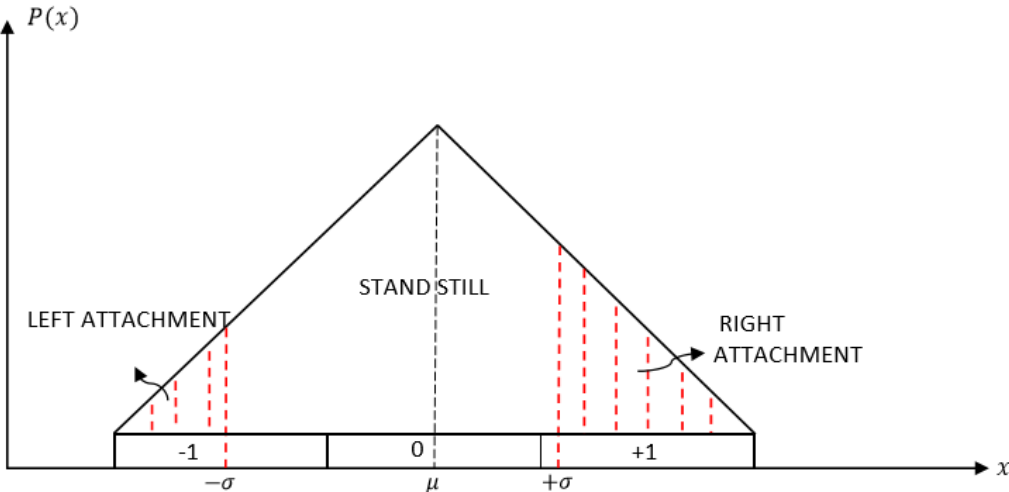


Figure B.6: Decision making model

The probabilistic model described in part 2, chosen symmetric and asymmetric decision boundaries changes the left and right jump probabilities. Therefore, they initiate the preferred direction just like the friction force on the bar in the first part. However, in this part existence of preferred direction is defined with probabilistic terms rather than friction force originated in Newtonian classical mechanics.

The symmetric decision boundaries chosen correspond to symmetric friction force and neither of them are sufficient to create a preferred direction but the system fluctuates about a constant mean in time. Nevertheless, asymmetric decision boundaries induces a preferred direction to the system as asymmetric friction force did because of the unequal probabilities of left and right jumps.

$$-\sigma \neq +\sigma \rightarrow \text{with friction} \tag{B.30}$$

$$-\sigma = +\sigma \rightarrow \textit{without friction} \quad (\text{B.31})$$

The results of our analysis also confirm the idea that we have put forward from the beginning.

## ANALYSIS

In this section, firstly we created a triangular distribution. Then random data are selected from this distribution and these random numbers are collected into an array. If the selected random data is less than the specified minimum standard deviation value ( $-\sigma$ ), it is equal to -1 that is to the left attachment state, if it is greater than the maximum standard deviation value ( $+\sigma$ ), it is equal to +1, that is to the right attachment state. In the last case if the values we randomly selected are greater than  $-\sigma$  value and less than  $+\sigma$  value, it is equal to 0, which means, stand still state.

### Case 1

In our first case, we took the  $\sigma$  values symmetrically, that is, equal to each other, and the right or left attachment was almost equal.

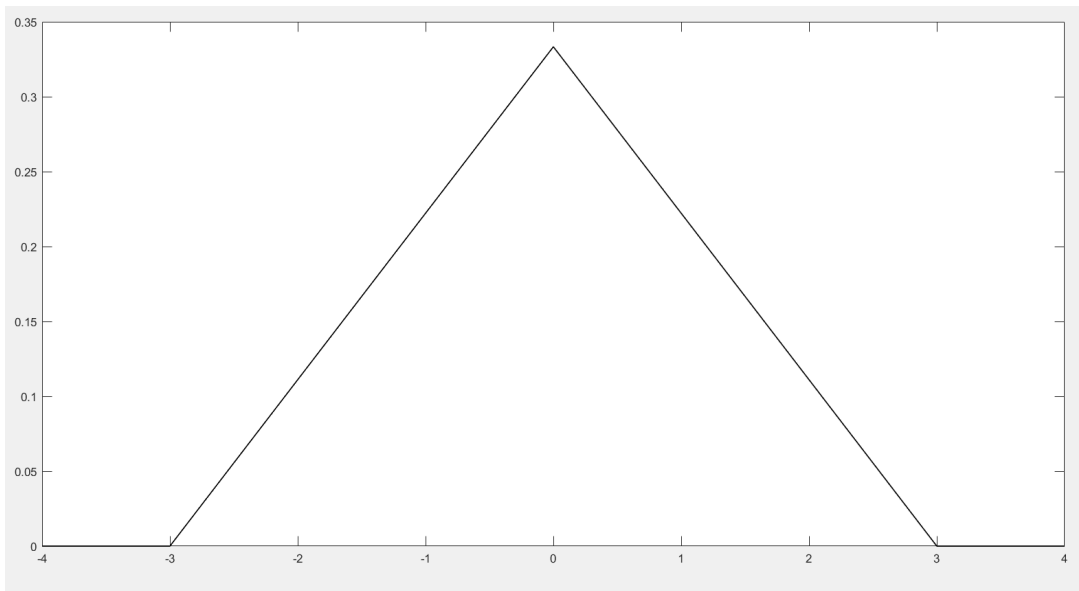


Figure B.7: Triangular Distribution

This is the triangular distribution we have created for our analysis. Mean value is 0 and while the lower limit is -3, the upper limit is +3. When we give equal standard



deviation values to keep symmetry of our distribution tent, right and left attachment histograms are almost equal to each other as you can see in Fig. B.7 (where  $+\sigma=+1$  and  $-\sigma=-1$ ). So jump to the right and left are equal and preferred direction does not exist.

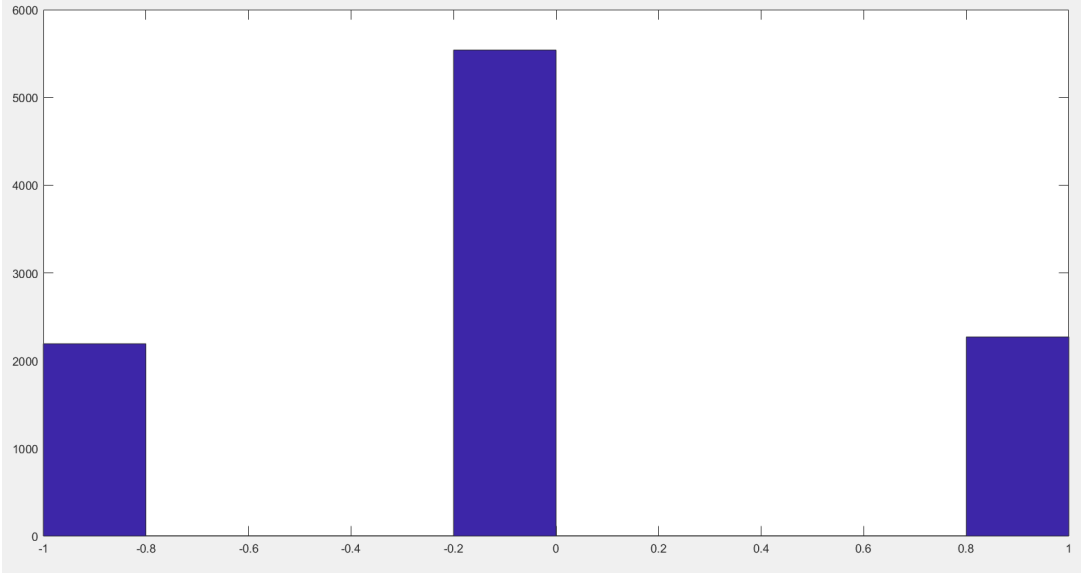


Figure B.8: Frequency Histogram of Decisions

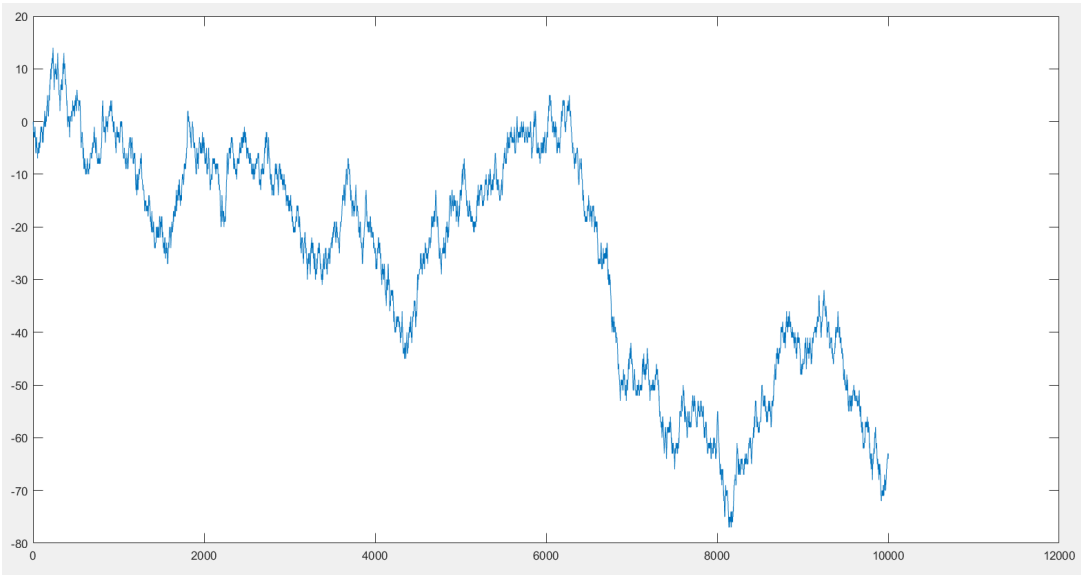


Figure B.9: Cumulative Triangular Distribution

**Case 2**

In this case, we eliminate the symmetry by giving different  $\sigma$  values and create a preferred direction. When we use the values  $+\sigma=+2.5$  and  $-\sigma=-1.5$ , we observe that the left attachment event is more probable (i.e. frequent) than the right and the system in the first case loses its symmetrical feature.

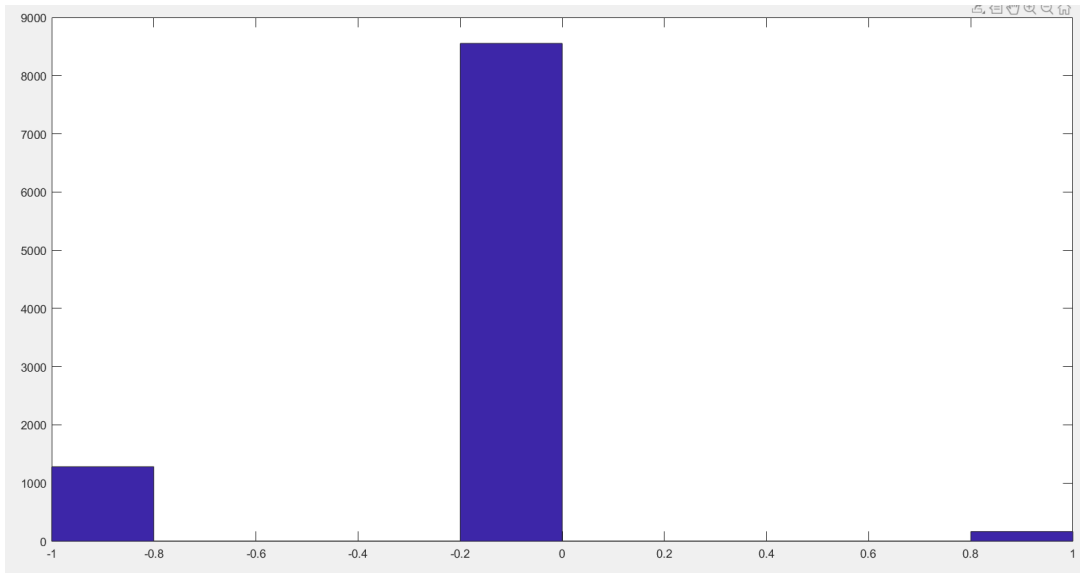


Figure B.10: Triangular Distribution Histogram

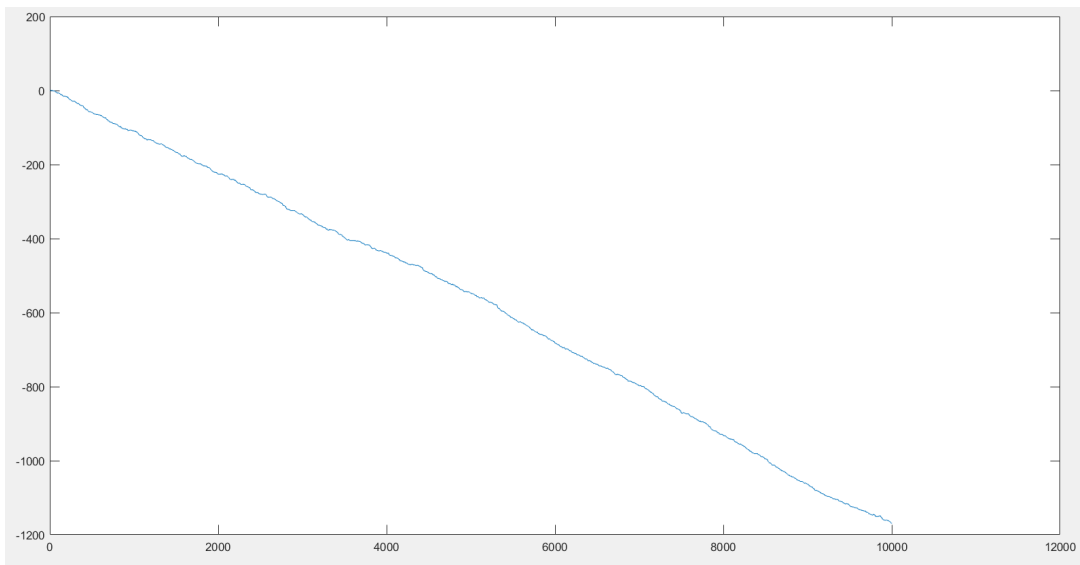


Figure B.11: Cumulative Triangular Distribution

### Case 3

In the last case, we give the values of  $+\sigma=+1$  and  $-\sigma=-2$  to realize the right-attachment event by giving different  $\sigma$  values again. As can be understood from the standard deviation values, as the number of random data selected in order to hold to the right is more than the ones selected for holding to the left so the preferred direction occurs to the right and this outcome can be easily observed in Fig.B.13

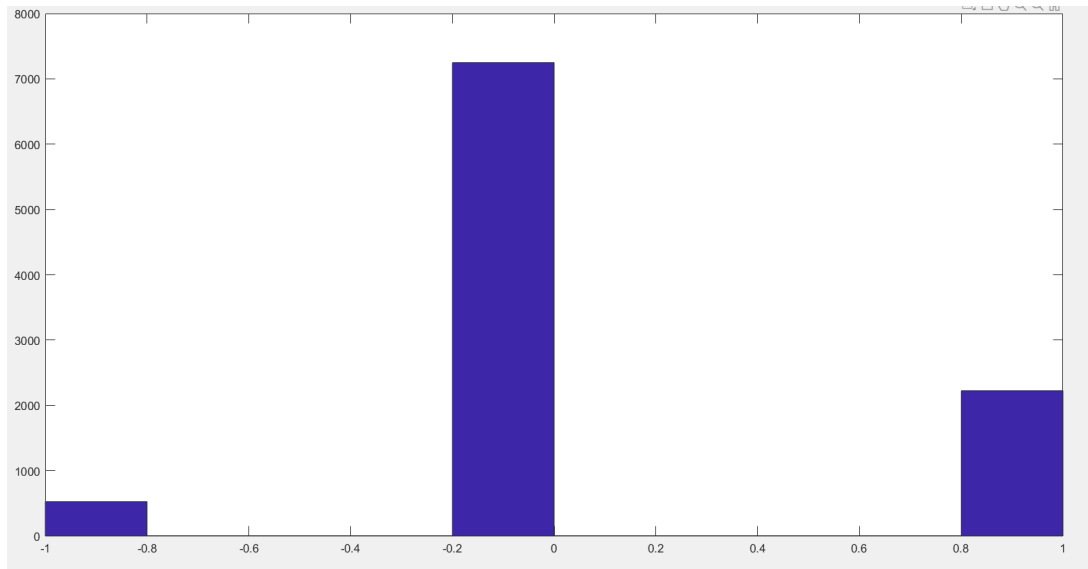


Figure B.12: Triangular Distribution Histogram

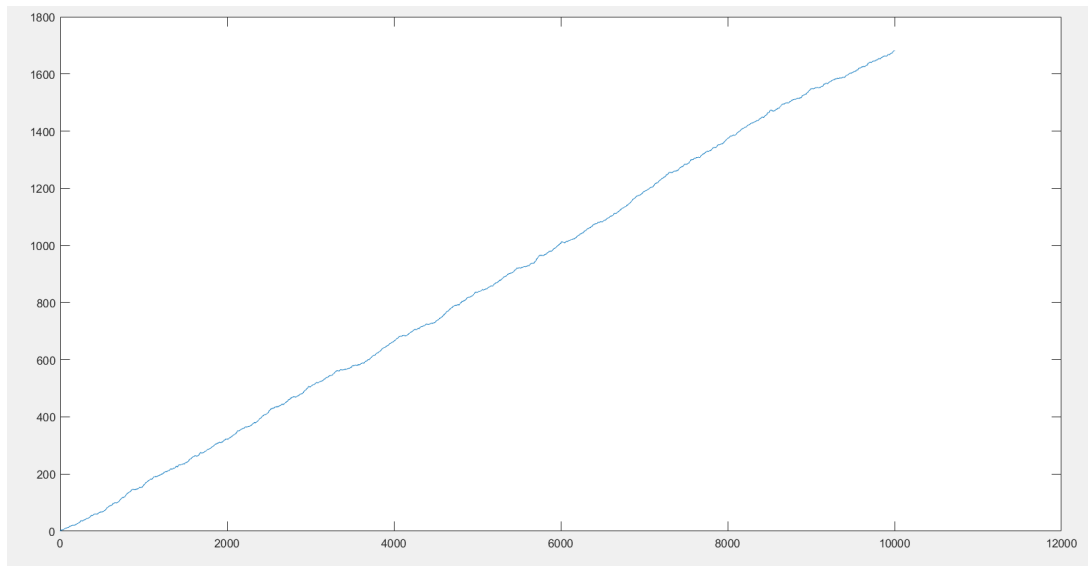


Figure B.13: Cumulative Triangular Distribution

Finally, when we draw in blue shows us the third state, that is the attachment to the left or in other words jump to right, the line shown in gray indicates not to move, that is, the stand still state, and the orange line shows us the state of right attachment

which means also jump to left.

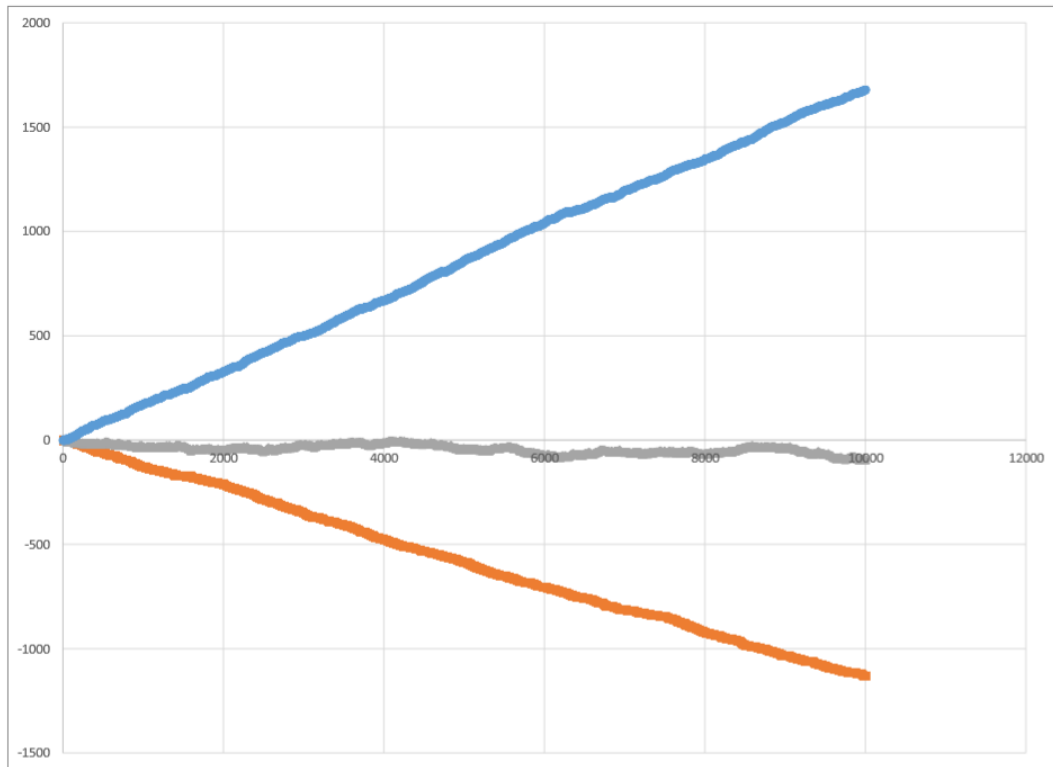


Figure B.14: Distribution for Three case

## Appendix C

### UNBIASED RANDOM WALK

In order to obtain unbiased random walk relation, the rate constant values in our equation must be equal to each other which means  $k_- = k_+$ . The unbiased random walk is analogous to frictionless case in 1D bar model in the first part and symmetric decision making case in the second part.

In the master equation (Equation C.1), when the rate constants are chosen equal to each other, master equation (Equation C.1) reduces to Fick's second law which describes unbiased diffusion.

Before making this analytical derivation, how the diffusion equation was obtained, and how it is equal to our master equation after making some numerical solutions is proved in detail below.

#### Diffusion Equation

According to Fick's first law the flux is linearly proportional to the concentration gradient in space.

$$j = -D \frac{\partial c}{\partial x} \quad (\text{C.1})$$

Where  $c$  is the concentration,  $x$  is the position,  $j$  is current density per unit time and  $D$  is the diffusion coefficient. Since the particles diffuse to the direction where concentration is less (downward the gradient), minus sign is necessary to be used. Otherwise the gradient and the flux directions would be the same, yet they must be in opposite directions. The unit of the current density ( $j$ ) is  $[j] = \frac{1}{\text{length}^2 * \text{time}}$ . So the unit of

the right hand side is  $\left[ \frac{\partial c}{\partial x} \right] = \frac{\text{number of particles}}{\text{length}^3} = \frac{\text{number of particles}}{\text{length}^3}$ . In the same way the unit of diffusion coefficient is determined as  $\frac{\text{length}^2}{\text{time}}$ . Moreover, the most important assumption of Fick's first law is the conservation of matter where the input and output are equal to each other for a differential space element in other words there is no accumulation in any of those differential elements.

First of all, the change in the number of particles ( $N_{\text{box}}$ ), per unit time is the change in concentration per unit time multiplied with the volume of the chosen box, then the relation can be written as

$$\frac{\partial N_{\text{box}}}{\partial t} = \frac{\partial c}{\partial t} \text{Volume} = \frac{\partial c}{\partial t} \Delta x \Delta y \Delta z \quad (\text{C.2})$$

In Equation C.3  $\Delta x \Delta y \Delta z$  represents the volume of the box. By conservation of mass, the result of the Equation C.3 must be equal to the number of particles which are flowing into the box per unit time and this relation is expressed as  $j(x, y, z) \Delta y \Delta z$ . Furthermore the number of particles leaving the box per unit time is denoted by,  $j(x + \Delta x, y, z) \Delta y \Delta z$ . When those two subtracted from each other to get the change in number of particles in the box, we can find the relation shown as below;

$$\frac{\partial c}{\partial t} \Delta x \Delta y \Delta z = j(x, y, z) \Delta y \Delta z - j(x + \Delta x, y, z) \Delta y \Delta z \quad (\text{C.3})$$

According to Taylor expansion around  $x$  to the first order,  $j(x + \Delta x, y, z)$  is determined as,

$$\frac{\partial c}{\partial t} \Delta x \Delta y \Delta z \cong j(x, y, z) \Delta y \Delta z - \left[ j(x, y, z) + \frac{\partial j}{\partial x} \Delta \right] \Delta y \Delta z \quad (\text{C.4})$$

If we now collect terms together, the local statement of conservation of mass can be written as

$$\frac{\partial c}{\partial t} = - \frac{\partial j}{\partial x} \quad (\text{C.5})$$

Equation C.5 gives the relation between space and time where it explicitly states change of concentration in time and change of flux in space. Please note that Equation C.1 can be substituted into it to find the second order differential relation of space in a differential time step all over the diffusive media as

$$\frac{\partial c}{\partial t} = D \frac{\partial^2 c}{\partial x^2} \quad (\text{C.6})$$

which is the classic law of diffusion in one dimension. Note that to derive this particular form of the diffusion equation, we had to assume that  $D$  is independent of concentration.

### Numerical Derivation of Diffusion Equation

Parabolic PDEs equations are employed to characterize time variable problems and these equations can be solved by substituting finite divided differences for the partial derivatives. Changes in time as well as in space in parabolic equations must be considered. As it can be seen in Fig. 4 parabolic PDEs are temporally open-ended. In order to solve the parabolic equations two fundamental solution approaches are used which are explicit and implicit schemes.

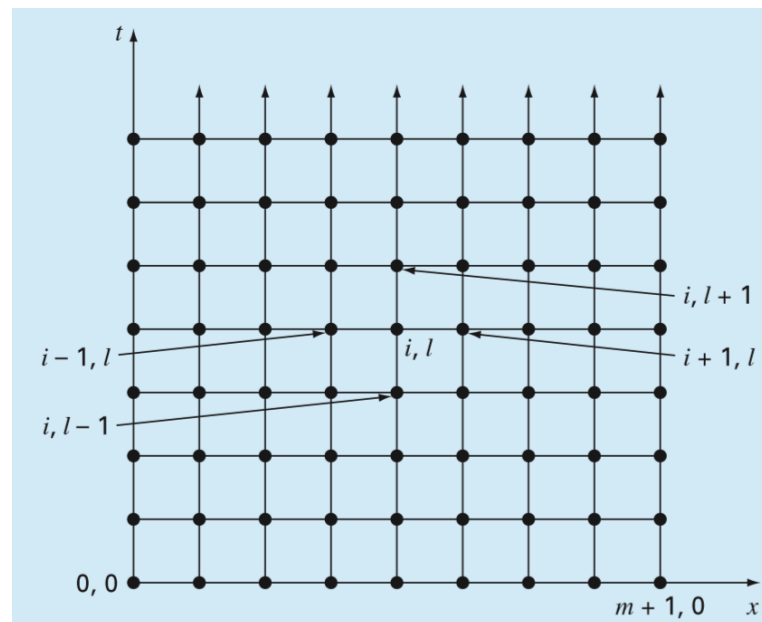


Figure C.1: Open-ended in the temporal dimension

In this assumption ( $k_- = k_+$ ) by using an explicit method we can obtain the one

dimensional diffusion law.

The classic law of diffusion requires approximations for the second derivative in space and the first derivative in time.

Where;

$$\frac{\partial^2 c}{\partial x^2} = \frac{c_{i+1}^l - 2c_i^l + c_{i-1}^l}{\Delta x^2} \quad (\text{C.7})$$

The superscript denotes the time. The forward finite-divided difference is used to approximate the time derivative

$$\frac{\partial c}{\partial t} = \frac{c_i^{l+1} - c_i^l}{\Delta t} \quad (\text{C.8})$$

Then if we substitute the Equation C.7 and Equation C.8 into the Equation C.6 we can obtain,

$$\frac{c_i^{l+1} - c_i^l}{\Delta t} = \frac{c_{i+1}^l - 2c_i^l + c_{i-1}^l}{\Delta x^2} \quad (\text{C.9})$$

$$c_i^{l+1} = D\Delta t = \left[ \frac{c_{i+1}^l}{\Delta x^2} - \frac{2c_i^l}{\Delta x^2} + \frac{c_{i-1}^l}{\Delta x^2} \right] + c_i^l \quad (\text{C.10})$$

$$c_i^{l+1} = \frac{D\Delta t}{\Delta x^2} c_{i+1}^l + \frac{D\Delta t}{\Delta x^2} c_{i-1}^l + c_i^l \left[ 1 - 2\frac{D\Delta t}{\Delta x^2} \right] \quad (\text{C.11})$$

Where  $c_i^{l+1}$  is analogous to  $p(x, t + \Delta t)$  so

$$\begin{aligned} \frac{D\Delta t}{\Delta x^2} c_{i+1}^l &\approx k_- \Delta t p(x, t + \Delta x, t) \\ \frac{D\Delta t}{\Delta x^2} c_{i-1}^l &\approx k_+ \Delta t p(x, t - \Delta x, t) \end{aligned} \quad (\text{C.12})$$

$$c_i^l \left[ 1 - 2\frac{D\Delta t}{\Delta x^2} \right] \approx [1 - (k_- + k_+) \Delta t] p(x, t)$$



By using these relations we can easily obtain that;

$$1 - 2\frac{D\Delta t}{\Delta x^2} \cong 1 - (k_- + k_+)\Delta t \quad \rightarrow \quad k_- + k_+ = \frac{2D}{\Delta x^2} \quad (\text{C.13})$$

And we know that  $k_- = k_+$  so

$$k_- = k_+ = \frac{D}{\Delta x^2} \quad (\text{C.14})$$

If we make a unit check we see that,  $D \rightarrow \left[ \frac{m^2}{sec} \right]$  and  $\Delta x^2 \rightarrow m^2$  so the unit of the rate constants is  $\frac{1}{sec}$ . Finally, it can be easily seen that the unbiased random walk equation is analogous to the classic diffusion equation.

### Analytical Solution of Master Equation

In order to obtain the master equation shown in Equation (C. 15) we sum over three microtrajectories which are jump to left, jump to right and no jump trajectories that can occur during a given time step.

$$\begin{aligned} p(x, t + \Delta t) = & k_- \Delta t p(x + \Delta x, t) + k_+ \Delta t p(x - \Delta x, t) \\ & + [1 - (k_- + k_+)\Delta t] p(x, t) \end{aligned} \quad (\text{C.15})$$

After making some simplifications

$$\begin{aligned} p(x, t + \Delta t) = & k_- \Delta t p(x + \Delta x, t) + k_+ \Delta t p(x - \Delta x, t) + p(x, t) \\ & - k_- \Delta t p(x, t) - k_+ \Delta t p(x, t) \end{aligned} \quad (\text{C.16})$$

$$\begin{aligned} p(x, t + \Delta t) = & k_- \Delta t [p(x + \Delta x, t) - p(x, t)] + k_+ \Delta t [p(x - \Delta x, t) - p(x, t)] \\ & + p(x, t) \end{aligned} \quad (\text{C.17})$$

$$\frac{p(x, t + \Delta t) - p(x, t)}{\Delta t} = k_- [p(x + \Delta x, t) - p(x, t)] + k_+ [p(x - \Delta x, t) - p(x, t)] \quad (\text{C.18})$$

At this point we use the Taylor expansion as follows,

$$p(x, t + \Delta t) = p(x, t) + \frac{\partial}{\partial t} p(x, t) \Delta t + \frac{1}{2} \frac{\partial^2}{\partial t^2} p(x, t) (\Delta t)^2 + \dots \quad (\text{C.19})$$

and

$$p(x \mp \Delta x, t) = p(x, t) \mp \frac{\partial}{\partial x} p(x, t) \Delta x + \frac{1}{2} \frac{\partial^2}{\partial x^2} p(x, t) (\Delta x)^2 + \dots \quad (\text{C.20})$$

After applying the Taylor expansion then we substitute the Equation C.19 and Equation C.20 into the Equation C.18 we get the relation as you can see below;

$$\begin{aligned} & \frac{p(x, t) + \frac{\partial}{\partial t} p(x, t) \Delta t - p(x, t)}{\Delta t} \\ k_- &= \left[ p(x, t) + \frac{\partial}{\partial x} p(x, t) \Delta x + \frac{1}{2} \frac{\partial^2}{\partial x^2} p(x, t) (\Delta x)^2 - p(x, t) \right] \\ k_+ &= \left[ p(x, t) - \frac{\partial}{\partial x} p(x, t) \Delta x + \frac{1}{2} \frac{\partial^2}{\partial x^2} p(x, t) (\Delta x)^2 - p(x, t) \right] \end{aligned} \quad (\text{C.21})$$

And after tedious simplifications;

$$\frac{\partial}{\partial t} p(x, t) \cong \frac{1}{2} \frac{\partial^2}{\partial x^2} p(x, t) (\Delta x)^2 (k_- + k_+) \quad (\text{C.22})$$

Where  $k_- = k_+$  and after making the necessary simplifications, the Equation C.22 can be written in the following compact form:

$$\frac{\partial}{\partial t} p(x, t) \cong ((\Delta x)^2 k) \frac{\partial^2}{\partial x^2} p(x, t) \quad (\text{C.23})$$

This is the diffusion equation derived in the previous part. The diffusion constant which is represented with D is equal to;

$$D = (\Delta x)^2 k \quad (\text{C.24})$$

if and only if  $k_- = k_+$ .

### BIASED RANDOM WALK

If  $k_- \neq k_+$ , the master equation turns into biased random walk, named as Smoluchowski Equation.

The Master equation is ;

$$p(x, t + \Delta t) = k_- \Delta t p(x + \Delta x, t) + k_+ \Delta t p(x - \Delta x, t) \\ [1 - (k_- + k_+) \Delta t] p(x, t) \quad (\text{C.25})$$

Then in order to make some simplifications we also follow the same procedure in unbiased random walk.

Where

$$p(x, t + \Delta t) = k_- \Delta t [p(x + \Delta x, t) - p(x, t)] + k_+ \Delta t [p(x - \Delta x, t) - p(x, t)] \\ + p(x, t) \quad (\text{C.26})$$

The Equation C.27 can be turned into more familiar form by Taylor expansion  $p(x, t + \Delta t)$  and  $p(x \mp \Delta x, t)$  similar to Equation C.23.

So the master equation can be written in the following form;

$$\frac{\partial}{\partial t} p(x, t) = k_- \frac{\partial}{\partial x} p(x, t) \Delta t + k_- \frac{1}{2} \frac{\partial^2}{\partial x^2} p(x, t) (\Delta t)^2 + k_+ \frac{\partial}{\partial x} p(x, t) \Delta x \\ + k_+ \frac{1}{2} \frac{\partial^2}{\partial x^2} p(x, t) (\Delta x)^2 \quad (\text{C.27})$$

Then;

$$\frac{\partial}{\partial t}p(x, t) = -\Delta x(k_+ - k_-)\frac{\partial}{\partial x}p(x, t) + \frac{1}{2}(\Delta x)^2(k_+ + k_-)\frac{\partial^2}{\partial x^2}p(x, t) \quad (\text{C.28})$$

The unit of the rate constants ( $k_-$  and  $k_+$ ) is  $\frac{1}{\text{sec}}$  so that this term  $\Delta x(k_+ - k_-) = \Delta x k_+ - \Delta x k_- = \Delta v$  represents the  $\frac{m}{\text{sec}}$  which is the velocity term denoted by  $v$  and the term  $\frac{(\Delta x)^2(k_+ + k_-)}{2}$  is the diffusion coefficient together with the unit  $\frac{m^2}{\text{sec}}$ .

So, If we rewrite the Equation C.29;

$$\frac{\partial p(x, t)}{\partial t} = -\Delta v \frac{\partial p(x, t)}{\partial x} + D \frac{\partial^2 p(x, t)}{\partial x^2} \quad (\text{C.29})$$

## Appendix D

### ADVECTION-DIFFUSION EQUATION

Advection diffusion equation is used to model spreading of pollutant. It governs the process of advection and diffusion at the same time. One dimensional advection diffusion equation is formulated in the following form;

$$\frac{\partial f}{\partial t} + U \frac{\partial f}{\partial x} = D \frac{\partial^2 f}{\partial x^2} \quad (\text{D.1})$$

#### Finite Difference Method

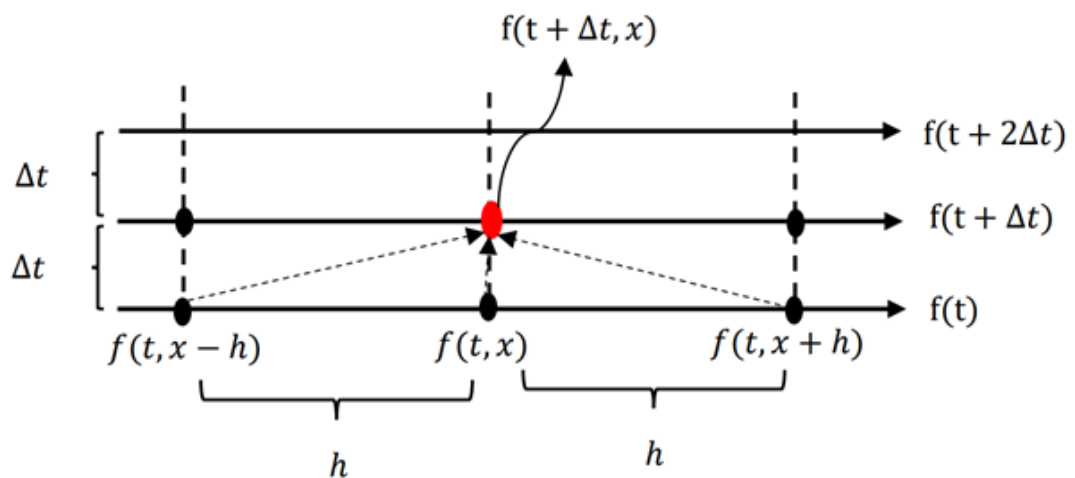


Figure D.1

#### The Time Derivative

Taylor expansion is used to describe the time derivative of the function.

$$f(t + \Delta t) = f(t) + \frac{\partial f(t)}{\partial t} \Delta t + \frac{1}{2} \frac{\partial^2 f(t)}{\partial t^2} \Delta t^2 + \text{HOT..} \quad (\text{D.2})$$

so, the time derivative can be obtained in the following form;

$$\frac{\partial f(t)}{\partial t} = \frac{f(t\Delta t) - f(t)}{\Delta t} - \frac{\Delta t}{2} \frac{\partial^2 f(t)}{\partial t^2} \quad (\text{D.3})$$

which is also called forward euler method.

### The Spatial First Derivative

When using finite difference approximations, the values of  $f$  are stored at discrete points.

By using Taylor series,

$$f(x + h) = f(x) + \frac{\partial f(x)}{\partial x} h + \frac{1}{2} \frac{\partial^2 f(x)}{\partial x^2} h^2 + \dots \quad (\text{D.4})$$

$$f(x - h) = f(x) - \frac{\partial f(x)}{\partial x} h + \frac{1}{2} \frac{\partial^2 f(x)}{\partial x^2} h^2 - \dots \quad (\text{D.5})$$

Subtracting Eqn.D.5 from Eqn D.4;

$$\frac{\partial f(x)}{\partial x} = \frac{f(x + h) - f(x - h)}{2h} \quad (\text{D.6})$$

which is called centered difference method.

### The Spatial Second Derivative

$$f(x + h) = f(x) + \frac{\partial f(x)}{\partial x} h + \frac{1}{2} \frac{\partial^2 f(x)}{\partial x^2} h^2 + \dots \quad (\text{D.7})$$

$$f(x - h) = f(x) - \frac{\partial f(x)}{\partial x} h + \frac{1}{2} \frac{\partial^2 f(x)}{\partial x^2} h^2 - \dots \quad (\text{D.8})$$

Adding Eqn D.7 to Eqn. D.8;

$$\frac{\partial^2 f(x)}{\partial x^2} = \frac{f(x + h) - 2f(x) + f(x - h)}{h^2} \quad (\text{D.9})$$

which is forward finite difference method.

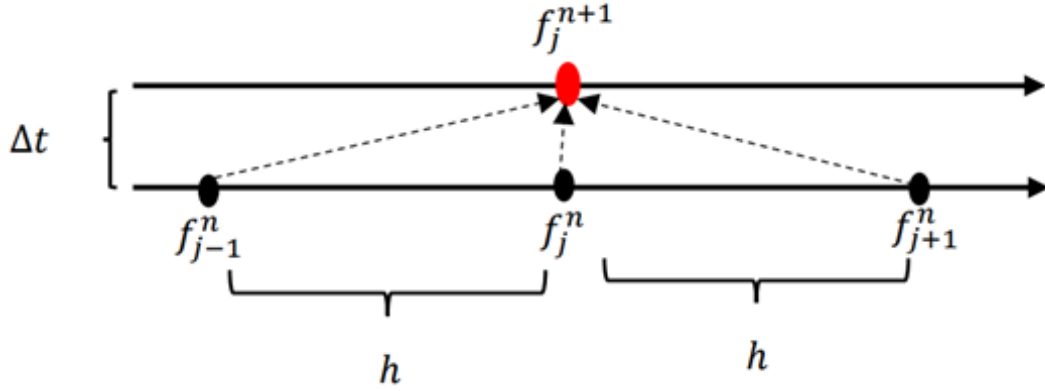


Figure D.2

In order to express space and time i will use  $j$  and  $n$  indices respectively so Eqn. D.3, Eqn. D.6 and Eqn. D.9 can be written in the indicial notation in the following form;

$$\left(\frac{\partial f}{\partial t}\right)_j^n = \frac{f_j^{n+1} - f_j^n}{\Delta t} \quad (\text{D.10})$$

$$\left(\frac{\partial f}{\partial x}\right)_j^n = \frac{f_{j+1}^n - f_{j-1}^n}{2h} \quad (\text{D.11})$$

$$\left(\frac{\partial^2 f}{\partial x^2}\right)_j^n = \frac{f_{j+1}^n - 2f_j^n + f_{j-1}^n}{h^2} \quad (\text{D.12})$$

Substituting Eqn. D.10, Eqn. D.11 and Eqn. D.12 into the Eqn. D.1 then the relation becomes as follows;

$$\frac{f_j^{n+1} - f_j^n}{\Delta t} + U \frac{f_{j+1}^n - f_{j-1}^n}{2h} = D \frac{f_{j+1}^n - 2f_j^n + f_{j-1}^n}{h^2} \quad (\text{D.13})$$

After making some simplifications;

$$f_j^{n+1} = f_j^n - \frac{U\Delta t}{2h}(f_{j+1}^n - f_{j-1}^n) + \frac{D\Delta t}{h^2}(f_{j+1}^n - 2f_j^n + f_{j-1}^n) \quad (\text{D.14})$$

Thus, given  $f$  at one time level,  $f$  at the next time level is given by using Eqn. D.14. The value of every point at level  $n+1$  is given explicitly in terms of the values at the level  $n$ .

In our problem, the unbound probability function changing over time is as follows;

$$\begin{aligned} \frac{\partial p_0}{\partial t} = & (k_B^- + k_A^+)p_1 + (k_B^- \delta - k_A^+ \Delta) \frac{\partial p_1}{\partial x} + \frac{1}{2}(k_B^- \delta^2 + k_A^+ \Delta^2) \frac{\partial^2 p_1}{\partial x^2} \\ & - (k_B^+ + k_A^-)p_0 \end{aligned} \quad (\text{D.15})$$

If we rewrite the Eqn. D.15 with the help of Eqn. D.14 (indicial form) we obtain the following relation;

$$\begin{aligned} p_{0j}^{n+1} = & p_{0j}^n + (k_B^- + k_A^+) \Delta t p_{1j}^n + (k_B^- \delta - k_A^+ \Delta) \Delta t \frac{p_{1j+1}^n - p_{1j-1}^n}{2\Delta} \\ & + \frac{1}{2}(k_B^- \delta^2 + k_A^+ \Delta^2) \Delta t \frac{p_{1j+1}^n - 2p_{1j}^n + p_{1j-1}^n}{\Delta^2} - (k_B^+ + k_A^-) \Delta t p_{0j}^n \end{aligned} \quad (\text{D.16})$$

If we follow the same steps for the bound probability function which is;

$$\begin{aligned} \frac{\partial p_1}{\partial t} = & p_0(k_A^- + k_B^+) + \frac{\partial p_0}{\partial x}(k_A^- \Delta - k_B^+ \delta) + \frac{\partial^2 p_0}{\partial x^2} \frac{1}{2}(k_A^- \Delta^2 + k_B^+ \delta^2) \\ & - p_1(k_A^+ + k_B^-) \end{aligned} \quad (\text{D.17})$$

and rewrite Eqn. D.17, the bound probability function can be written by using time ( $n$ ) and space ( $j$ ) indices like this;

$$\begin{aligned} p_{1j}^{n+1} = & p_{1j}^n + (k_A^- + k_B^+) \Delta t p_{0j}^n + (k_A^- \Delta - k_B^+ \delta) \Delta t \frac{p_{0j+1}^n - p_{0j-1}^n}{2\Delta} \\ & + \frac{1}{2}(k_A^- \Delta^2 + k_B^+ \delta^2) \Delta t \frac{p_{0j+1}^n - 2p_{0j}^n + p_{0j-1}^n}{\Delta^2} - (k_A^+ + k_B^-) \Delta t p_{1j}^n \end{aligned} \quad (\text{D.18})$$